Precision flavor physics from Lattice QCD

Candidate: Francesco Sanfilippo
Supervisor: G. Martinelli

December 13, 2011

Contents

Chapter 1

Introduction

1.1 Motivations

The Standard Model is the modern theory describing the fundamental interactions among elementary particles.

The Model has been tested with success over a very large set of observables, showing to be able to predict the experimental values of cross sections and decay rates for all processes up to the explored scale of energy (the electroweak scale, of $\mathcal{O}(100)$ GeV), and has passed a large number of different checks. Despite of its remarkable successes however, the Model suffers from various problems, among which: the instability of the Higgs mass to radiative corrections, the lack of a mechanism explaining the bariogenesis, the absence of a candidate for the dark matter, and its failure to unify truly all the fundamental forces together.

The model itself limits to parametrize the observed hierarchy of particles mass and of flavor mixing amplitude, and does not explain them. From this reason the model is generally considered to be a low-energy approximation of a more fundamental theory.

All these problems suggest that the validity of the model is limited to energies of the order of the TeV scale. It is common opinion that at this scale of energy a new physics beyond the Standard Model has to show. This scale is experimentally accessible only by means of very high energy particle accelerators (previously only from TeVatron, now only from LHC). On the other hand, the effects caused by new physics should manifest indirectly at energies below the TeV scale, as small corrections to the Standard Model predictions [1]. These observables are accessible also from dedicated low energy but high energy luminosity accelerators (e.g the past B-factories BaBar, Belle, and the to-be constructed SuperB [2]).

In the perspective of highlighting and quantifying the effects of new physics, a deep and careful comparison of the experimental observables to the prediction of the Standard Model can give remarkable information. A dominant role is played in this field by flavor physics, which in the hadronic sector involves the elements of the Cabibbo-Kobayashi-Maskawa (CKM) matrix. The extraction of the values of the CKM matrix elements performed from different experimental inputs and with the help of different theoretical calculations represents the most tighten test of the Standard Model [3]. Here we will briefly review the quantities which have been subject our analysis and give motivation for the work which we have carried out (see chapter in will be reviewed in chapter 2 for more extensively informations on such quantities).

One of the most relevant and actual flavor physics problem is the precise determination of

hadronic matrix elements relevant for the B physics. The b quark decay physics are highly sensitive to new physics effects and very sensible to test presence of physics beyond the standard model. These tests already provides some small indications of deviations from Standard Model prediction, but actual statistic errors and systematics uncertainty do not allow them to be relevant and demand for deeper study. From the experimental side the building of new generation of B factories will allow to improve substantially the measurement of b quark quantities. From the theoretical side, a precise determination (at the $\sim 1\%$ level of accuracy) of hadronic matrix element related to b quark will be needed in order to give relevance to statistically improved measurement of $B_{(s)}$ meson leptonic and semi-leptonic decay width and of neutral B mixing amplitude.

Experiments measuring leptonic and semi-leptonic decay amplitude of K system, together with lattice calculation of leptonic K meson decay constant f_K and semi-leptonic form factors give access to the V_{us} element of the CKM matrix. These experiments reach already such level of precision that theoretical computations of K decay constant and form-factors need to take into account the small isospin breaking effects related to the mass and charge difference of u and d quarks in order to give meaningful results. This effects are typically added to the computations using effective theory, but first principle and more precise computation of such corrections would be very useful in order to make the V_{us} determination more accurate.

Quark masses can be determined using different physical inputs, so that the comparing the results obtained in different lattice computations from different groups one can over-constrain the Standard Model. Their values are also used as physical inputs for subsequent computations, and is therefore of primary importance to measure them as accurately as it is possible.

1.2 Methodology

On the theoretical side, the calculations are challenging due to the effects of the strong interaction, which in the Standard Model is described by the Quantum Cromodynamics (QCD).

At short distances (or equivalently at high energies) the quarks interact weakly, so that it is possible to study the theory with perturbative techniques; the other way round, the interaction increases with the increase of the distance (or with the decrease of the energy), and at distance larger than $\sim 1\,\mathrm{fm}$ (energy lower than $\sim 1\,\mathrm{GeV}$) the theory is not perturbative anymore. For this reason every calculation between low energy hadronic states needs a non perturbative treatment. This is the case for many observables playing important role in the context of flavor physics, as for example the form factors, the decay constants, and numerous matrix elements involved in meson mixings, whose relevance has been explained previously.

The only available method to calculate physical observables non perturbatively starting from first principles, in which all sources of systematic errors can be kept under control and whose accuracy can be arbitrarily increased with time is Lattice QCD. This method has been the tool used in the work of this thesis. In Chapter 3 we introduce Lattice QCD presenting examples of calculations and discussing in details the various systematics effects which must be taken in consideration when dealing with a modern Lattice computation.

1.3 Main results

Most part of the present thesis work has been devoted to the determination of Standard Model parameters, in particular quark masses and CKM matrix elements. Here we report the main

results of the thesis, which will be described more extensively in separate chapters.

Quark masses

In Chapter 4 we perform a non-perturbative determination of the u/d, s and c quark masses including a careful discussion of the continuum and chiral extrapolations. In this way we reduced the most important source of systematics errors in the current lattice calculation. Renormalization has been performed non-perturbatively and quark masses has been tuned in such a way to reproduce the pseudo-scalar meson masses.

The quark masses in the $\overline{\rm MS}$ scheme at 2 GeV read:

$$\begin{aligned} \overline{m}_l^{\overline{\rm MS},\,2\,{\rm GeV}} &= 3.6\,(1)\,(2)\ {\rm MeV} &= 3.6\,(2)\ {\rm MeV}\,, \\ \overline{m}_s^{\overline{\rm MS},\,2\,{\rm GeV}} &= 95\,(2)\,(6)\ {\rm MeV} &= 95\,(6)\ {\rm MeV}\,, \\ \overline{m}_c^{\overline{\rm MS},\,2{\rm GeV}} &= 1.14\,(3)\,(3)\ {\rm GeV} &= 1.14\,(4)\ {\rm GeV}\,. \end{aligned} \tag{1.1}$$

B physics

Determination of the b quark related quantities suffers from additional systematic errors caused by the needed extrapolation in the heavy quark mass. We have designed a specific approach to deal with such extrapolation, which is described in Chapter 5, that allowed us to perform a precise computation of the b quark mass and B and B_s leptonic decay constants f_B and f_{B_s}, obtaining them with a 2-3% level of precision. This poses our results among the most precise available at present. Moreover we explored various new techniques which in future will allow, with an increase computational power, to reach the level of accuracy required by future experiments, and allow to extract the CKM matrix elements related to b quark (V_{ub}, V_{cb}) with an unprecedented accuracy and add strong constraints to the Standard Model.

The main results of this chapter are:

- the b quark mass:

$$\begin{aligned} \overline{m}_b(\overline{m}_b) &= 4.29(13)(4)\,{\rm GeV} = 4.29\,(14)\ {\rm GeV}\,, \\ \overline{m}_b^{\overline{\rm MS},\,2\,{\rm GeV}} &= 4.92\,(13)\ {\rm GeV}\,. \end{aligned}$$

- the B and B_s mesons leptonic decay constants f_B and f_{B_s}:

$$f_{Bs} = 232(10)\ \ {\rm MeV}\,, \qquad f_B = 195(12)\ \ {\rm MeV}\,, \qquad \frac{f_{Bs}}{f_B} = 1.19(5)\,. \tag{1.2}$$

Isospin breaking effects

In Chapter 6 we present a new fully non-perturbative method to compute the $u-d$ quark mass difference and to take into account the isospin breaking effects on physical quantities related to this difference. The method is then applied to the computation of the leptonic K-meson decay constant, and proves to be very effective in decreasing the error on the computation on its isospin breaking corrections. We also provide a preliminary determination of the proton-neutron mass splitting, and of the isospin correction to the K semi-leptonic form factors.

The main results of this analysis are:

- the value of the up-down quark mass difference, which in $\overline{\text{MS}}$ at 2 GeV reads:

$$[m_d - m_u]^{\overline{\text{MS}},\,2\text{GeV}} = 2.27(24)\ \text{MeV}\,, \tag{1.3}$$

- the isospin breaking corrections on the K leptonic decay constant:

$$\left[\frac{f_{K^+}}{f_K} - 1\right] = -0.38(6)\%\,, \tag{1.4}$$

- the proton-neutron mass splitting, which at fixed lattice spacing results:

$$[M_n - M_p]^{QCD} = 2.7(9)\ \text{MeV}\,. \tag{1.5}$$

Strange and Charm unquenching

All the computations presented up to this point are performed in partially quenched setup accounting for $N_f = 2$ light sea quark. This is equivalent to performing the perturbative calculations by ignoring the presence of quark different form u and d in fermionic loops in the diagrammatic formalism. Although believed to have small effects on observable, this approximation must be removed in order to increase the reliability of lattice QCD calculations. In Chapter 7 we present preliminary results obtained in new computations which take into accounts two heavier flavors of quarks (strange and charm) with respect to previous computations. We will show in particular a preliminary computation of the B_K parameter involved in neutral K mixing, and a preliminary computation of the pion electromagnetic form factor. When terminated, these results will be the first to take into account both strange and charm dynamical quarks.

Chapter 2

Flavor physics

2.1 CKM matrix

The Standard Model group the six observed flavor of quarks in two sets of three generations:

$$\begin{aligned} \mathrm{u} &= (u,\, c,\, t) \\ \mathrm{d} &= (d,\, s,\, b)\,. \end{aligned}$$

The quarks of types u have $+2e/3$ charge, while quarks of types d have $-e/3$ charge. Quark mass increase going from u/d generation to t/b. The SM lagrangian contains a therm which mixes allow interaction vertexes between u and d types quarks:

$$\mathcal{L}_{f.v} = \frac{g}{\sqrt{2}} W_\mu^+ \sum_{f,g=1}^{n} \bar{\mathrm{u}}^f \gamma^\mu V_{fg}^{CKM} \mathrm{d}^g + \mathrm{h.c}\,, \tag{2.1}$$

where g is the Fermi constant, W the field of the charged vector boson mediating weak force, and V^{CKM} is the Cabibbo-Kobayashi-Maskawa matrix, a unitary matrix parameterizing the mixing between different flavors of quarks. Its entries are fundamental parameters of the Standard Model which must be extracted from experiments:

$$V^{CKM} = \begin{pmatrix} V_{ud} & V_{us} & V_{ub} \\ V_{cd} & V_{cs} & V_{cb} \\ V_{td} & V_{ts} & V_{tb} \end{pmatrix}. \tag{2.2}$$

Being a rank $n = 3$ unitary matrix, it is parameterized by $n^2 = 9$ parameters, of which $2n - 1 = 5$ of them are not physically relevant because of the possibility to redefine quark fields, so the number of significant parameters is actually 4, of which 3 are rotation angles between different quarks, and the remaining one is a complex phase causing CP violations.

The unitarity of the CKM matrix can be expressed by numerous unitarity relations. In particular, the sum of squared entries of each rows (or columns) must be equal 1.

Given the fact that different entries of CKM matrix can be independently measured, it is possible to test SM by verifying such relation to be experimentally satisfied. In particular the most precise bound comes from the analysis of the first line of the matrix, that is proving the relation:

$$|V_{ud}|^2 + |V_{us}|^2 + |V_{ub}|^2 = 1. \tag{2.3}$$

The value of V_{ud} is very precisely known from the measurement of nuclear β decays, and the remaining two parameters can be determined experimentally from leptonic and semi-leptonic decays of K, D and B mesons. Large part of this thesis work is dedicated to topics related to the determination of such CKM matrix elements, and in next sections we will discuss how lattice computations help in performing such tasks.

Another interesting propriety of unitary matrices is that each row (or column) is orthogonal to the other, so that it is possible to build various other relations to prove the SM. In particular considering the first and third columns of the matrix one gets:

$$V_{ud}V_{ub}^* + V_{cd}V_{cb}^* + V_{td}V_{tb}^* = 0\,. \tag{2.4}$$

Each of the three addend of such relation define a vector in the complex plane. Using the Wolfeinstein parameterization of the CKM matrix they read respectively:

$$\begin{aligned} V_{ud}V_{ub}^* &= A\lambda^3\left(1-\lambda^2/2\right)(\rho+i\eta) \\ V_{cd}V_{cb}^* &= -A\lambda^3 \\ V_{td}V_{tb}^* &= A\lambda^3\left(1-\rho-i\eta\right). \end{aligned}$$

These three vectors define a triangle in the complex plain, whose apex has coordinates $(\bar{\rho},\,\bar{\eta}) = \left(1-\lambda^2/2\right)\times(\rho,\,\eta)$ in units of $A\lambda^3$. The area of the triangle quantify the amount of CP violation in the SM: if all CKM entries were real, η would be null and thus the triangle would have zero area. Therefore the triangle, which is called *unitary triangle*[1] is strongly related to CP violation phenomena.

Various experiments can measure different proprieties of this triangle, such as side lengths, angles amplitudes, etc. In general it is very useful to show the various bounds on the CKM matrix elements as bands on the complex plain which must intersect on the apex of the triangle. In Fig. 2.1 we show the fit of all the present bounds to the values of $\bar{\rho}$ and $\bar{\eta}$ performed by UTfit collaboration.

All the constraints to the triangle intersect in the same region, thus indicating quite a good agreement between SM predictions and experiments. The increase of precision both on the theoretical and experimental sides will allow in future to perform more an more stringent fit and possibly highlight the presence of New Physics.

Now that we have given a general overview of the flavor topics considered in the present thesis work we can go in details on particular arguments, explaining how non-perturbative computation pose problems on the computation of flavor quantities, and how lattice allow to solve them.

2.2 Leptonic decay constants

Among the most simples flavor-related hadronic quantities measurable on lattice there are the leptonic decay constants of mesons. Quite a large part of our work has been devoted to the determination of decay constants for various pseudo-scalar mesons.

Their values provides some of the most important bounds on the values of the CKM matrix elements, and therefore of great relevance in the contest of flavor physics.

A pseudo-scalar meson composed by an up and down type quarks can decay into a $(\mu,\,\bar{\nu}_\mu)$ pair through the emission of a W meson. Diagrammatically this happens through diagram shown in Fig. 2.2.

[1] Actually other 5 similar triangles exists.

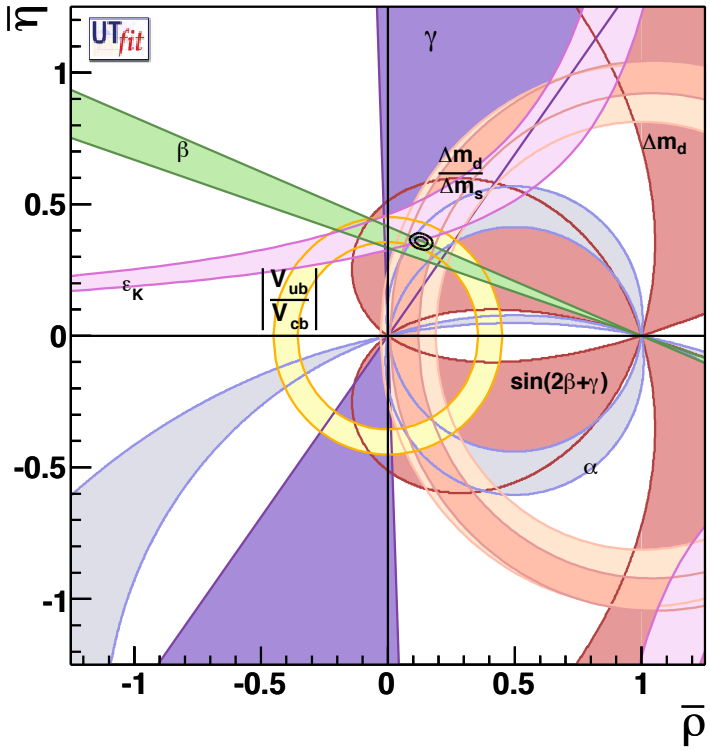

Figure 2.1: Fit of all the bound to the values of $\bar{\rho}$ and $\bar{\eta}$ obtained by UTfit collaboration.

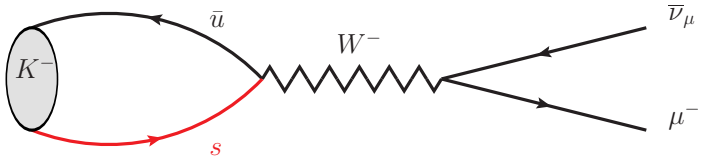

Figure 2.2: Diagrammatic representation of the leptonic decay of $K^- \to \mu^- \bar{\nu}_\mu$.

The branching ratio of such decay mode is given by:

$$\Gamma\left(PS \to \mu\bar{\nu}_\mu\left(\gamma\right)\right) = \frac{G_F^2 \left|V_{PS}\right|}{8\pi} f_{PS}^2 M_{PS}^2 M_\mu^2 \left(1 - \frac{M_\mu^2}{M_{PS}^2}\right)\left[1 + \frac{\alpha}{\pi} C_{PS}\right], \tag{2.5}$$

where G_F is the Fermi constant, M_μ and M_{PS} are the muon and pseudo-scalar particle masses, C_{PS} is a coefficient parameterizing the electromagnetic radiative corrections, and α the QED coupling. V_{PS} is the CKM matrix appropriate for the coupling between the u and d type quark contained in the pseudo-scalar meson (so for example it is V_{us} when we look at the K meson and V_{ud} when we look at the Pion), and f_{PS} parameterize the hadronic matrix element between pseudo-scalar meson state and the vacuum of the axial current:

$$f_{PS} P_\mu = \langle 0 | A_\mu | PS \rangle \ , \tag{2.6}$$

where we have defined the axial current: $A_\mu = \bar{u}\gamma_\mu\gamma_5 d$. The experimental measurement of such branching ratios, together with the knowledge of the decay constants f_{PS} allow to determine CKM matrix elements with great precision.

One of the most precise determination of the value of the ratio $|V_{us}/V_{ud}|$ comes from the measurement of the ratio of $K \to \mu\bar{\nu}_\mu(\gamma)$ and $\pi \to \mu\bar{\nu}_\mu(\gamma)$ branching ratios. In particular it is known [4] that:

$$\frac{\Gamma(K \to \mu\bar{\nu}_\mu(\gamma))}{\Gamma(\pi \to \mu\bar{\nu}_\mu(\gamma))} = \left|\frac{V_{us}}{V_{ud}}\right|^2 \left(\frac{f_K}{f_\pi}\right)^2 \left(\frac{M_K^2 - M_\mu^2}{M_\pi^2 - M_\mu^2}\right)^2 \times 0.9930(35). \tag{2.7}$$

In this expression the last coefficient parametrize long term and radiative corrections. Matrix element $|V_{ud}| = 0.97425(22)$ is very precisely known from the measurement of nuclear beta decays, so that the ratio f_K/f_π allow to determine precisely the value of $|V_{us}|$.

Lattice QCD calculations is the only method that allow to determine the value of the decay constants non-perturbatively starting directly from first principles, through the direct evaluation of matrix element 2.6.

These computations are performed typically considering the isospin symmetric theory in which $m_u = m_d$ and $q_u = q_d$. Given the precision reached from experiments measuring K and π leptonic branching ratios, it is necessary to go beyond this approximation. In Chapter 6 we will present novel method to take into account corrections related to the u/d mass difference. Taking into account these corrections will allow to improve the current bounds on $|V_{us}|$ and thus perform improved test on the SM.

Other two particularly important cases of study are the leptonic decays $B \to \tau\nu_\tau$ and $B_s \to \mu^+\mu^-$.

The first process is particularly sensitive to potential New Physics contributions mediated, at tree level, by charged Higgs. The relevant entries in the Standard Model prediction for the decay rate are the CKM matrix element V_{ub}, which can be extracted from the study of semi-leptonic $B \to \pi\,\ell\,\nu_\ell$ decays without significant New Physics contributions (for $\ell = e, \mu$), and the pseudo-scalar decay constant f_B. The measured values of the $B \to \tau\nu_\tau$ decay rate deviate, at present, by about 3 sigma from the Standard Model prediction [5], within relatively large experimental and theoretical uncertainties. In this respect, improving the lattice determination of f_B would be an important ingredient for increasing the chances of detecting the contribution of New Physics effects to this decay.

The second process of interest is the rare leptonic decay $B_s \to \mu^+\mu^-$, which is being studied with unprecedented accuracy at LHCb. In this case the relevant hadronic parameter to be determined on the lattice, which enters the theoretical prediction of the decay rate, is the pseudo-scalar decay constant f_{B_s}.

The determination of both f_B and f_{B_s}, together with a prediction for the b quark mass m_b, are part of the present work and will be discussed extensively in chapter 5.

2.3 Semi-leptonic form factors

Lattice QCD allows to compute non-perturbatively hadronic form factors for both baryons and mesons. In the following we will show how the determination of the $K \to \pi$ vector form factor

allows to provides the most precise determination of the CKM matrix element $|V_{us}|$ through the analysis of the semi-leptonic $K \to \pi\ell\nu$ decay (also known as $K_{\ell 3}$ decay). At zero momentum transfer q^2 of the lepton pair this decay rate is given by:

$$\Gamma_{K\to\pi\ell\nu} = \frac{G_F^2 M_{KW}^5}{192\pi^3} S_{EW} \times |V_{us}|^2 \left|f_+^{K\pi}(0)\right|^2 I_{K\ell} \left(1 + \delta_{EM}^{K\ell} + \delta_{SU(2)}^{K\pi}\right)^2 , \tag{2.8}$$

where $S_{EW} = 1.0232\,(3)$ is the short distance electroweak correction, G_F is the Fermi constant, M_K is the K mass, $\delta_{EM}^{K\ell}$ represents the channel-dependent long-distance EM corrections, $\delta_{SU(2)}^{K\pi}$ the correction for isospin breaking, and $I_{K\ell}$ is a phase-space integral that is sensitive to the momentum dependence of the form factors. The latter describe the matrix element of the vectorial current between K and π, defined by:

$$\langle \pi^i(p')|V_\mu|K^i(p)\rangle = C_i \left[f_+^i(q^2)(p+p')_\mu + f_-^i(q^2)(p-p')_\mu\right] , \qquad q^2 = (p-p')^2 , \tag{2.9}$$

where C_i is a Clebsch-Gordan coefficient equal to 1 ($2^{-1/2}$) for neutral (charged) Kaons.

This form factor can be measured very precisely on lattice in a fully non-perturbative way. In chapter 7 we will report on a preliminary calculation of such quantity, again computed in the isospin symmetric approximation mentioned previously.

The precision reached by the experiments in the measurement of $K_{\ell 3}$ branching ratios need to take into account the effects of the breaking of isospin symmetry, which are contained in term $\delta_{SU(2)}^{K\pi}$ in Eq. 2.8 and typically computed with Ch-PT. In chapter 6 we will present a new method to compute non-perturbatively the effects of mass difference between u/d quark in the $K \to \pi$ vector form factor. This correction

2.4 B_K parameter

The neutral Kaon mesons system is quite a non-trivial one, given the fact that mass eigenstate $\left|K^0\right\rangle \equiv |d\bar{s}\rangle$ and its antiparticle $\overline{K}^0 \equiv \left|\bar{d}s\right\rangle$ are neither CP neither weak interactions eigenstates. The CP even and odd eigenstates are $K_{1,2} = \frac{1}{\sqrt{2}}\left(K^0 \pm \overline{K}^0\right)$; the long-time and short-time decaying modes, which are eigenstates of the weak interaction, are almost but nor exactly CP eigenstates, and in particular (by making an opportune definition of these modes) it is possible to write them as:

$$|K_S\rangle = \frac{1}{\sqrt{1+\epsilon_K^2}} \left(|K_1\rangle + \epsilon_K |K_2\rangle\right) \tag{2.10}$$

$$|K_L\rangle = \frac{1}{\sqrt{1+\epsilon_K^2}} \left(\epsilon_K |K_1\rangle - |K_2\rangle\right) . \tag{2.11}$$

The nonequivalence between weak decay modes and CP eigenstates is just caused by the possibility of neutral kaon mass eigenstates to mix among themselves. Therefore the small parameter ϵ_K quantify the amount of indirect CP violation in the weak interaction decay modes caused by the mixing of mass eigenstates. Studying the neutral K decaying modes it is possible to measure the value of ϵ_K.

In the Standard Model this take place through a second order weak interaction involving the exchange of two W mesons, as sketched in the left panel of picture 2.3. The box diagram can be

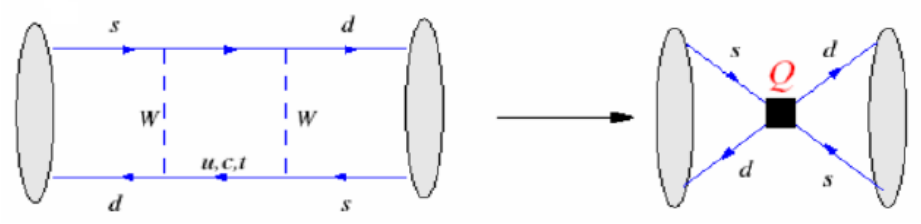

Figure 2.3: *Left panel*: interaction causing neutral K mixings in the SM. *Right panel*: low energy effective description of the phenomenon.

contract to a point as shown in the right panel of picture 2.3, so that the interaction causes the mixing is given by the effective hamiltonian:

$$\mathcal{H}_{eff}^{\Delta S=2} \equiv \frac{G_F M_W^2}{16\pi^2} \underbrace{\left[\sum_{l,m=u,c,t} C_1^{(l,m)}(\mu)\, V_{ls}^* V_{ld} V_{ms}^* V_{md} \right]}_{\text{perturbative}} \underbrace{\hat{Q}_1(\mu)}_{\text{non pert.}} , \tag{2.12}$$

where:

$$Q_1^{bare} \equiv \frac{1}{4} \left[\bar{s}\gamma_\mu (1-\gamma_5) d\right] \left[\bar{s}\gamma_\mu (1-\gamma_5) d\right] , \tag{2.13}$$

is a four-point operator dimension 6 operator, and $C_1^{(l,m)}$ are *Wilson coefficients* matching the effective theory with the full theory, which is a scale-dependent operator whose value is renormalization scale depending. It is customary to parameterize the matrix element of the renormalized $\hat{Q}_1$ operator between K^0 and $\overline{K}^0$ states as:

$$\left\langle \overline{K}^0 \right| \hat{Q}_1(\mu) \left| K^0 \right\rangle = \left\langle \overline{K}^0 \right| \hat{Q}_1(\mu) \left| K^0 \right\rangle_{VIA} \hat{B}_1(\mu) , \tag{2.14}$$

where the VIA stands for "Vacuum Insertion Approximation", where one inserts only vacuum between the two $[\bar{s}\gamma_\mu (1-\gamma_5) d]$ factors contained in Eq. 2.13, that is given by:

$$\left\langle \overline{K}^0 \right| \hat{Q}_1(\mu) \left| K^0 \right\rangle_{VIA} = \frac{8}{3} \left\langle \overline{K}^0 \left| \bar{s}\gamma_0\gamma_5 d \right| 0 \right\rangle^2 = \frac{8}{3} f_K^2 M_K^2 , \tag{2.15}$$

where the factor 8/3 comes from Feirz rearrangement of the gamma matrices.

The value of $\hat{B}_1(\mu)$, known also simply as B_K quantify therefore the deviation from the VIA of the matrix element 2.14. It is related to the value of ϵ_K through the relation:

$$\epsilon_K = \frac{G_F^2 M_W^2 f_K^2 M_K^2}{6\sqrt{2}\Delta M_K} \hat{B}_1(\mu)\, \mathrm{Im} \left[\sum_{l,m=u,c,t} C_1^{(l,m)}(\mu)\, V_{ls}^* V_{ld} V_{ms}^* V_{md} \right] . \tag{2.16}$$

From the experimental measure of ϵ_K and the lattice computation of $\hat{B}_1(\mu)$, one can put a constraint on the unitary triangle. In particular one can put a constraint on the quantity:

$$constant = \bar{\eta}(1-\bar{\rho}) , \tag{2.17}$$

which correspond to the bound plotted in fig. 2.4.

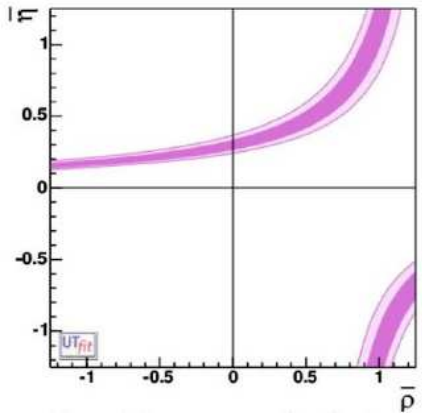

Figure 2.4: Constraint on the apex of the unitary triangle imposed by the knowledge of ϵ_K.

The operator defined in 2.12 is the only one contributing to neutral Kaon mixing according to the Standard Model. In general, New Physics model predict a larger number of possible interaction which can mediate the mixing, which are globally described by an enlarged set of operator in which all possible current contribute to the hamiltonian 2.12 in addition to the axial one. Each of these current is associated to a different parameter B_i for a total of 5 coefficient (including also the standard B_K). The calculation of these coefficients allow to put bound on New Physics models, and is therefore of very strong interest.

In Chapter 7 we will present preliminary results for the calculation of the B_K parameter performed within new $N_f = 2 + 1 + 1$ simulations.

Chapter 3

Lattice QCD

Lattice Quantum Field Theory is a ay to regularize Field Theory in which the continuum and infinite space-time is replaced with a discretized grid of points in a finite volume. Lattice spacing a between the hyper-cubic grid of points acts as ultra-violet cut-off, while the box length L acts as infrared cut-off. This regularization is very suitable to perform non-perturbative computations. We will illustrate the various steps involved in a lattice computation by starting from a particular case, the hadron mass determination, on which much part of this Ph.D thesis work is based.

3.1 QCD in the continuum

3.1.1 QCD Lagrangian

The continuum lagrangian density for QCD with a set of n_f quark of mass m_i, $i \in \{1...n_f\}$ reads, in the slashed Dirac notation and omitting color and Dirac indices:

$$\mathcal{L}(x) = \sum_{f=1}^{n_f} \overline{q}^{(f)}(x) \left(\not{D}(x) + m_f \right) q_f(x) + \frac{1}{4} F_{\mu\nu} F^{\mu\nu} , \tag{3.1}$$

where

$$F_{\mu\nu} \equiv \frac{1}{ig} \left[D_\mu, D_\nu \right] , \tag{3.2}$$

being g the coupling, and where the covariant derivative D is definite in terms of the gauge field A as:

$$D_\mu(x) \equiv \partial_\mu + igA_\mu(x) . \tag{3.3}$$

Fermions transform according to the fundamental representation of the $SU(3)$ group while gauge fields transform according to the adjoint.

3.2 Hadron masses determination

3.2.1 General strategy

Mass spectrum of a quantum theory for a certain set of field Φ defined by a certain action $S[\Phi]$ can be determined by analyzing the large euclidean time behavior of correlation functions of appropriate operators, as following.

Let us suppose that we want to determine the mass of a particle with certain quantum number. First of all we have to choose two operator O_1, O_2 (not necessarily different) carrying the same quantum numbers of the particle we are interested in. We have to compute the two-points correlation function:

$$C_T(t) \equiv \left\langle O_2(t) O_1^\dagger(0) \right\rangle_T = \frac{1}{Z_T} \mathrm{Tr}\left[e^{-i(T-t)H} O_2 e^{-itH} O_1^\dagger \right] , \tag{3.4}$$

where T is the time extent of the system, H is the hamiltonian of the theory and we have defined the partition function: $Z_T = \mathrm{Tr}\left[e^{iH}\right]$.

In the path-integral formulation of quantum field theory this correlation function is obtained as:

$$C_T(t) = \frac{1}{Z_T} \int D[\Phi] \, e^{iS[\Phi]} O_2[\Phi(t)] \, O_1^\dagger[\Phi(0)] , \tag{3.5}$$

where $\int D[\Phi]$ is the functional integral over all possible field configurations.

In the limit of large T it is possible to show that $C_T(t)$ correspond to the vacuum matrix element of the operator $O_2(t) O_1^\dagger(0)$:

$$C(t) \equiv \lim_{T\to\infty} C_T(t) = \langle 0 | O_2(t) O_1^\dagger(0) | 0 \rangle . \tag{3.6}$$

By inserting the sum over intermediate states we can write it as:

$$\begin{aligned} C(t) &= \langle 0 | O_2(t) \left(\frac{\sum_m |m\rangle \langle m|}{2m} \right) O_1^\dagger(0) | 0 \rangle = \\ &= \sum_m \frac{e^{-itE_m}}{2m} \langle 0 | O_2 | m \rangle \langle m | O_1^\dagger | 0 \rangle . \end{aligned}$$

In this way the correlation is decomposed as a sum of complex exponential, one for each state m predicted by the theory, each oscillating with a factor equal to the mass of the state, and each multiplied by the product of the matrix elements of $O_1^\dagger$ and O_2. The operators $O_1^\dagger$, O_2 have the role of creating and destructing the particle of our interest out from the vacuum, and so are called *interpolating operators.*

In order to isolate the ground state we apply the Wick rotation passing from Minkowskian to Euclidean time. This is performed by applying the transformation $t \to -i\tau$ to the system, which implies also changing $\partial_0 \to i\partial_0$, $\gamma_i \to -i\gamma_i$, $i \in \{1,2,3\}$ and so on. In Euclidean space time the metric matrix is given by $g_{\mu\nu} = \mathrm{Diag}[1,1,1,1]$ so that there is no need to distinguish between upper and lower indices.

In the limit $\tau \to \infty$ only the ground state contributes to the correlation function:

$$= \lim_{t\to\infty} C(\tau) = \frac{e^{-\tau E_f}}{2m} \langle 0 | O_2 | f \rangle \langle f | O_1^\dagger | 0 \rangle , \tag{3.7}$$

so the lower lying state mass can be determined by looking at the large euclidean time behavior of an appropriate correlation functions.

3.2.2 Pion mass determination in QCD

Now we will consider a concrete example and we will describe how to determine the pion mass. According to what said in section 3.2 we have first of all to choose an operator O carrying the same quantum numbers of the charged pion, that is a pseudo-scalar particle. The simplest operator is:

$$O_{\pi^+} = \bar{d}\gamma_5 u\,, \tag{3.8}$$

where u, d are the fields of the up and down quarks respectively.

Having chosen an interpolating operator we can write the formal expression of the time correlation function of this operator:

$$C_{PS,PS}(t) = \frac{1}{\mathcal{Z}} \int D\left[\bar{q}^{(f)}, q^{(f)}, A\right] \left\{ \left(\bar{u}(t)\gamma_5 d(t)\right)\left(\bar{u}(0)\gamma_5 d(0)\right) e^{-S_E} \right\}. \tag{3.9}$$

This kinds of expression has no real meaning, as they involve an infinite number of integrals (one per space-time point). In order to make it sensible we need to *regularize* it, transforming it into a canonical multi-dimensional integral. This will be the topic of next section.

3.3 Lattice regularization of QCD

There are various ways to make a field theory finite, each having its advantages and problems. Dimensional regularization is by far the most popular among regularization prescriptions, and it is the most useful in perturbative computations, by expanding functional integrals in powers of the couplings. Lattice QCD (LQCD)instead allows to deal with non-perturbative problems, allowing one to evaluate directly the full functional integrals numerically, with a precision limited only by available computational power. In this section we will introduce the subject of lattice regularization starting from the *Wilson regularization* (section 3.3.1), followed by the detailed discussion of the continuum limit (section3.3.2) and then we briefly review how to improve the continuum scaling through the so-called Symanzik program (section 3.3.3). In the end we will review the Twisted Mass regularization (section 3.3.4), which have been used in all the computations presented in this thesis.

We will not discuss other formulation of LQCD such as Staggered or Domain Wall, neither will discuss recent development as Stout smeared actions, as these tools have not been used in any part of the present work.

3.3.1 Wilson regularization of QCD

The first lattice regularization was proposed in 1974 by K. Wilson in the pioneering paper [6]. Over the past years many developments of this technique have been proposed, and lattice computations are rarely performed using straightly this regularization nowadays. Nonetheless in many cases the Wilson regularization remained the basic ingredient to build more sophisticated lattice actions, and so we will discuss it extensively in the following sections.

3.3.1.1 Regularization of the free fermion field

In any regularization one starts defining the hyper-cubic grid of points $\{n\}$, of extent L in space and T in time, and first-neighbor separation a. Fields are associated to lattice points, so that a field f is defined by the collection of the values f_i, $i \in \{n\}$.

The discretized derivative is defined as $\hat{\partial}_\mu f_n \equiv \frac{f_{n+\hat{\mu}} - f_{n-\hat{\mu}}}{2a}$, where $\hat{\mu}$ is the vector of length a pointing in the direction $\hat{\mu}$.

The Wilson lattice regularized action for a free fermion field $\psi(x)$ of mass m is given in euclidean space-time by:

$$\hat{S}_{euc}^{free} = \hat{\bar{\psi}}_{i;\alpha} M_{i,j;\alpha,\beta} \hat{\psi}_{j;\beta}\,, \tag{3.10}$$

where we have defined the *fermionic matrix*:

$$M_{i,j;\alpha,\beta} = \frac{1}{2}\left\{\kappa^{-1}\delta_{i,j}\delta_{\alpha\beta} - \sum_\mu \left[\left(1+\gamma_{\mu;\alpha,\beta}\right)\delta_{i+\hat{\mu},j} + \left(1-\gamma_{\mu;\alpha,\beta}\right)\delta_{i-\hat{\mu},j}\right]\right\}, \tag{3.11}$$

and the *hopping parameter*:

$$\kappa^{-1} = 2\hat{m} + 8r. \tag{3.12}$$

All the quantities with "$\hat{}$" are to be intended as expressed in terms of a, for example the dimensionless mass $\hat{m} \equiv am$, and spin indices have been omitted for simplicity. Fermionic field at different space-time point anti-commutate so for each lattice point ψ is a *Grassman variable.* From now on, all the quantities have to be intended to be computed in Euclidean space-time (where not else indicated) so that we will omit the *eucl* for simplicity.

By substituting all the quantities with their dimensional counterpart we can rewrite it as:

$$\frac{\hat{S}^{free}}{a^4} = m\bar{\psi}_n\psi_n - \bar{\psi}_n\gamma_\mu \underbrace{\frac{\psi_{n+\hat{\mu}} - \psi_{n-\hat{\mu}}}{2a}}_{\partial_\mu\psi_n} - ar\underbrace{\sum_\mu \frac{\psi_{n+\hat{\mu}} - 2\psi_n + \psi_{n-\hat{\mu}}}{2a^2}}_{\partial^2\psi_n} = \bar{\psi}_n\left[m - \hat{\not{\partial}} - ar\hat{\Box}\right]\psi_n\,, \tag{3.13}$$

where we have defined the euclidean laplacian:

$$\hat{\Box} \equiv \sum_\mu \left[\delta_{n,n+\hat{\mu}} - 2\delta_{n,n} + \delta_{n,n-\hat{\mu}}\right]. \tag{3.14}$$

In the "naive" continuum limit (that is, taking the $a \to 0$ limit of previous expression) this reduces to the well known continuum action:

$$S_{naive}^{free} = \lim_{a\to 0}\frac{\hat{S}^{free}}{a^4} = \int d^4x\bar{\psi}\left[m - \not{\partial}\right]\psi\,. \tag{3.15}$$

The laplacian in this contest is known as "Wilson term" and do not contribute to the continuum limit because it is multiplied by a. Apparently this term is inessential to reproduce the continuum limit. Moreover at finite a its presence breaks the chiral symmetry of the action at $m = 0$. We could get a simpler expression for $\hat{S}$ setting $r = 0$ from the beginning (this is known as the *naive* regularization), with the advantage of having to deal with a discretized theory for which the chiral symmetry is preserved at finite lattice spacing.

Actually the presence of the Wilson term is necessary to avoid the so-called *fermion doubling* problem which affects the theory if r is set to zero. In order to explain it more in details, let us calculate the field propagator. This will also give us the possibility to show an example of an analytical computation with lattice regularization.

3.3.1.2 Propagator computation

The propagator is defined as the two points green function: $S_{\alpha\beta}(x,y) = \left\langle \bar{\psi}_\beta(y)\,\psi_\alpha(x)\right\rangle$ which in continuum path-integrals formulation is expressed as:

$$S_{\alpha\beta}(x,y) = \frac{\int D\left[\psi,\bar{\psi}\right]\bar{\psi}_\beta(y)\,\psi_\alpha(x)\,e^{-S\left(\psi\bar{\psi}\right)}}{\int D\left[\psi,\bar{\psi}\right]e^{-S\left(\psi\bar{\psi}\right)}}\,. \tag{3.16}$$

In lattice discretization this expression is replaced by its discrete counterpart:

$$S_{m,n;\alpha\beta} = \frac{\int\prod_{p;\gamma}d\hat{\bar{\psi}}_{p;\gamma}\prod_{r;\delta}d\hat{\psi}_{r;\delta}\,e^{-\hat{\bar{\psi}}M\hat{\psi}}\hat{\bar{\psi}}_{n,\alpha}\hat{\psi}_{m,\beta}}{\int\prod_{p;\gamma}d\hat{\bar{\psi}}_{p;\gamma}\prod_{r;\delta}d\hat{\psi}_{r;\delta}\,e^{-\hat{\bar{\psi}}M\hat{\psi}}}\,, \tag{3.17}$$

The computation of integrals such as 3.17 can be performed using the *Wick theorem*, which in this case assert simply that: $\Delta_{i,j;\alpha\beta} = \left(M^{-1}\right)_{i,j;\alpha\beta}$.

The inverse of the matrix M can be computed easily in momentum space, and passing to dimensional variables we can see that its limit is given by:

$$S_{\alpha,\beta}(x_i,\,x_j) = \sum_{c=1}^{16}\int_{-\infty}^{+\infty}\frac{d^4k\,e^{ik(x_i-x_j)}}{(2\pi)^4}\lim_{a\to 0}\frac{\left(m+\frac{r}{2a}\ell_c\right)\delta_{\alpha,\beta} - i\left(\not{k}\right)_{\alpha,\beta}}{\left(m+\frac{r}{2a}\ell_c\right)^2+k^2}\,, \tag{3.18}$$

where $\ell_c = \{0,1,1,1,1,2,2,2,2,2,2,3,3,3,3,4\}$.

This means that at finite lattice spacing the propagator contains 16 poles, and so describe 16 particles. One of them has the pole at m and so describe the correct particle, while the others get an additional mass contribution $\frac{r}{2a}\ell_c$. For any finite value of r the mass of these 15 additional particles, known as *doublers*, gets larger and larger with the decreasing of the lattice spacing, and eventually decouples from the system in the continuum. In particular setting $r=1$, in a typical lattice simulation with an inverse lattice spacing of $\sim$ 2GeV the 15 doublers have a mass of at least 4GeV, so their presence can be ignored in any computation.

If r had been put to zero (that is, if had removed the Wilson term), the additional particles would have been degenerate in mass with the physical one and so the continuum limit of the theory would have been wrong: the Wilson term is needed to get the correct continuum limit.

The presence of this term in an interacting theory such as QCD has a bad side effects: the chiral symmetry is broken at finite lattice spacing. This comes from a more general property of QCD, expressed by the No-Go Nielsen and Ninomiya, which states that it is impossible to define a discretization of QCD simultaneously free from the fermion doubling problem which reproduce the correct chiral limit when the mass parameter m is set to zero.

Without chiral symmetry,mass term is not protected from additive renormalization. This means that the renormalized quark mass is different from zero when the bare quark mass is set to zero. The true chiral limit will instead be obtained at a particular value of the hopping parameter κ_{crit} whose value depends on the particular details of the regularization (gauge action, number of quarks, lattice spacings, etc), corresponding to a particular value m_{crit} of the bare quark bass. In can be shown that the renormalized quark mass m_R is given by:

$$m_R = Z_m\left(m - m_{crit}\right)\,, \tag{3.19}$$

with Z_m is the multiplicative renormalization constant and the value of m_{cr} has to be determined non-perturbatively. The additive renormalization can be solved working with *twisted mass* Wilson fermions, which will be discussed in section 3.3.4 and have been used through all our work.

3.3.1.3 Regularization of Yang-Mills theory

In order to regularize the QCD we have to make gauge invariant the lattice Lagrangian for fermionic field described in the previous chapter.

Let us define a lattice $SU(3)$ gauge transformation $\{\Omega_n\}$, being n a generic lattice site.

Fermionic fields must transform according to the fundamental representation of the transformation:

$$\hat{\psi}_n \to \Omega_n \hat{\psi}_n, \qquad \hat{\bar{\psi}}_n \to \hat{\bar{\psi}}_n \Omega_n^\dagger \,, \tag{3.20}$$

where we have omitted the color indices for simplicity.

Mass lagrangian term is automatically invariant under the gauge transformation:

$$\hat{m}\hat{\bar{\psi}}_n \hat{\psi}_n \to \hat{m}\hat{\bar{\psi}}_n \Omega_n^\dagger \Omega \hat{\psi}_n = \hat{m}\hat{\bar{\psi}}_n \hat{\psi}_n \,, \tag{3.21}$$

as $g_n g_n^\dagger = 1$. For the discretized derivative this is not true, for example:

$$\hat{\bar{\psi}}_n \hat{\psi}_{n+\hat{\mu}} \to \hat{\bar{\psi}}_n \Omega_n^\dagger \Omega_{n+\hat{\mu}} \hat{\psi}_{n+\hat{\mu}}. \tag{3.22}$$

As in the continuum, in order to make the whole lagrangian gauge invariant we have to introduce some kind of covariant derivative. This can be achieved by defining for each link connecting two nearest neighbor lattice site $n, n+\hat{\mu}$ a *link variable* $U_{n;\mu}$, an element of $SU(3)$ transforming under the gauge transformation Ω as:

$$U_{n;\mu} \to \Omega_n U_{n;\mu} \Omega_{n+\hat{\mu}}^\dagger \,, \tag{3.23}$$

playing the role of parallel transport between n and $n+\hat{\mu}$, and by making the substitution:

$$\delta_{i+\hat{\mu},j} \to \delta_{i+\hat{\mu},j} U_{i;\mu} \,, \qquad \delta_{i-\hat{\mu},j} \to \delta_{i-\hat{\mu},j} U_{i-\hat{\mu};\mu}^\dagger \,. \tag{3.24}$$

in the fermionic matrix (3.11):

$$M_{i,j;\alpha,\beta} = \frac{1}{2}\left\{ \kappa^{-1}\delta_{i,j}\delta_{\alpha\beta} - \sum_\mu \left[\left(1 + (\gamma_\mu)_{\alpha,\beta}\right) U_{i;\mu}\delta_{i+\hat{\mu},j} + \left(1 - (\gamma_\mu)_{\alpha,\beta}\right) U_{i-\hat{\mu};\mu}^\dagger \delta_{i-\hat{\mu},j} \right] \right\}. \tag{3.25}$$

In this way the lagrangian is gauge invariant under the defined Ω transformation, because the links U transform exactly in the way needed to cancel the spurious term in equation 3.22:

$$\hat{\bar{\psi}}_n U_{n+\hat{\mu}} \hat{\psi}_{n+\hat{\mu}} \to \hat{\bar{\psi}}_n \Omega_n^\dagger \Omega_n U_{n;\mu} \Omega_{n+\hat{\mu}}^\dagger \Omega_{n+\hat{\mu}} \hat{\psi}_{n+\hat{\mu}} = \hat{\bar{\psi}}_n U_{n+\hat{\mu}} \hat{\psi}_{n+\hat{\mu}} \,. \tag{3.26}$$

Link variable $U_{n;\mu}$ elements of $SU(3)$ and so can be wrote in terms of a generating element $A_\mu = A_\mu^a T^a$ of the algebra SU (3):

$$U_{n;\mu} = \exp\left(iagA_\mu\right) \,, \tag{3.27}$$

where we have introduced the coupling g, so that in the continuum the Lagrangian density defined by fermion matrix (Eq. 3.25) reduces correctly to the fermionic part of the QCD Lagrangian for a single flavor (3.1 rotated to the Euclidean):

$$\mathcal{L} = \bar{\psi}\left\{ m + \not{\partial} + ig\not{A} \right\} \psi \,. \tag{3.28}$$

3.3.1.4 Gauge dynamic term

The gauge fields so introduced do not still have a proper dynamic, so we have to introduce a kinetic term S_G for them in the action. In the continuum this is given by the space-time integral of the lagrangian density:

$$\mathcal{L}_G = \frac{1}{4}\mathrm{Tr}F_{\mu\nu}F_{\mu\nu}\,, \tag{3.29}$$

being $F_{\mu\nu} \equiv [D_\mu, D_\nu]$ the field strength tensor:

$$F_{\mu\nu} = \partial_\mu A_\nu - \partial_\nu A_\mu + ig\,[A_\mu, A_\nu]\ . \tag{3.30}$$

The simplest expression which in the continuum limit reduces to S_G has been found by Wilson and is expressed in terms of the *plaquettes* $U_{n;\mu\nu}$, defined as the ordered product of the four links variables lying over the border of the square defined by the points n and $n + \hat{\mu} + \hat{\nu}$:

$$U_{n;\mu,\nu} \equiv U_{n;\mu}U_{n+\hat{\mu};\nu}U^\dagger_{n+\hat{\nu};\mu}U^\dagger_{n;\nu}\,. \tag{3.31}$$

In particular the Wilson expression for the gauge action is given by:

$$S_{G,W} \equiv \frac{2}{g^2}\sum_n\sum_{\mu<\nu}\left(3 - \Re\mathrm{Tr}\,U_{n;\mu\nu}\right)\,, \tag{3.32}$$

It is easy to show that this quantity is gauge invariant, and that near the continuum limit by making use of the Baker-Hausdorff formula the plaquette can be wrote as:

$$U_{n;\mu,\nu} = \exp\left[iga^2\left(\partial_\mu A_{n;\nu} - \partial_\nu A_{n;\mu} + ig\,[A_{n;\mu}, A_{n;\nu}]\right) + O\left(a^3\right)\right]U_{n;\mu,\nu} = \exp\left[iga^2F_{n;\mu\nu} + O\left(a^3\right)\right]\,, \tag{3.33}$$

so that expanding at second order in a, 3.32 reduces to the correct continuum expression.

Reassuming, the expression for the Wilson discretized action of QCD is given by

$$S_{LQCD} \equiv \sum_f S^f_Q + S_{G,W}\,, \tag{3.34}$$

where for each quark flavor we have defined:

$$S^f_Q \equiv \hat{\bar{\psi}}^f M^f \hat{\psi}^f\,, \tag{3.35}$$

being M^f the fermionic matrix 3.25 wrote in terms of the mass m_f of the quark f.

The partition function for this theory reads:

$$\mathcal{Z} \equiv \int\prod_p\left(\prod_f d\hat{\bar{\psi}}^f_p d\hat{\psi}^f_p\prod_\mu dU_{p;\mu}\right)e^{-\sum_f\hat{\bar{\psi}}^f M^f\hat{\psi}^f + S_{G,W}}\,. \tag{3.36}$$

3.3.2 Continuum limit

We have shown that Wilson regularization of both fermionic and gauge action reduces to the correct expressions in the continuum limit $a \to 0$. This feature is needed but is not sufficient to ensure that the fully quantized theory reproduces QCD in the continuum.

The calculation of any observable requires to evaluate functional integral, whose behavior as function of a is highly nontrivial, as we have already discovered in Sec. 3.3.1.2, where we have shown that an apparently correct regularization do not have the correct propagator. We need therefore a more convincing argument than the simple observation that the goodness of the $a \to 0$ limit of the action.

When taking the continuum limit the cut-off is removed, so the action must be renormalized, by tuning appropriately parameters such as g and the quark masses $\{m\}$ in order to leave finite the computed quantities. In general at a given lattice spacing a, we have to fix all the N parameters $\{\lambda\}$ of the theory, by imposing to the theory to reproduce the physical value of N observables $\{G\}$, by solving the set of equations:

$$\begin{cases} G_1\left(\lambda_1 \dots \lambda_n, a\right) = G_1^{phys} \\ \dots \\ G_n\left(\lambda_1 \dots \lambda_n, a\right) = G_n^{phys}. \end{cases} \tag{3.37}$$

The value of parameters λ depends on the lattice spacing in a nontrivial way, particular to the precise detail of the regularization took into account. Let us assume that all the quarks in the theory are massless, so that the theory depends only from the parameter g. In this case we must impose:

$$\lim_{a \to 0} G\left(g\left(a\right), a\right) = G^{phys}. \tag{3.38}$$

The relation between g and a can then be obtained by requiring the observable not to depend from a when it is sufficiently small, that is imposing:

$$\frac{dG\left(g\left(a\right), a\right)}{d \ln a} = 0 \to \left(\frac{\partial}{\partial \ln a} + \beta \frac{\partial}{\partial g}\right) G\left(g\left(a\right), a\right) = 0\,. \tag{3.39}$$

This reveals us that the relation between g and a is given by the β-function of QCD $\beta \equiv \frac{\partial}{\partial \ln a}$. It can be shown perturbatively that in any regularization of QCD we have:

$$a\left(g\right) = \frac{1}{\Lambda_L} \left(b_0 g^2\right)^{-\frac{b_1}{2b_0^2}} \exp\left[-1/\left(2b_0 g^2\right)\right] \left(1 + O\left(g^2\right)\right)\,, \tag{3.40}$$

with:

$$b_0 = \frac{1}{16\pi^2} \frac{\left(11 n_c - 2 n_f\right)}{3}, \qquad b_1 = \frac{1}{\left(16\pi^2\right)^2} \frac{34 n_c^3 - 10 n_c^2 n_f - 3 n_f \left(n_c^2 - 1\right)}{3 n_c}\,, \tag{3.41}$$

being n_c the number of colors of the theory ($n_c = 3$ for QCD) and n_f the number of flavor of the quarks (assumed to be massless), and Λ_L is a parameter depending from the details of the regularizations. The functional relation between a and g depends from the regularization details only from order g^2.

The crucial point of this discussion is that for $n_f < 11 n_c/2$ the lattice spacing a is a monotonically increasing function of g, and that:

$$\lim_{g \to 0} a\left(g\right) = 0\,. \tag{3.42}$$

We have therefore proved that the continuum limit is realized sending the coupling g to zero: this is well known *asymptotic freedom* of QCD. In presence of quarks of finite mass the β-function cannot be computed in a closed form, and the continuum limit must be checked numerically. However one still expects the relation (3.42) to hold also for the massive case, and the large consensus on this is supported by strong numerical evidence.

3.3.3 Symanzik improvement of lattice regularizations

Being not possible to choose arbitrary small lattice spacing, it is advisable to use any possible strategy which can minimize discretization effects and make the extrapolation simpler.

We have already shown that Wilson gauge action (Eq. 3.32) reproduces the continuum limit up to terms $O\left(a^2\right)$. Wilson regularized fermionic action defined by the matrix (Eq. 3.25) instead reproduces the continuum limit up to terms of order $O\left(a\right)$.

One possibility to improve the approaching to the continuum of the discretized action is to add operators of dimension greater than 4, which vanish in the continuum limit. These operators must not modify the symmetries of the regularized action in order not to spoil the continuum limit, but can suppress lattice artifacts and remove a part of the discretization effects. The idea is that when the regularized action is expanded in powers of a, all possible operator compatible with the regularization symmetries:

$$S^{latt} = S^{cont} + ac_1 S_1 + a^2 c_2 S_2 + \mathcal{O}\left(a^3\right). \tag{3.43}$$

The terms S_i are irrelevant operators, suppressed by increasing powers of the cut-off a. It should be possible to add these operators explicitly to the action with appropriate coefficients such to cancel their effect:

$$S^{latt} \to S^{latt} - ac_1 S_1 - a^2 c_2 S_2 + \mathcal{O}\left(a^3\right) = S_{cont} + \mathcal{O}\left(a^3\right). \tag{3.44}$$

The value of the parameters $c_1, c_2 \ldots$ in the renormalized action are unknown a-priori, so they must be found non-perturbatively or computed in lattice perturbation theory.

The addition of these operators is known as *Symanzik improvement program* [7].

At order a the only operator needed to improve Wilson action is given by the Pauli term:

$$O^{Pauli}_{n;\mu\nu} = \hat{\psi}^{\dagger}_n \sigma_{\mu\nu} \hat{\psi}_n \hat{F}_{n;\mu\nu}\,, \tag{3.45}$$

where $\hat{F}_{\mu\nu}$ is the discretized version of the field strength tensor, which can be for example expressed as:

$$\hat{F}_{n;\mu\nu} = \frac{-i}{8}\left(Q_{n;\mu\nu} - Q_{n;\nu\mu}\right), \tag{3.46}$$

being $Q_{n;\mu\nu}$ the sum of the plaquettes in the μ,ν plane containing the site n:

$$Q_{\mu\nu} \equiv U_{n;\mu\nu} + U_{n;-\mu,\nu} + U_{n;-\mu,-\nu} + U_{n;-\nu,\mu}\,, \tag{3.47}$$

The term in the continuum scales as a^5 and so do not contribute to the continuum limit. It can be added to the regularized action as:

$$S_{\rm sw} \equiv \frac{c_{\rm sw}}{2} \sum_{n;\mu<\nu} O^{Pauli}_{n;\mu\nu}. \tag{3.48}$$

The coefficient $c_{\rm sw}$ is known as *Sheikholeslami–Wohlert coefficient* from the name of the authors which firstly proposed it [8]. Its value must be tuned appropriately in order to remove order a effects from the action.

A complete application of the Symanzik program requires also to improve interpolating operators used to compute correlation functions (which as the action, differs from their continuum

counterpart for terms of order a), adding appropriate counter-terms with coefficient to be tuned separately for each correlation function.

As all the improvement coefficient must be determined non perturbatively, this strategy of improvement is quite tedious and expensive. In our works we have chosen a different strategy of improvement for the fermionic action, which we will illustrate in section 3.3.4.

It has been shown that the problem of exceptional configuration occurring with Wilson fermions when working at small quark masses is ameliorated when the Symanzik improvement program is applied to the gauge action. At first order this requires to write the gauge action in terms of all possible length 6 and 4 paths (which means to add rectangle and chair-shaped paths to the simple plaquette). These can be heuristically understood as being an effect of the more non-locality of the action: an action wrote in terms of longer paths enhances in functional integrals the relevance of smoother configurations, associated to larger eigenvalues of the fermionic matrix, and so suppresses exceptional configurations.

For this reason, although not necessary in order to achieve $\mathcal{O}(a)$ improvement, we have used improved gauge actions in our computations, namely the *tree-level Symanzik improved action* for the $N_f = 2$ simulations and the *Iwasaki improved action* for the $N_f = 2 + 1 + 1$ simulations, in which all the $\mathcal{O}\left(a^4\right)$ discretizations effects are removed from the continuum limit. In the first case one includes only rectangles so that the gauge action reads:

$$S_{sym} = S_{G,W} \equiv \frac{2}{g^2} \sum_n \left[c_0 \sum_{\mu<\nu} \left(3 - \Re\mathrm{Tr}\, U^{1x1}_{n;\mu\nu}\right) + c_1 \sum_{\mu<\nu} \left(3 - \Re\mathrm{Tr}\, U^{1x2}_{n;\mu\nu}\right) \right], \tag{3.49}$$

where $U^{1x1}_{n;\mu,\nu}$ is the plaquette defined in eq. 3.31 while

$$U^{1x2}_{n;\mu,\nu} = U_{n;\mu} U_{n+\hat{\mu};\nu} U_{n+2\hat{\mu};\nu} U^\dagger_{n+\hat{\mu}+\hat{\nu};\mu} U^\dagger_{n+\hat{\nu};\mu} U^\dagger_{n;\nu}\,, \tag{3.50}$$

is the rectangle originating on site n lying on plane μ, ν, and coefficients c_0 and c_1 are fixed perturbatively to $c_1 = -1/12$, $c_0 = 1 - 8c_1$.

In the Iwasaki action also chair-shaped paths are included, and coefficients are fixed non-perturbatively and thus allow to achieve a better suppression of exceptional configurations.

3.3.4 Twisted mass regularization

We have shown in details how to regularize QCD in the scheme proposed by Wilson. All our computations have been performed with a modified version of Wilson regularization, called *Twisted Mass QCD*.

In its simplest form, Twisted Mass lattice QCD describes two degenerate quark flavors:

$$\chi \equiv \begin{pmatrix} \chi_1 \\ \chi_2 \end{pmatrix}. \tag{3.51}$$

whose action:

$$S = \bar{\chi} D_{twist} \chi \equiv \bar{\chi} D_{Wilson} \mathbf{1}^{flav} \chi + S_{twist}\,, \tag{3.52}$$

contains an additional term:

$$S_{twist} \equiv \bar{\chi} i\mu\gamma_5 \tau_3^{flav} \chi\,, \tag{3.53}$$

where $\tau_3 = \mathrm{diag}\,\{1, -1\}$.

This lattice regularization has many advantages with respect to the simple Wilson lattice QCD which we will discuss in the following sections.

3.3.4.1 Physical basis and continuum limits

For future discussions it is useful to define the *polar mass* M and the *twist angle* α*:*

$$M = \sqrt{m^2 + \mu^2}, \quad \alpha = \arctan(\mu/m) \,, \tag{3.54}$$

and rewrite the action (3.52) in terms of the more convenient variables:

$$\psi \equiv R(\alpha)\,\chi, \quad R(\alpha) \equiv \exp(i\alpha\gamma_5\tau_3/2) \,. \tag{3.55}$$

This is the so-called *physical base* (in opposition to the χ called *twisted basis*). In this basis the non trivial flavor term is just associated to the value of the parameter r contained in the fermionic matrix, which (omitting Dirac index) reads:

$$D_{i,j} = 4f(\alpha)\,\delta_{i,j} - \frac{1}{2}\sum_{\mu}\left[(f(\alpha)+\gamma_\mu)\,U_{i;\mu}\delta_{i+\hat{\mu},j} + (f(\alpha)-\gamma_\mu)\,U^{\dagger}_{i-\hat{\mu};\mu}\delta_{i-\hat{\mu},j}\right] , \tag{3.56}$$

where $f(\alpha) \equiv re^{-i\alpha\gamma_5\tau_3}$, and the full action is:

$$S = \bar{\psi}_i\left[D_{i,j} + M\delta_{i,j}\mathbf{1}^{flav}\right]\psi_j \,. \tag{3.57}$$

After taking the continuum limit the action simply reads:

$$S = \int d^4x\bar{\psi}\left(\not{D} + M\right)\mathbf{1}^{flav}\psi \,. \tag{3.58}$$

Therefore in the continuum the twisted mass QCD describes two usual degenerate flavors of quarks, while at finite lattice spacing the two quarks differ for discretization effects.

The relation between usual and twisted mass QCD (in the following often abbreviated as tmQCD) is dictated by equation (3.55). Appropriate relation between tmQCD and QCD correlation functions must be considered when performing computations in the twisted basis.

3.3.4.2 Historical motivation

Twisted term was originally introduced in [9] to add an infrared regulator to the Dirac matrix (3.11). The eigenvalues of the Dirac matrix fluctuate configuration per configuration, and at small quark mass *exceptional configurations* with anomalously low eigenvalues may appear, whose presence put strong problems in the numerical analysis, and in particular limits the smallness of the quark masses which can be analyzed at a fixed lattice spacing. By making use of the γ_5-hermiticity of the Wilson operator:

$$(\gamma_5 D_{Wilson})^{\dagger} = \gamma_5 D_{Wilson} \,, \tag{3.59}$$

it can be shown that:

$$\det D_{twist} = \det\left[(D+m)(D+m)^{\dagger} + \mu^2\right] , \tag{3.60}$$

with D being the massless Wilson fermionic matrix.

Eigenvalues of the quadratic form $(D+m)(D+m)^{\dagger}$ are real and non-negative, and twisted term expels all the eigenvalues of the Dirac matrix from a strip of size 2μ from the real axis, thus allowing to analyze lower quark masses.

3.3.4.3 Automatic order a improvement at maximal twist

In the case in which $\alpha = \frac{\pi}{2}$ all the quark mass comes from the twisted term, and $f(\alpha)$ reduce to $\gamma_5 \tau_3 r$. In this situation called *maximal twist* the theory at finite lattice spacing describes two flavor of Wilson fermions regularized with two opposite value of r, each carrying a nontrivial Dirac structure γ_5 [9].

This situation has a very nice property: parity even correlation function (which include all the physical correlation functions) are automatically $\mathcal{O}(a)$ improved, and $\mathcal{O}(a)$ discretization effects will affect only parity odd (unphysical) correlation functions. Let us sketch a proof of this remarkable features of tmQCD.

Through Symanzik expansion (section 3.3.3) it can be shown that $\mathcal{O}(a)$ discretization effects in parity even correlation functions computed in Wilson regularized QCD are odd with respect to the sign of r. Therefore it could be possible to get rid of all the $\mathcal{O}(a)$ discretization effects by averaging correlation functions computed with $r = +1$ with the same functions computed with $r = -1$: but this is exactly what happens in tmQCD at maximal twist, where the average is automatically performed between the two quarks of the doublet.

3.3.4.4 Tuning to maximal twist

We have already stressed that the interaction renormalizes additively the quark mass, and in particular the untwisted term m. This means that in the full renormalized theory the maximal twist condition cannot be realized by just setting $m = 0$ (that is, $\kappa = 1/8$). On the contrary, one has to tune m (and thus κ) to a particular value in such a way that the *renormalized* Wilson mass m_R defined by equation (3.19) is 0.

This can be achieved by making use of the *Partially Conserved Axial Current* relation:

$$m_R = \frac{Z_A \left\langle \left(\partial_\mu A^a_\mu(x)\right) P^a(0) \right\rangle}{2 Z_P \left\langle P^a(x) P^a(0) \right\rangle}, \tag{3.61}$$

descending from the axial untwisted Ward identity [10], through which the renormalized Wilson mass can be determined. Being interested in getting a null m_R, it is sufficient to tune k to get a null value of the correlation function $\left\langle \left(\partial_\mu A^a_\mu(x)\right) P^a(0) \right\rangle$. It is worth mentioning that this is not the only possible way to tune the theory to the maximal twist. Different choice are possible and in principle they might provide slightly different critical value for κ. These difference are however higher order discretization effects.

3.3.4.5 Simplifications in renormalization and main drawbacks

The usage of Twisted Mass regularization at maximal twist is fruitful also for simplifying the renormalization of some hadronic matrix element, and make easier to perform some computations. For example the decay constant f_{PS} of a pseudo-scalar meson PS composed of two quarks of mass μ_1, μ_2 discussed in chapter 2 in Wilson regularization is computed as:

$$f_{PS} P_\mu = \left\langle 0 \left| A^R_\mu \right| PS(P) \right\rangle, \tag{3.62}$$

with A^R_μ being the renormalized axial current, which can be computed on lattice only through an appropriate renormalization procedure.

In Twisted mass in particular it requires to compute the renormalization constant Z_V, but making use of the already cited PCVC relation holding at maximal twist, it can be also computed as:

$$f_{PS} = (\mu_1 + \mu_2) \frac{\langle 0 | P | PS \rangle}{M_{PS}^2} . \tag{3.63}$$

Being these all bare quantities, they do not require any renormalization procedure, and are therefore simpler. Also other more complicated hadronic matrix elements, such as the B_K parameter involved in the neutral K mixing, can be renormalized more easily than in plain Wilson regularization, by carefully choosing the sign of the r parameter regularizing the quark composing the K meson [11].

From the other side, the Twisted terms break parity and isospin at finite lattice spacing.

The breaking of the parity induces mixing between pseudo-scalar and scalar particles, for example mesons. Being scalar heavier than pseudo-scalar mesons, this is not a problem when one is interested in looking at the lighter ones, because scalar mesons appear as excited states whose presence goes away in the continuum, but can be more troublesome if one is interested in looking at the scalar mesons.

Isospin breaking instead leads to a breaking of the SU (2) vectorial symmetry of QCD with two degenerate flavor, which induces a non-cancellation of disconnected contribution to neutral hadron correlation functions. The lack of this symmetry at finite lattice spacing means for example that $M_\pi^+ = M_\pi^- \neq M_\pi^0$ for discretization effects, and that the neutral pion contains contribution coming from disconnected terms. This can also lead to a greater number of mixing between hadronic operator and make renormalization more difficult.

3.4 Numerical analysis

Apart from the free theory case already considered, the integrals of the kind (3.36) cannot be solved in a closed analytical form, so they have to be computed numerically. This means that one has to perform computations at fixed lattice spacing a and volume V, by making use of a numerical integration scheme, and to extrapolate to the continuum and infinite volume the observables of interest. We will review carefully all the steps involved in the procedure.

3.4.1 Integration over fermionic degrees of freedom

Let us consider the partition function (3.36). Fermionic fields are anti-commutating variables, which in order to be treated numerically should be represented in terms of matrices of rank equal to the lattice volume. This would make the computations unfeasible already at very small volumes. One can avoid dealing with such representation by making use of the relation:

$$\int D[\psi, \psi^*] \exp[-\psi^* M \psi] = \det M , \tag{3.64}$$

coming from a particular case of the Wick theorem. In this way one get rids of the integrals over the quark fields at the cost of having to deal with a much non local integrand. The partition function can be expressed as the integral over all the configurations of fields $U_{i;\mu}$:

$$\mathcal{Z} = \int \prod_{i;\mu} dU_{i;\mu} \prod_f \det M^f \, \exp(-S_{G,W}) . \tag{3.65}$$

The value of a quantity O will be computed as:

$$\langle O \rangle = \int \prod_{i;\mu} dU_{i;\mu} O(U) \rho[U] , \tag{3.66}$$

where we have defined:

$$\rho[U] \equiv \prod_f \det M^f \exp(-S_{G,W}) / \mathcal{Z} , \tag{3.67}$$

and with $O(U)$ being expressed in terms of the field $U_{i;\mu}$, according to the Wick theorem.

3.4.2 Monte Carlo methods for the gauge degrees of freedom

Having get rid of the fermionic degrees of freedom we are left with the integral over the gauge fields, for which no relation such as 3.66 exists and so have to be computed in a numerical form.

It is clear that already with lattice grids of few points per size, the number of degrees of freedom is too large to allow for a direct evaluation of integrals with technique such as Simpson integration, so one need to relies on Monte Carlo techniques. These class of numerical integration methods can be applied whenever the integral assumes the form of a weighted average over the integrand space, and is very suitable when the weight is highly peaked over a limited region of the integrand space.

In Wilson discretization it can be shown that $\det M$ is real (and positive on non-exceptional configurations) so that Eq.3.66 can be regarded as the average value of O over the space U weighted with the probability distribution ρ.

Let us indicate with U^a a certain realization of the gauge fields $U_{i;\mu}$. The first part of the evaluation of O consists in generating a set S_N of N configurations U^a, $a \in [1 \dots N]$ according to the distribution function $\rho[U^a]$. This is performed by making use of hybrid techniques which mix normal Monte Carlo methods with molecular dynamics in order to avoid the explicit evaluation of the fermionic matrix determinant. Being this a very technical point which has not been subject of the thesis work, we will not review it and we will assume to be able to generate such set S_N.

For each gauge configuration U^a one measures the value of the observable O^a on such configuration, and then an approximate estimate $\bar{O}_N$ of the observable is given by simple average of the N determinations O^a:

$$\bar{O}_N \equiv \frac{1}{N} \sum_{a=1}^{N} O^a . \tag{3.68}$$

Under the assumptions of the central limit theorem, for a sufficiently large N the estimator $\bar{O}_N$ will be distributed as a Gaussian with mean O and variance given by

$$\mathrm{Var}_\rho \bar{O}_N \equiv \frac{C}{N} \mathrm{Var}_\rho \mathrm{O} , \tag{3.69}$$

where C is a constant depending by the correlation between gauge configuration contained in the ensemble. If all the configurations in the ensemble were independent each other, then $C = 1$. Algorithms used to produce the gauge configurations instead make the configuration contained in the ensemble S_N correlated each other, so that we will always have $C > 1$ and unknown a priori. In order to make an accurate estimate of the error $\epsilon_{\bar{O}_N} \equiv \sqrt{\mathrm{Var}_\rho \bar{O}_N}$ jackknives and bootstrap techniques have been used through all this work.

After generating the gauge configurations, these can be used many times in order to determine different quantities of interest. Let us come back to our original problem of computing correlation functions and let us see in concrete how they can be obtained from gauge configurations.

3.4.3 Hadronic correlation functions

The discretized expression of the pion correlation function 3.9 reads:

$$C^{u,\bar{d}}_{x,t} = \frac{1}{\mathcal{Z}} \int \left(\prod_f d\bar{q}^f_i \, dq^f \prod_\mu dU_{i;\mu} \right) \left\{ \left(\bar{d}_{x,t} \gamma_5 u_{x,t} \right) \left(\bar{u}_0 \gamma_5 d_0 \right) \, e^{-\sum_f \bar{\psi}^f M^f \psi^f - S_{G,W}} \right\} , \tag{3.70}$$

where for simplicity we have omitted the $\hat{}$. By making use of the Wick theorem one can again get rid of the fermionic integrals and write the correlation function in term of the *contraction*:

$$C_{\vec{x},t} = - \left\langle \mathrm{Tr} \left[\gamma_5 S^u_{(\vec{x},t);0} \gamma_5 S^d_{0;(\vec{x},t)} \right] \right\rangle , \tag{3.71}$$

where $S^q_{a;b}$ is the propagator from a to b for quark q:

$$S^q_{a;b} \equiv (M^q)^{-1}_{a;b} , \tag{3.72}$$

and for simplicity we have defined:

$$\langle f \rangle \equiv \frac{1}{\mathcal{Z}} \int f \prod_{i;\mu} dU_{i;\mu} e^{-S_{G,W}} \prod_f \det M^f . \tag{3.73}$$

This expression has a simple physical interpretation: $(M^u)^{-1}_{(\vec{x},t);0}$ propagates an up quark from the origin to the point $(\vec{x},t)$ while $\left(M^d\right)^{-1}_{0;(\vec{x},t)}$ propagates a down quark in the opposite direction, as depicted with diagrams in fig. 3.1.

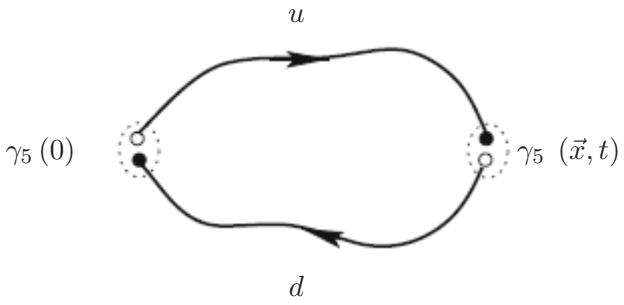

Figure 3.1: Pictorial depiction of correlation function.

In this way the pion correlation function can be computed as a product of inverse matrix. In particular one need actually only one row of each matrices, which can be obtained by solving an appropriate linear system. The hadronic correlation function can then be obtained by contracting the Dirac indices according to the present gamma structure, and taking the trace over the color indices.

We are left with a free space index $\vec{x}$. As already stated, the correlation function $C_{\vec{x},t}$ represent the propagation of meson between the origin and the point $\vec{x}, t$, so that the quark do has a

completely undefined momentum. In order to have mesons with definite spatial momentum $\vec{p}$ (in lattice units) one should have used the appropriate convolution of the interpolating operators, which is the Fourier transformed of the creation operators at a fixed point:

$$\tilde{O}_{\vec{p},t} \equiv \frac{1}{\sqrt{N}} \sum_{\vec{x}} e^{-i\vec{p}\vec{x}} O_{\vec{x},t}, \quad N \equiv \sum_{\vec{x}} . \tag{3.74}$$

By making use of the space translation invariance of the theory one can avoid using such operator on the source, and factorize the Fourier transform out from the trace:

$$C_{\vec{p},t} = \sum_{\vec{x}} e^{-i\vec{p}\vec{x}} C_{\vec{x},t} . \tag{3.75}$$

In the case we want the meson to be at rest one simply has to sum the correlation function $C_{\vec{x},t}$ over the space index $\vec{x}$.

After projecting to zero momentum the correlation function, by inserting the sum over all intermediate state we get:

$$C_t^{A,B} = \left\langle \tilde{O}^A_{\vec{0},t} \bar{O}^B_0 \right\rangle = \sum_k \frac{e^{-tE_k}}{2E_k} \langle 0| O^A |k\rangle \langle k| O^{B\dagger} |0\rangle = \sum_k \frac{e^{-tE_k}}{2E_k} Z^A_k Z^{B*}_k , \tag{3.76}$$

having defined the matrix elements:

$$Z^{A,B}_k \equiv \langle 0| O^{A,B} |k\rangle . \tag{3.77}$$

3.4.4 Ground state mass measurement

The summation gets contributions from the states $|k\rangle$ with definite momentum coupling to the operator O^A and O^B. At finite time this in general is a sum of infinite exponentials:

$$C_t = c_0 e^{-E_0 t} + c_1 e^{-E_1 t} + \dots . \tag{3.78}$$

Let us call E_1 the state with the lowest energy after the fundamental. If we collect the term relative to the lowest state, and indicating with $\Delta E_i \equiv E_i - E_0$ the summation reads:

$$C_t = c_0 e^{-E_0 t} \left(1 + \frac{c_1}{c_0} e^{-\Delta E_1 t} + \dots \right) . \tag{3.79}$$

At short times all the terms contribute in the sum, but at times t larger than the reciprocal of the first energy gap all the terms inside the bracket are suppressed, so that only the ground states survive. The energy E_0 can then be determined by looking at the slope of the logarithm of the correlation function at times larger than $1/\Delta E_1$:

$$\log C_t \overset{t \gg \frac{1}{\Delta E_1}}{\longrightarrow} q - E_0 t . \tag{3.80}$$

Actually the energy gap is not known a priori, as well as E_0. It is therefore necessary to determine it by looking at the correlation function itself, by searching for the time interval where the logarithm of the correlation function shows a linear behavior.

3.4.4.1 Effective mass

In order to better quantify the contamination from excited states in the correlation function, it is very useful to define for each time point the *effective mass:*

$$m_t^{eff} \equiv \log \frac{C_t}{C_{t+1}} \,. \tag{3.81}$$

At times large enough where only the lowest states dominate the correlation function $C_t = ce_0^{-E_0 t}$ and the effective mass is constant in time: $m_t^{eff} = E_0$. Where more than one state contributes to the correlation function, the effective mass deviate from the constant behavior.

In general the simple exponential behavior is modified by periodic boundary conditions: operator $\bar{O}_0^B$ creates states propagating from $t = 0$ both in the positive and in the negative direction.

Meson correlators are symmetric with respect to the exchange $t \to T - t$ up to a possible minus sign:

$$C_t^{mes} = \pm C_{T-t}^{mes} \,, \tag{3.82}$$

so that where the lower lying state dominates the correlation function shows in the symmetric case the behavior:

$$C_t^{A,B} = \frac{Z_0^A Z_0^{B*}}{E_0} e^{-TE_0/2} \cosh\left[E_0 \left(T/2 - t\right)\right] \,, \tag{3.83}$$

and in the anti-symmetric case:

$$C_t^{A,B} = \frac{Z_0^A Z_0^{B*}}{E_0} e^{-TE_0/2} \sinh\left[E_0 \left(T/2 - t\right)\right] \,. \tag{3.84}$$

This is not the case for baryons, where after projecting to definite parity states, particles with opposite parity having different masses propagate in the two halves of the lattice, so that the correlation function takes a more general form of the kind:

$$C_t^{A,B;\,bar\,p} = c_0^{(p)} e^{-tE_0^{(p)}} + c_0^{(-p)} e^{-tE_0^{(-p)}} \,. \tag{3.85}$$

If one wants to take into account properly the periodicity for mesons, the effective mass has to be computed by solving iteratively for m_t^{eff} the equation:

$$\frac{C_t}{C_{t+1}} = \frac{\cosh\left[m_t^{eff}\left(T/2 - t\right)\right]}{\cosh\left[m_t^{eff}\left(T/2 - t - 1\right)\right]} \,, \tag{3.86}$$

for the symmetric case, and similarly with sinh instead than cosh for the anti-symmetric.

The computation of the effective mass for a certain time t is done in terms of C_t and C_{t+1} so the effective mass is always defined up to $t = T/2 - 1$.

In Fig. 3.2 we illustrate an example of computation of the correlation function for Pions composed of quark of various masses on lattice of time extent $T = 48$, plotted in logarithmic scale. The correlation function is periodic around $t = 24$, and the linear behavior expected from equation 3.80 is apparently visible from $t \simeq 6$.

In Fig. 3.3 we show the effective mass computed according to equation 3.81 (dashed lines) and to equation 3.86 (continuous lines), computed after symmetrizing the correlation function. It

is clear that neglecting the periodicity of the correlation function leads to an error which becomes larger and larger as t gets nearer $T/2$. The error gets instead smaller as the meson gets heavier: light hadrons propagate for longer distance and feel boundaries more than heavy particles.

It is also clear that the contribution from excited states cannot be neglected before $t \simeq 10-12$, revealing the great importance of the effective mass analysis in the determination of the region of domination of ground states.

3.4.4.2 Correlated vs uncorrelated fits

After having identified the region where the lowest state dominates we can proceed to determine the mass of the ground state. As the computation of correlators is done numerically, with finite statistics the value of the correlation is known only within an error. Therefore the hadron must be determined by fitting the correlation C_t with the function (3.83), (3.84) or (3.85) (according to the correlation periodicity) over an appropriate time range. In general there is no theoretical argument for omitting points far both from 0 and T, so that when one is sure that the error is properly computed the time range should be of the form $[t_{min}; T - t_{min}]$ for mesons and $[t_{min}; T/2]$ for baryons. In the following we will always assume to treat appropriately the possible symmetry of the correlation functions and quote time range as $[t_{min}; T/2]$.

Being typically computed over the same gauge ensemble, values of correlation function at different times are correlated each other, that is:

$$\langle C_t C_{t'} \rangle \neq \langle C_t \rangle \langle C_{t'} \rangle . \tag{3.87}$$

Therefore in theory one should perform a two-parameters fit of the correlation function by minimizing the correlated χ^2:

$$\chi^2_{corr} \equiv \delta_t \Sigma^{-1}_{t,t'} \delta_{t'} , \tag{3.88}$$

where we have defined the deviation between data and theoretic function:

$$\delta_t \equiv C_t - f(t) , \tag{3.89}$$

and Σ is the (exact) correlation matrix of C:

$$\Sigma_{t,t'} = \langle C_t C_{t'} \rangle - \langle C_t \rangle \langle C_{t'} \rangle . \tag{3.90}$$

The matrix Σ can be estimated only from the configuration per configuration fluctuations of the correlation function, so that with finite statistics the matrix is known only approximatively. The correlated fit should be advisable in all the cases in which the off diagonal elements of Σ are not negligible, that is when correlation between different elements of fitted data is sizable. Unfortunately in these cases the matrix Σ is very often badly conditioned (the ratio between the larger and smaller eigenvalues of the matrix is large), and then matrix Σ^{-1} is known with large errors. Using such kind of matrix can spoil the results of the fit, and lead to unphysical results, so in all fits of correlation functions we have used the diagonal approximation:

$$\Sigma_{t,t'} = \sigma_t \delta_{t,t'} . \tag{3.91}$$

3.4.4.3 Hadron mass determination

If one is interested both in the determination of the matrix elements and the hadron mass, a two-parameters fit is necessary. If instead one is interested only in the determination of the hadron mass, it is possible to perform a constant fit of the effective mass m^{eff}: being constructed (qualitatively) as a ratio between correlated quantity C_t and C_{t+1}, the error on m_t^{eff} this quantity is in general smaller than those of C_t, and m_{eff} at different times more uncorrelated than C_t.

In Fig. 3.4 we show the results of the 2 parameters fit of the correlation function C_t with the function 3.83 (with the constraint $Z_0^A = Z_0^B = Z_0$) together with the constant fit of the effective mass, plotted over the effective mass. It is clear that the fit of the effective mass provide a more precise estimate of E_0.

In all the situations in which we have been interested only in the energy determination of the hadrons, we have used the effective mass (or similar quantities built for more complicated correlators). In the cases in which instead both energy and matrix element were needed, we have used the direct fit of the correlation function in order to have a better control of the correlation between the errors of E and Z so obtained.

3.5 Systematics effects

Let us analyze the various problems affecting a typical lattice computation and the techniques used to treat them. We will put special care on the solution adopted in our work.

3.5.1 Finite size effects

When performing computations on lattice, the volume act as infrared cut-off on the obtained observable that has to be removed at the end of the computation. The effects of the finite volume is to modify the energy levels of the particle described by the theory. In a finite box the energy levels become discrete and are shifted. The shift of the energy levels can be shown to be related to the scattering length of particles in the box, and thus in general can be computed analytically and removed without performing explicitly the $V \to \infty$ limit.

The relevant scales for determining the finite size effects (FSE) are the side L of the box simulated and the mass of the lowest particle of the theory, therefore the pion mass M_π which having a greater propagation length is the most affected by the presence of borders.

It can be shown that when the final state contains not more than one particle, FSE are exponentially suppressed[1] functions of the quantity LM_π. It can be shown that when constraint: $L \gtrsim 2\,\mathrm{fm}$ and $M_\pi L \gg 1$ Chiral Perturbation Theory (ChPT) [12] can be used to compute the effects of finite borders [13].

In most of our computations the parameter $M_\pi L$ is larger than 4, so FSE are expected to be small and therefore their presence treatable in ChPT. We checked explicitly the amount of FSE by performing in one case two simulations, at the same parameters but the volume. By comparing the results obtained at different volumes it is possible to quantify these effects. The only case in which these effects have been found sizable and taken into account is the computation of the light quark average mass (see section 4.2), while for other quantities the effects are negligible compared to other errors.

[1] In presence of multiple particles in the final state, FSE are power functions of a.

3.5.2 Quenching effects

Up to the late nineties computational power available was not sufficient to allow to take into account the relevance of the fermionic determinant in lattice computations. For this reason all lattice calculations were performed neglecting the $\det M$ contribution in the action. This corresponds to perform the $m_{quark} \to \infty$ limit of the action, so that "sea" quark do not propagate. For these reason this approximation is known as *quenching* of the fermionic degrees of freedom.

3.5.2.1 Quenching and non-unitarity

The generation of the gauge configurations at that time was performed in the pure Yang-Mills theory, so that fermions appear as external "valence" classical fields only when computing fermionic correlation functions. It is easy to understand that perturbatively this corresponds to neglect diagrams containing fermionic loops in the computation of the correlation functions.

In general it is always possible to perform computation choosing different regularization for the sea and valence quarks (respectively the quarks associated to the generation of the gauge configurations and to the computation of correlation functions). These regularization scheme are called *non-unitary*. If the renormalized mass of the sea and valence quark[2] is chosen equal, the non-unitarity leads only to modified cut-off effects which do not affect the continuum physics, but in general this is not the case. In particular taking the chiral limit for non unitary valence quark can lead to divergences in correlation, so that special cares must be taken.

3.5.2.2 Light quark unquenching and chiral limit

The quenched theory in the continuum describes a theory quite different from QCD, so that one expect all the quenched computations to be affected by a non evaluable systematic error, and would like ultimately to remove the quenching effect and perform computation in full QCD.

In the last 10 years the development in algorithms and machines made it possible to start performing calculation taking into account the presence of the fermionic determinant. In all regularizations, lower value of the quark mass corresponds enhance the density of low eigenvalues of the fermionic matrix, and this makes computations more and more demanding and difficult as the value of m_{quark} is lowered. With Wilson family regularization the lowest value of quark masses considerable without exceptional configuration problem to occurs is an increasing function of the lattice spacing, so that in order to simulate lower quark masses one has to decrease the lattice spacing. From the other side, one is forced to increase simulated volume in order not to have large finite volume effects as explained in section 3.5.1. Therefore in general the number of lattice point has to be increased in order to simulate lower quark masses. Given the present amount of available computational power it is not possible to perform computations at physical light quark mass having at the same time under control the lattice discretization and finite volume effects, and one has to sacrifices one or more of these requirement: in particular one typically works with nonphysically large quark masses, thus performing a partial quenching of the fermionic degrees of freedom.

In our computations we have worked with light quark masses ranging from 15 up to ˜3 times the physical up/down quark average mass. The effect of the partial quenching is taken into

[2]Sea quarks are those appearing in the determinants of the lagrangian used to generate the gauge configuration. Valence quarks are those from which external states are built.

account by performing an accurate *chiral limit* $m_{light} \to m_{physical}$ during the computations, as will be described carefully in an appropriate section of each studied quantities.

Generally speaking in most of the hadronic matrix elements the unquenching effects have been found to be quite small, if not negligible.

3.5.2.3 Strange and charm unquenching

Computations presented in chapters 4, 6 and 5 are performed by taking into account only the propagation of the two light quarks (up, down) and therefore will be indicated as $N_f = 2$ simulations. The inclusion of the other quarks is expected to play a marginal role (especially those of the three heavier quark, charm bottom and top). Moreover the twisted mass regularization in its simple form is well suited to simulate pairs of degenerate quarks, therefore the up/down doublet, and requires modification in order to deal with a non degenerate doublet such as strange/charm.

The effect of the quenching of an heavy quark (such as the charm, or possibly the strange) could be kept into account (or at least roughly quantified) by performing a *reweighting* of the gauge ensemble, that is by computing:

$$\langle O \rangle_{unq} = \frac{\int D\left[U\right] \det M_q O e^{-S_w}}{\int D\left[U\right] \det M_q e^{-S_w}} = \frac{\frac{\int D[U] \det M_q O e^{-S_w}}{\int D[U] e^{-S_w}}}{\frac{\int D[U] \det M_q e^{-S_w}}{\int D[U] e^{-S_w}}} = \frac{\langle O \det M \rangle}{\langle \det M \rangle} \,. \tag{3.92}$$

As an effect of the difficulties related to the evaluation of the determinant of the fermionic matrix, this method has never been tested. For these reasons the mentioned computations are affected by an unpredictable quenching effect, which is expected to be much smaller than the already small quantified light quark quenching (see comment in the ending of previous section).

For example a comparison of our $N_f = 2$ result for the B and B_s decay constants, to existing results from $N_f = 2+1$ quark flavor simulations [14,15] suggests that the error due to the partial quenching of the strange quark is smaller at present than other systematic uncertainties.

Nonetheless ultimately one would like to get rid also of this effect: for this reason ETM collaboration has started the generation of a new set of $N_f = 2+1+1$ gauge ensembles including also the unquenching of the strange and charm quarks, on which we will comment in chapter 7.

3.5.3 Discretization effects and continuum limit

Lattice regularized theory reproduces the original theory only in the continuum limit $a \to 0$. Observables computed at finite lattice spacing will differ from its continuum counterpart for finite terms which go to zero only in the continuum limit, generally called *discretization effects*.

In order to extract continuum physics it is therefore necessary to compute observables at various finite lattice spacings and extrapolate them to $a \to 0$.

This extrapolation induces errors on the observables, so one should try to work at the smaller possible lattice spacing. As the lattice spacing is decreased, the number of lattice points for each direction has to be increased in order to keep the same fixed physical volume, thus the computational efforts required to make any calculation increases with the decreasing of a. The minimal lattice spacing affordable is dictated by the available computational power.

Assuming to be able to remove from observables discretization effects up to order a through some kind of improvement, we will be left with effects of order a^2 and superiors. Discretization effects are typically parametrized as polynomial in a. Data computed at finite lattice spacing is

fitted with such polynomial and the extrapolation is done numerically extrapolating the fitted function.

3.5.4 Lattice spacing determination

When choosing the lattice spacing a at the beginning of the computations, one has to fix the gauge coupling g at the value $g(a)$ that it assumes at the chosen scale. The running of g with a is given by the β-function (see Eq. 3.40), which is known only perturbatively up to few orders in g, and the absolute relation between the two quantities is fixed by Λ_{QCD}, which is only known within error.

Therefore in general is not possible to fix exactly g to the value required for the chosen lattice spacing, and an error will be committed. Looking the problem the other way around, as g fixes univocally the lattice spacing, a will be different from what is expected. This means that at the beginning of the computation one cannot choose exactly at which lattice spacing he is working, but can only fix it roughly, by taking a more or less reasonable value of g, with the help of the information coming from previous studies.

All quantities determined on lattice are known only in terms of lattice spacing. In order to convert all quantities to physical units, a good knowledge of the lattice spacing is needed, so after performing the computations one needs to re-determine it. This can be done by choosing a quantity G of dimension d and computing its value in lattice units $\hat{G}$. The lattice spacing will then be given by the ratio:

$$a = \left(G/\hat{G}\right)^{1/d} . \tag{3.93}$$

3.6 Non perturbative renormalization

Although some observables such as hadron masses can be computed and directly related to their physical counterpart, in general this is not true: the process of quantization of the theory re-define parameters (mass, couplings) and operators, so that the before been able to compare quantity computed in a regularized theory with physical observables, one has to identify their correct quantum definition. This process is achieved through the renormalization of the theory.

Different kinds of renormalization can take place. An operator $\mathcal{O}$ can renormalize multiplicatively: $\mathcal{O}^{ren}(a) = Z_{\mathcal{O}}(a)\,\mathcal{O}$, where $Z_{\mathcal{O}}$ can in general be a function of the cut-off a; can have an additive renormalization constant $\mathcal{O}^{ren}(a) = C_{\mathcal{O}}(a) + \mathcal{O}$; it can mix with operator carrying the same quantum numbers $\mathcal{O}(a) = c_1(a)\,\mathcal{O}_1 + \cdots + c_n(a)\,\mathcal{O}_n$, where $\mathcal{O}_i$ are all operators carrying the quantum numbers of $\mathcal{O}$. All these possibility can occur simultaneously, and complicate scenarios can happen.

When renormalizing the theory one need to define a renormalization scheme imposing some kind of condition on operators matrix elements that fix the values of renormalization constants and mixings coefficients.

In the continuum the most used scheme is the $\overline{\text{MS}}$ scheme, which is very suitable when dealing with perturbative computation. On lattice, perturbation theory suffer from various complication which makes almost impossible to perform any calculation beyond the second order, and therefore one often prefer to rely on non-perturbative methods. The more used is by far the RI/MOM scheme [16], which been used extensively through all the present thesis work. However having not worked directly with it, we limit to sketch it in the following.

In order to keep the discussion simple we consider only the case of bilinear operators such as:

$$\mathcal{O}_\Gamma \equiv \bar{u}\Gamma d\,, \tag{3.94}$$

where Γ is a combination of gamma matrices, and let us call Z_Γ the multiplicative renormalization constant of such operator, so that $\mathcal{O}_\Gamma^{ren} = Z_\Gamma \mathcal{O}_\Gamma$. One compute non-perturbatively in the full quantized theory the expectation value of the operator $\mathcal{O}_\Gamma$ between quark fields status $|p\rangle$ at momentum p, and choose Z_Γ such that:

$$Z_\Gamma \left\langle p\right| \mathcal{O}_\Gamma \left|p\right\rangle \Big|_{p^2=\mu^2} = \left\langle p\right| \mathcal{O}_\Gamma \left|p\right\rangle_{tree} \Big|_{p^2=\mu^2}\,, \tag{3.95}$$

where $\left\langle p\right| \mathcal{O}_\Gamma \left|p\right\rangle_{tree}$ is the matrix element computed at the tree level, and μ is a scale such that:

$$\Lambda_{QCD}^2 \ll \mu^2 \ll 1/a^2\,. \tag{3.96}$$

This ensure from one side ($\mu^2 \ll 1/a^2$) that cut-off effects are small, and from the other side ($\Lambda_{QCD}^2 \ll \mu^2$) that one is working in a perturbative regime and therefore can connect RI/MOM with other schemes such as $\overline{\text{MS}}$ through continuum perturbation theory [17] (a typical value for μ is 2 GeV).

The matrix element on the left side of equation 3.95 is the amputated two points Green function and might be computed as

$$\left\langle p\right| \mathcal{O}_\Gamma \left|p\right\rangle = \frac{1}{12}\text{tr}\left(S^{-1}(p) G_O\left(p\right) S^{-1}\left(p\right)\right)\,, \tag{3.97}$$

with $G_O\left(p\right)$ being the Fourier transform of the un-amputated Green function

$$\begin{aligned}
G_O\left(p\right) &= \int d^4x\, d^4y\, e^{-ip\cdot(x-y)} G_O\left(x,y\right) = \\
&= \int d^4x\, d^4y\, e^{-ip\cdot(x-y)} \left\langle S\left(x,0\right)\Gamma S\left(0,y\right)\right\rangle = \\
&= \left\langle \left(\int d^4x\, e^{-ip\cdot x} S\left(x,0\right)\right)\Gamma\gamma_5 \left(\int d^4y\, e^{-ip\cdot y} S\left(y,0\right)\right)^\dagger \gamma_5 \right\rangle = \\
&= \left\langle S\left(p\right)\Gamma\gamma_5 S^\dagger\left(p\right)\gamma_5 \right\rangle\,,
\end{aligned}$$

where we have defined the Fourier transform of the propagator

$$S\left(p\right) = \int d^4x\, e^{-ip\cdot x} S\left(x,0\right)\,, \tag{3.98}$$

and its inverse $S^{-1}\left(p\right)$, and we have made use of the γ_5 hermiticity property of the propagator.

In order to make the renormalization procedure mass independent, the 3.95 must be imposed at null value of all quark masses. This means that, being impossible to work directly at null mass, a chiral extrapolation must be performed in order to fulfill the renormalization condition. Other complications arising in the case of power divergence, mixing with other operators, etc must be treated in a case-by-case approach.

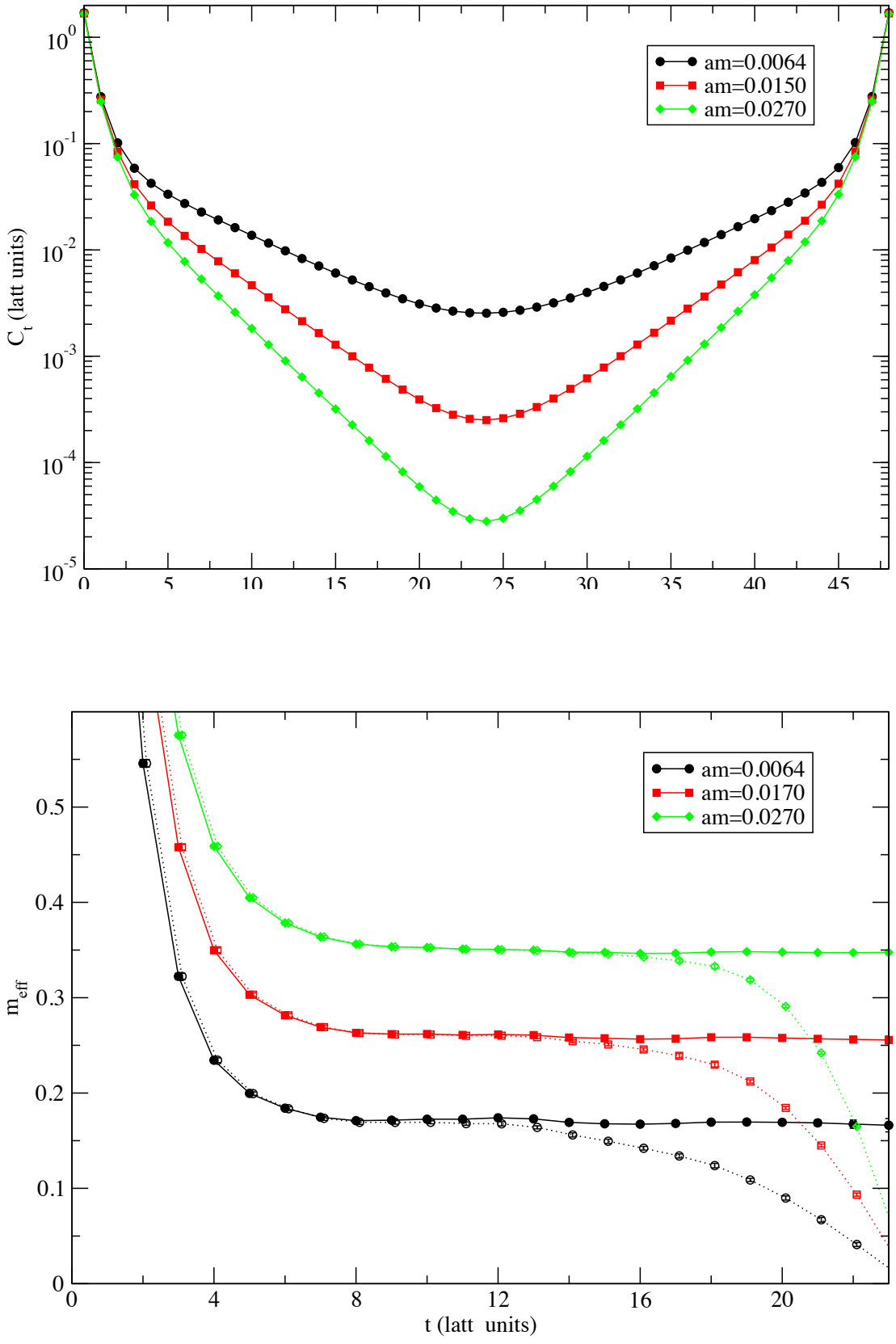

Figure 3.3: Effective mass computed with (continuous) and without (dashed and slightly displaced) taking into account the periodicity of correlation functions.

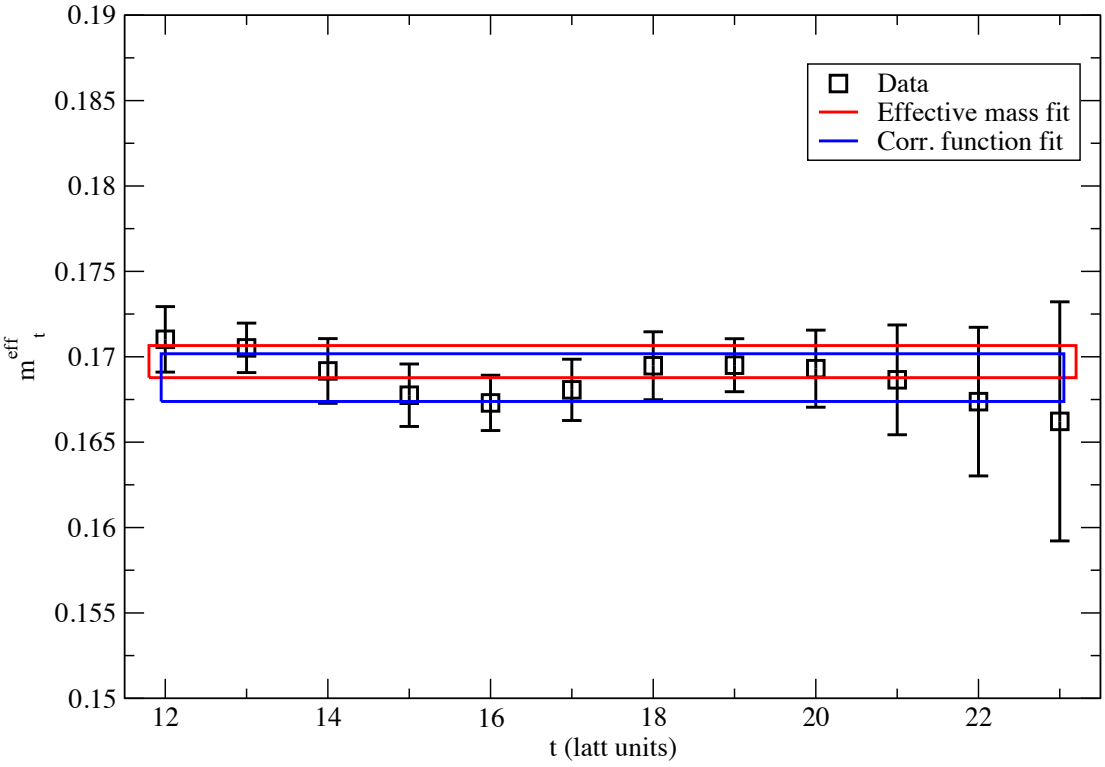

Figure 3.4: Comparison between the determination of the lower lying state energy from the 2 parameters fit of the correlation function C_t (in blue) and from the constant fit of the effective mass (red). The correlation function is $am = 0.0064$ in Fig. 3.2.

Chapter 4

Quark masses

Quark masses are fundamental parameters of the Standard Model. A precise knowledge of their values is of great importance for many different reasons.

From a phenomenological point of view, several useful observables to constrain the SM or to search for New Physics depend on quark masses, thus requiring their accurate values in order to make significant theory vs. experiment comparisons.

From a more theoretical side, explaining the quark mass hierarchy, which is not predicted by the SM, is a deep issue and a great challenge.

From a practical point of view, quark masses are parameters of the lattice QCD lagrangian and their values need to be fixed as well as that of the strong running coupling α_s.

Although many different observations indicate that hadrons are constituted by quarks, as a consequence of their peculiar interactions quarks are not observed as free objects in nature, therefore the their masses cannot be directly measured and have to be inferred.

4.1 Lattice determination with $N_f = 2$ gauge ensembles

Lattice QCD allow one to determine quark masses non-perturbatively starting from first principle. Bare quark masses appear explicitly as parameters in the QCD lagrangian, and can be fixed to their physical values by imposing to a certain observable $G(m_q)$ to reproduce its experimental value G_{phys}.

One of the more common and more suitable choices is to fix the quark masses through the mass of the pseudo-scalar mesons M_{PS}. This strategy has many advantages: meson masses are simple to extract from lattice simulations thanks to the good signal/noise ratio, their physical value are very well known, and many of the systematic effects involved in the analysis can be treated with the help of Chiral Perturbation Theory. Most important, the pseudo-scalar mesons are quasi-Goldstone bosons, so their squared mass is directly related to the mass of the valence quarks, namely:

$$M_{PS}^2 \propto (m_{q_1} + m_{q_2})\,. \tag{4.1}$$

In order to fix the value of a quark mass one has to solve numerically the equation $M_{PS}(m_q) = M_{PS}^{phys}$, by tuning the quark mass m_q iteratively up to reproducing the physical mass of the pseudo-scalar meson PS. In order to avoid the demanding computation to become prohibitive, we evaluate M_{PS} over a discrete set of quark masses, find an analytical function describing the data, and use it to interpolate or extrapolate to the physical meson mass.

In the real world all quark masses contribute simultaneously to every observable, so that in theory one should determine quark masses all at once. In the following instead we will consider the determination of each mass in a separate analysis, starting from the lightest Up/Down up to the case of the Charm. We will perform our analysis over the gauge configurations obtained with $N_f = 2$ light sea quarks, and therefore only the quark u and d are treated in a fully unquenched way. This corresponds to having neglected the effect of all the other quarks in virtual loops, so that the value of their masses can affect only quantities in which they appear as external states.

Stating it the other way around, having neglected all quarks but the lights means that observables might differ from the value in "full" QCD. These differences are generally expected to be very small, as explained in section (3.5.2).

This part of the work is organized in this way. In Section7.1.4 we discuss the details of the performed computation. In section 4.2 we discuss the determination of the average up/down quark mass, while in sections 4.3 we determine the strange and in section 4.4 the charm masses.

This chapter is based on the published paper [18].

4.1.1 Simulation details

Our calculation is based on a set of 13 ensembles of gauge field configurations generated by the European Twisted Mass Collaboration (ETMC) using the tree-level improved Symanzik gauge action discussed in section 3.3.3 and the twisted mass quark action at maximal twist, discussed in section 3.3.4. Gauge configurations contains two mass degenerate dynamical quarks. In order words, strange and charm quarks are quenched in this calculation. More details on the gauge ensembles used in this work can be found in [19, 20].

As discussed in previous chapter, we implement non-degenerate valence quarks in the twisted mass formulation by formally introducing a twisted doublet for each non-degenerate quark flavor. In the present analysis we thus include in the valence sector three twisted doublets, (u, d), (s, s') and (c, c'), with masses am_l, am_s and am_c, respectively. Within each doublet, the two valence quarks are regularized in the physical basis with Wilson parameters of opposite values, $r = -r' = 1$. Moreover, we only consider in the present study pseudo-scalar mesons composed of valence quarks regularized with opposite r. This choice guarantees that the squared meson mass m_{PS}^2 differs from its continuum counterpart only by terms of $O(a^2 m_q)$ and $O(a^4)$. Details of the ensembles of gauge configurations used in the present analysis are collected in Table 4.1.

In order to investigate the properties of the various light, strange and charmed mesons, we simulate the sea and valence up/down quark mass in the range $(14 - 48)$ MeV (in $\overline{\text{MS}}$ at 2 GeV), the valence strange quark mass within $(77 - 144)$ MeV, and the valence charm quark mass within $(1 - 2)$ GeV (again in $\overline{\text{MS}}$ at 2 GeV). Strange and charm ranges have been chosen in such a way to cover the physical value of relative quarks.

Quark propagators with different valence masses are obtained using the so called multiple mass solver method, which allows to invert the Dirac operator for several valence masses at the same time, with a mild increase in computational cost with respect to the computation of the single propagator.

The statistical accuracy of the meson correlators is significantly improved by using the so-called one-end stochastic method [21], which includes all spatial sources at a single time-slice.

β	$a\left(10^{-3}fm\right)$	$N_x^3 \times N_t$	am_l	$M_\pi\,(MeV)$	$M_\pi L$	N_{conf}
3.80	98	$24^3 \times 48$	0.0080	410	5.0	240
			0.0110	480	5.8	240
3.90	85	$24^3 \times 48$	0.0040	315	3.3	480
			0.0064	400	4.1	240
			0.0085	450	4.7	240
			0.0100	490	5.0	240
		$32^3 \times 64$	0.0030	275	3.7	240
			0.0040	315	4.3	240
4.05	67	$32^3 \times 64$	0.0030	300	3.3	240
			0.0060	420	4.5	240
			0.0080	485	5.2	240
4.20	54	$32^3 \times 64$	0.0020	270	3.5	80
		$48^3 \times 96$	0.0065	495	4.3	240

Table 4.1: Details of the 13 gauge ensembles considered. See following section for a discussion concerning the determination of the lattice spacing.

In this method one start defining a set of 4 random field $\eta^{t_w,\beta}_{n;\alpha;a},\ \beta \in [1;4]$ such as:

$$\eta^{t_w,\beta}_{n;\alpha;a} = \delta_{\alpha(\beta)}\delta_{n_0,t_w} Z_{n;a},\ \beta \in [1,4]\ , \tag{4.2}$$

where n_0 is the time coordinate of site n, t_w is the time coordinate of the spatial source, and$Z_{n;a}$ is a random number extracted according to an appropriate distribution, satisfying the propriety:

$$\left\langle Z^*_{n;a} Z_{m;b} \right\rangle = \sum_r Z^{r*}_{n;a} Z^r_{m,b} = \delta_{m,n}\delta_{a,b}\,, \tag{4.3}$$

where r indicate the different realizations of η.

Starting from this definition one compute:

$$\phi^q_{n;\alpha,\beta;a} = S^q_{n,m;\alpha,\rho;a,b}\eta^\beta_{m;\rho;b}\,. \tag{4.4}$$

where S^q is the propagator for the quark q. It is easy to show that the quantity:

$$C^{q_1,q_2}_{t;A,B} = \sum_{r\,conf;\,n} \mathrm{tr}\left[\gamma_5 \phi^{r,q_1\dagger}_n \gamma_5 \Gamma_A \phi^{r,q_2}_n \delta_{n_0,t+t_w}\right]\ , \tag{4.5}$$

is a good estimator of the two points correlation functions such as 3.71. In fact using orthogonality relation 4.3 and γ_5 hermiticity this can be rewritten as:

$$C^{q_1,q_2}_{t;A,B} = \sum_{\vec{x};\,conf} \mathrm{tr}\left[S^{\dagger,q_1}_{t,\vec{x};0}\Gamma_A S^{,q_2}_{0;t,\vec{x}}\Gamma_B\right]\ . \tag{4.6}$$

In typical situation one consider $Z_{n;a}$ distributed according to a gaussian or uniform over Z_4, and only one realization of η per configuration. Indeed, therms which averages to 0 performing summation over r are also gauge variant, so that the summation over configurations already contains an implicit summation over r.

4.1.2 General remarks

4.1.2.1 Statistical methods

Statistical errors on the meson masses are evaluated using the jackknife procedure. We have used 16 jackknife bins for each configuration ensemble, verifying that bin length in each ensemble is larger than autocorrelation time of the ensemble. Statistical errors on the fit results which are based on data obtained from independent ensembles of gauge configurations are evaluated using a bootstrap procedure, with 100 bootstrap samples.

4.1.2.2 Renormalization

The analysis is based on a study of the dependence of meson masses on renormalized quark masses, with data at the four simulated values of the lattice spacing simultaneously analyzed. In twisted mass QCD, when working at maximal twist, the renormalized quark mass $\bar{m}$ is given by

$$\bar{m}^{\mu} = Z_m^{\mu} m \,, \tag{4.7}$$

with m being the twisted mass parameter Z_m the renormalization constant at the scale μ , which making use of the Partially Conserved Vectorial Current (PCVC) relation can be shown to be equal to the reciprocal of the axial current renormalization constant Z_m:

$$Z_m = Z_P^{-1} \,, \tag{4.8}$$

For this quantity we use the results obtained in [22], which read:

$$Z_P = \{0.411\,(12)\,,\, 0.437\,(7)\,,\, 0.477\,(6)\} \quad \text{at} : \beta = \{3.80,\, 3.90,\, 4.05\}\ , \tag{4.9}$$

in the $\overline{\rm MS}$ scheme at 2 GeV. Here, and in the following, we denote by "bar" the quark masses renormalized in the $\overline{\rm MS}$ scheme and, if not otherwise specified, at the scale of 2 GeV. The errors given in Eq. 4.9 do not account neither the discretization errors nor the uncertainty associated with the perturbative conversion from the RI-MOM (see sec. 3.6) to the $\overline{\rm MS}$ scheme. The former are taken care of by performing on the renormalized quark masses the extrapolation to the continuum limit. The uncertainty associated to the conversion from the RI-MOM to the $\overline{\rm MS}$ scheme is included in our final estimate of the systematic error on the quark masses. For the renormalization constant at $\beta = 4.20$, not calculated in [22], we use the preliminary value $Z_P^{\overline{\rm MS}}\,(2\,{\rm GeV})\Big|_{4.20} = 0.501\,(20)$.

The uncertainty on Z_P has been taken into account by including in the definition of the χ^2 to be minimized in the fits a term:

$$\left(\frac{\tilde{Z}_P^i\,(a) - Z_P^i\,(a)}{\delta Z_P^i\,(a)}\right)^2 \,, \tag{4.10}$$

for each value of the lattice spacing and in each bootstrap sample, where $Z_P^i\,(a) \pm Z_P\,(a)$ is the input value for the renormalization constant at the lattice spacing a and for the bootstrap i, and e $Z_P^i\,(a)$ the corresponding fit parameter. This procedure corresponds to assuming for the renormalization constant a Bayesian Gaussian prior [23].

4.1.2.3 Scale setting

The simultaneous analysis of data at different values of the lattice spacing also requires the data conversion from lattice units to a common scale. For the analysis in the pion sector, we have expressed all quantities in appropriate units of the Sommer parameter r_0 [24]. This is defined in terms of purely gauge quantities, as the distance at which the force $F(r)$ between two statics quarks behaves like:

$$F(r_0)\, r_0^2 = 1.65\,. \tag{4.11}$$

We use for r_0/a in the chiral limit the values:

$$r_0/a = \{4.54(7), 5.35(4), 6.71(4), 8.36(6)\} \text{ at } \quad \beta = \{3.80,\ 3.90, 4.05,\ 4.20\}\ , \tag{4.12}$$

obtained from an extension of the analyses in [23,25] with the inclusion of all four lattice spacings. As in [23], the chiral extrapolation of r_0/a is performed by using three ansatze for the sea quark mass dependence: linear only, quadratic only and quadratic+linear. The size of mass-dependent discretization effects is verified by including in the fits $\mathcal{O}(a^2 m_l)$ and $\mathcal{O}(a^2 m_l^2)$ terms, which turn out to be negligible. The uncertainties on the results given in Eq. 4.12 include the systematic errors estimated as the spread among the values obtained from the above-mentioned fits. In the present analysis the uncertainty on the r_0/a values is taken into account by adding a term to the χ^2 of the fit in a similar way to Z_P, as explained above.

The analysis in the pion sector is also used to determine, besides the value of the average up/down quark mass at the physical point, the lattice spacing at each coupling. The physical input used for this determination is the pion decay constant f_π, whose computation in terms of hadronic correlation function is explained in the next section.

In the successive determination of the strange and charm quark masses, the data are analyzed directly in physical units.

4.2 Light quarks (up, down) average mass

In the following we will focus on the determination of the average light quarks mass:

$$m_l \equiv \frac{m_u + m_d}{2}\,. \tag{4.13}$$

Light quark average mass is much simpler to determine than the two separate masses for various reasons. The difference between their mass is estimated to be of the same order of magnitude of their average value, so one would expect large differences between observables related to hadrons composed of different combinations of these two quarks. However the relevant scale for almost all of these observables is Λ_{QCD}, whose value is of some hundreds of MeV, and so much larger than up and down quark masses. Moreover, the fermionic determinant of a theory containing two light quarks with different masses is guaranteed to be definite positive only in a regularization with an exact chiral symmetry (overlap fermions), which are very demanding in terms of computational power.

In a numerical analysis any direct effect of the mass splitting would be of the same order of magnitude of the statistical errors, therefore a direct determination of the two light quark masses would be affected by a large error. In other words this means that at the present level of accuracy it is enough in many cases to determine this quantity and use it in further computations. Correction to the isospin degenerate case might be determined separately as we will discuss in section 6.

In order to fix the light quark mass we have considered the Pion neutral meson mass $M_{\pi^0} = 135.0\,\mathrm{MeV}$ as physical input. In the isospin symmetric world the mass of charged and neutral pion should be equals, and it is known that the difference in mass between neutral and charged pions induced by the light quark mass difference is quadratic in this quantity. Moreover the electromagnetic effects on neutral pion mass are very small, so for these reasons, M_{π^0} is the quantity nearer to the value of the pion mass in the isospin symmetric limit light, and therefore is the more suitable quantity to fix m_l.

4.2.1 Correlation functions analysis

As already explained in section (3.2.2), a good interpolating field for pseudo-scalar mesons is given by the local pseudo-scalar bilinear $O_{PS}^{q_1 q_2} = \bar{\psi}_{q_1}\gamma_5\psi_{q_2}$. For this analysis we have computed the correlation function:

$$C_{PS}^{l}(t) = \left\langle \overline{O_{PS}^{ll}}(t)\, O_{PS}^{ll}(0) \right\rangle . \tag{4.14}$$

The two light quark entering the correlation functions have been regularized with opposite r: in this case the correlation is obtained by computing the single connected contraction:

$$C_{PS}^{l,+-} = -\sum_{conf}\sum_{n,m} \mathrm{tr}\left[\gamma_5 D_{+}^{-1}(n,m)\,\gamma_5 D_{-}^{-1}(m,n)\right] , \tag{4.15}$$

where the $\pm$ refers to the sign of r. This contraction is equivalent (apart from small $\mathcal{O}\left(a^2\right)$ effects) to the $C_{PS}^{l,-+}$, and the two have been averaged in order to improve statistics.

These contractions correspond to the so-called r-charged (or "twisted mass") meson, which are known to have better signal to noise ratio and much lower cut-off effects than the corresponding r-neutral or "Osterwalder–Schrader") meson (see section 3.3.4.5).

For each gauge ensemble we have considered only unitary Pions, e.g. those with the same valence quark mass of the sea. Pion mass has been determined by fitting over an appropriate interval $[t_{min}, T - t_{min}]$ the correlation function $C_{PS}^{l}(t)$ with the single exponential state expression:

$$C(t) = \frac{Z_\pi^2 e^{-aM_\pi T/2}}{aM_\pi}\cosh\left[aM_\pi\left(T/2 - t\right)\right] , \tag{4.16}$$

where Z_π and aM_π have been let as free minimization parameters, and where the "cosh" arises instead of the simple exponential due to the backward propagating states as explained in section 3.4.4.1. The value of t_{min} has been chosen by examining the the effective mass and taking the part at which it shows a plateau. In Fig. 4.1 we show an example of the effective mass for various mesons at the same lattice spacing ($\beta = 3.90$) together with the mass resulting from the fit of the correlation function.

After determining aM_π and Z_π we build af_π according to section 3.3.4.5. In order to determine m_l, a combined fit in terms of m_l and a is needed.

4.2.2 Combined chiral and continuum fit

We have studied the dependence of the pion mass and decay constant on the renormalized quark mass. For these quantities the predictions based on NLO-ChPT and the Symanzik expansion up to $O\left(a^2\right)$ can be written in the form:

$$M_\pi^2 = \mathbf{2B_0}m_l \cdot \left[1 + \frac{\mathbf{2B_0}m_l}{16\pi^2\mathbf{f_0}^2}\log\frac{\mathbf{2B_0}m_l}{16\pi^2\mathbf{f_0}^2} + \mathbf{P_1}m_l + a^2\cdot\left(\mathbf{P_2} + \mathbf{P_3}\log\frac{\mathbf{2B_0}m_l}{16\pi^2\mathbf{f_0}^2}\right)\right] \tag{4.17}$$

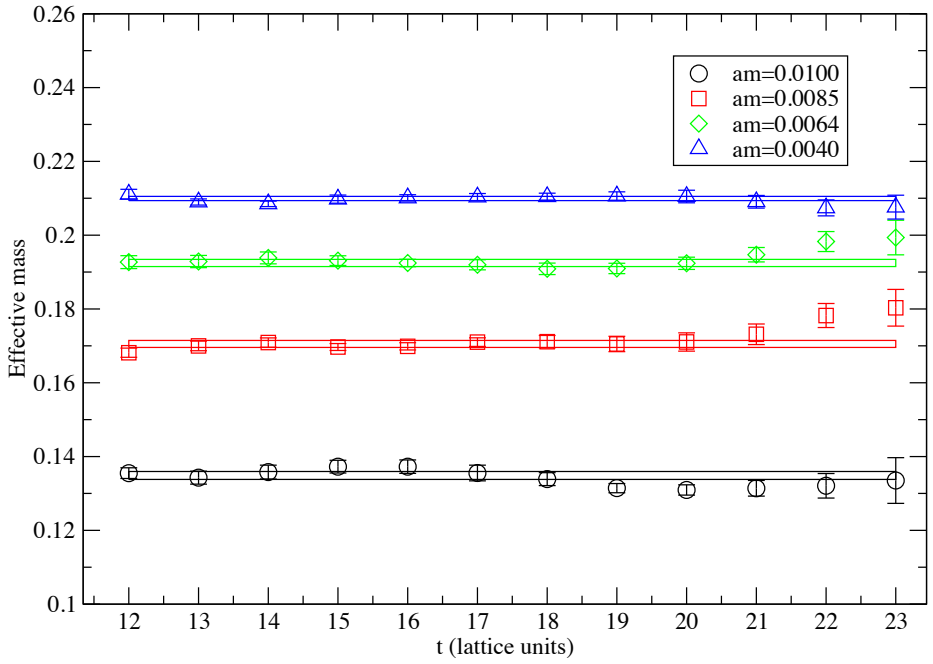

Figure 4.1: Plot of the effective mass at four different values of the light quark mass at the same lattice spacings. Fit lines are the values of M_π obtained from the fit of the correlation functions, plotted together with their errors. Light quark valence mass is equal to the sea one and is indicated with am.

$$f_\pi = f_0 \cdot \left[1 - 2\frac{\mathbf{2B_0}m_l}{16\pi^2\mathbf{f_0}^2}\log\frac{\mathbf{2B_0}m_l}{16\pi^2\mathbf{f_0}^2} + \mathbf{P_4}m_l + a^2 \cdot \left(\mathbf{P_5} + \mathbf{P_6}\log\frac{\mathbf{2B_0}m_l}{16\pi^2\mathbf{f_0}^2}\right)\right], \tag{4.18}$$

were m_l is the renormalized quark mass and f_0 is normalized such that $f_{\pi^{phys}} = 130.7\,\mathrm{MeV}$.

We have fitted expressions (4.17) and (4.18) simultaneously over all available lattice data, leaving bold quantities (discussed in more details below) as free fit parameters. We have checked that the correlation between M_π^2 and f_π is quite small and can be safely neglected in building the χ^2.

In order to fit lattice data, we have converted pion mass and decay constant into units of r_0 by multiplying them for the appropriate power of r_0/a, thus:

$$(r_0 M_\pi)^2 = (aM_\pi)^2 \cdot (r_0/a)^2 \tag{4.19}$$

$$(r_0 f_\pi) = (a f_\pi) \cdot (r_0/a)\,. \tag{4.20}$$

Also the fitting expression are to be intended in units of r_0: therefore from the fit we have determined $2B_0 r_0$, $r_0 f_0$, a/r_0, etc that have been converted in physical units after determining r_0 (see below).

In fig. 4.3 we show the dependence of $(r_0 m_\pi)^2/m_l$ on the renormalized light quark mass at the four β, and the curves corresponding to the best fit of the lattice data according to Eq. (4.17), while in fig. 4.3 we show a similar plot for $r_0 f_\pi$ fitted according to Eq. (4.18).

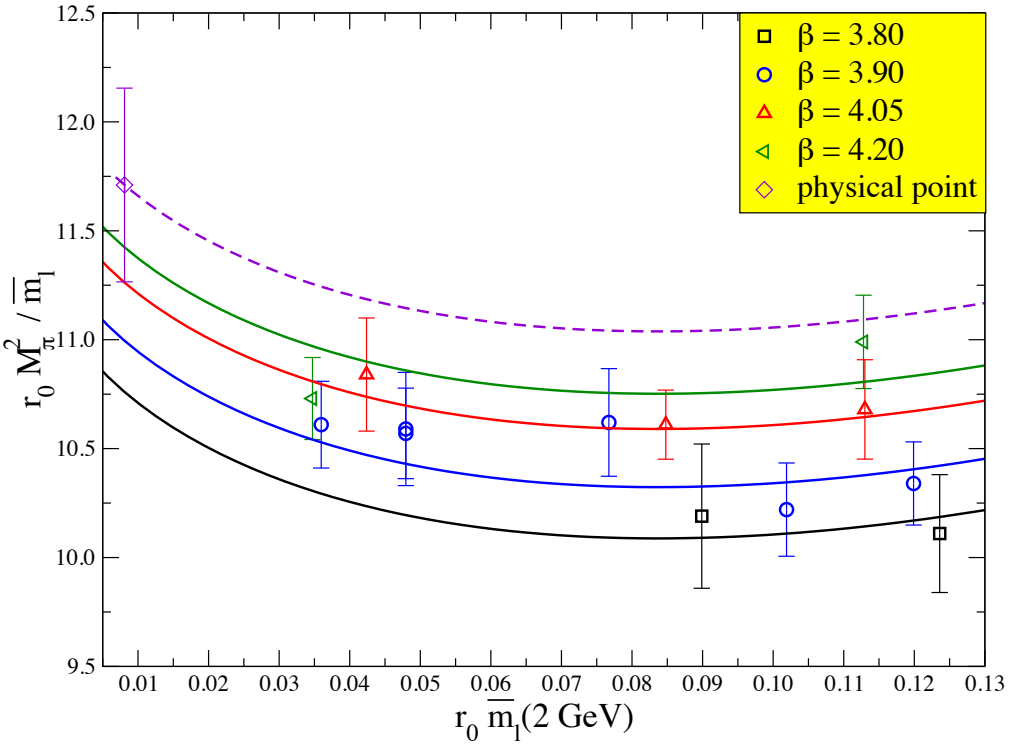

Figure 4.2: Dependence of $(r_0 f_\pi)^2$ on the renormalized light quark mass at the four lattice spacings.. Empty diamonds represent the results obtained after extrapolating to the continuum limit. Quark mass is renormalized in $\overline{\text{MS}}$ at 2 GeV.

4.2.3 Systematic errors

Let us discuss the various sources of systematic errors that affect the determination of the quark masses.

4.2.3.1 Chiral extrapolation

For estimating the systematic uncertainty due to the chiral extrapolation we have also considered a fit including a next-to-next-to leading order (NNLO) local contribution proportional to the light quark mass square. In particular we neglected the logarithmic dependance from quark mass and considered only polynomial term in m_l^2. In this case we are not able to determine all the fitting parameters and we are thus forced to introduce priors on the additional LECs. In this way we find that the result for m_l increases by 6%.

4.2.3.2 Discretization effects

As already mentioned, discretization effects on squared pseudo-scalar meson mass have been shown to be proportional to $a^2 m_l$. Pion mass is an exception to this rule: it has been recently pointed out in [26] that in twisted mass regularization additional terms originate from the splitting between charged and neutral pion mass. The cut-off dependence terms P_3 and P_6 in formulas 4.17 and

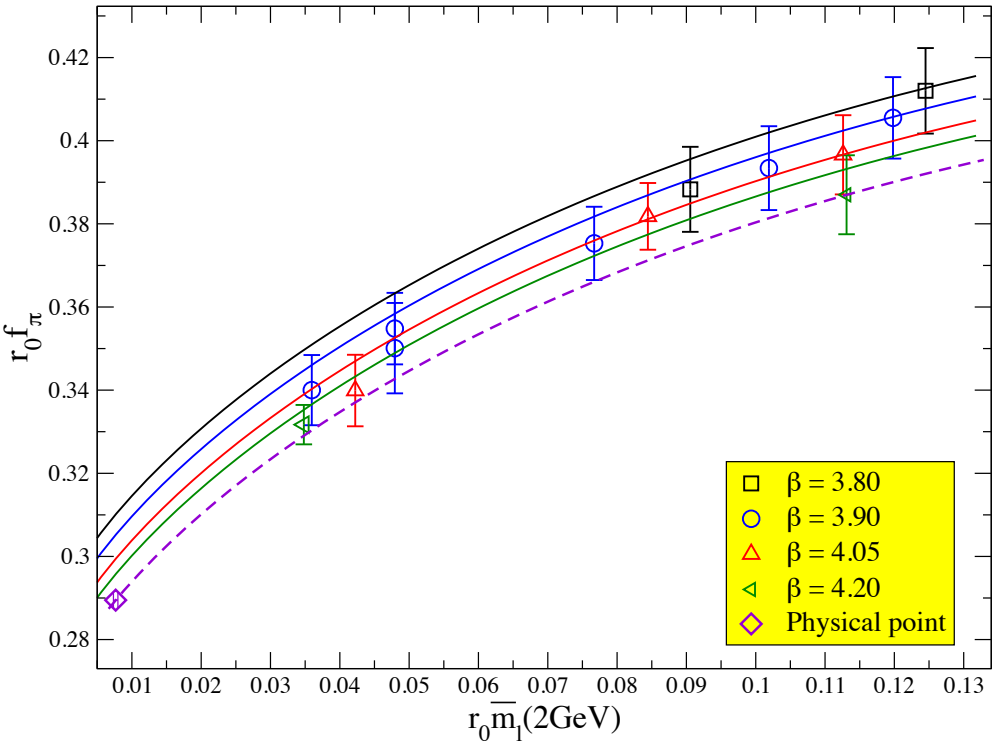

Figure 4.3: Dependence of $(r_0 m_\pi)^2 / m_l$ on the renormalized light quark mass at the four lattice spacings. Empty diamonds represent continuum limit results. Quark mass is in $\overline{\text{MS}}$ at 2 GeV.

4.18 are obtained by expanding the expression computed in 1-loop twisted chiral perturbation theory [26]. Parameters P_3 and P_6 are directly related to the charged-neutral pion mass splitting induced by twisted term so that it is possible to determine this splitting from their fitted values. The squared mass splitting turns out to be $\Delta M_\pi^2 = -(33 \pm 19)\, a^2 \Lambda_{QCD}^4$, consistent with a direct evaluation performed by ETMC [27] (where it was determined to be $\Delta M_\pi^2 = -50 a^2 \Lambda_{QCD}$).

In order to illustrate the dependence of the pion mass on the lattice cutoff, we have interpolated the lattice data for M_π^2 at the four values of the lattice spacing to a common reference value of the light quark mass, $\overline{m}_{ref} = 50\,\text{MeV}$ (in $\overline{\text{MS}}$ at 2 GeV), which is the only mass value where data at the four different lattice spacings is simultaneously available. In other words we have taken for each lattice spacing a the mass $M_\pi^{a,\overline{m}_{near}}$ of the pion made from the quark having renormalized mass $\overline{m}_{near}$ more near to $\overline{m}_{ref}$, and have defined:

$$M_\pi^{a,ref} = M_\pi^{a,\overline{m}_{near}} \sqrt{\frac{M_\pi^2\left(\overline{m}_{ref}, a\right)}{M_\pi^2\left(\overline{m}_{near}, a\right)}} \tag{4.21}$$

where $M_\pi^2(m_l, a)$ is fit function 4.17. The resulting values of $(r_0 m_\pi)^2$ obtained in this way are shown in fig. 4.4 as a function of $(a/r_0)^2$, together with the corresponding continuum extrapolation. We see that discretization errors on the pion mass square are below 10% at $\beta = 3.90$ and negligible within the fitting errors at $\beta = 4.20$.

In order to estimate the systematic uncertainty due to discretization effects we have performed both a fit without the logarithmic discretization terms, i.e. with $P_3 = P_6 = 0$ in Eq. 4.2, and a fit

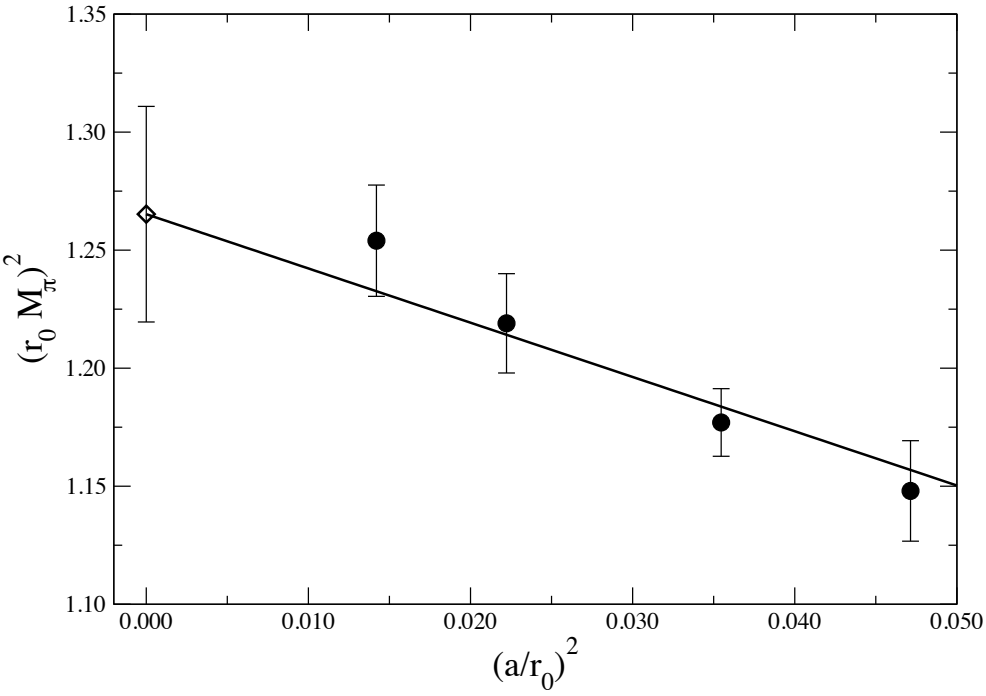

Figure 4.4: Dependence of $(r_0 M_\pi)^2$ on the squared lattice spacing, for a fixed reference light quark mass ($\overline{m}_{ref} = 50\,\mathrm{MeV}$ as explained in the text). Empty diamonds represent continuum limit results.

without all $\mathcal{O}\left(a^2\right)$ corrections, i.e. with $P_2 = P_3 = P_5 = P_6 = 0$. Both these ansatze turn out be compatible with the lattice data. We find that the result for the up/down quark mass decreases by approximately 2% and increases of about 6% in the two cases respectively, so that we estimate an overall uncertainty due to residual discretization effects of $\pm 4\%$. We have also tried to add in the fit discretization terms of $\mathcal{O}\left(a^2 m_l^2\right)$ or $\mathcal{O}\left(a^4\right)$. In both cases these terms turn out to be hardly determined with our data, leading for m_l to results consistent with those obtained from the other fits, but with uncertainties larger by a factor three.

4.2.3.3 Finite volume effects

Lattice results for pion masses and decay constants have been corrected for finite size effects (FSE) evaluated using the resumed Luscher formulae. The effect of the $\mathcal{O}\left(a^2\right)$ isospin breaking has been taken into account also in these corrections, according to the formulae computed in [28]. On our pion data, FSE vary between 0.2% and 2%, depending on the simulated mass and volume. The inclusion of the pion mass splitting in the FSE induces a variation of about $15 - 40\%$ in the finite size correction itself. This effect is at the level of one third of the statistical error for our lightest pion mass at $\beta = 3.90$ on the smaller volume, and even smaller in the other cases.

4.2.3.4 Renormalization

We also include in the final result a systematic uncertainty coming from the perturbative conversion of the quark mass renormalization constant from the RI-MOM to the $\overline{\text{MS}}$ scheme. Using the results of the 3-loop calculation of [29], one can write the relation between the quark mass in the two schemes as:

$$\frac{\overline{m}(\mu)}{m^{\text{RI}}(\mu)} = 1 - 0.424\,\alpha_s(\mu) - 0.827\,\alpha_s(\mu)^2 - 2.126\,\alpha_s(\mu)^3 + \mathcal{O}\left(\alpha_s(\mu)^4\right). \tag{4.22}$$

The uncertainty due to the truncation of the perturbative series has been conservatively estimated by assuming the unknown $\mathcal{O}\left(\alpha_s^4\right)$ term to be as large as the $\mathcal{O}\left(\alpha_s^3\right)$ one. Evaluating this term at the renormalization scale $\mu \simeq 3GeV$, which is the typical scale of the non-perturbative RI-MOM calculation in our simulation [22], and using $\alpha_s(3\,\text{GeV}, N_f = 2) = 0.202$, we then find that this uncertainty corresponds to be less than 2%.

4.2.4 Determination of $\bar{m}_l$

The value of the physical up/down quark mass is determined by solving numerically the equation:

$$\frac{M_\pi^2(\bar{m}_l)}{f_\pi^2(\bar{m}_l)} = (M_\pi/f_\pi)^2_{phys}\ , \tag{4.23}$$

where the left hand side of equation is the ratio of the fitted function, while the right hand side is the experimental value of the ratio.

To summarize previous discussions and for future reference, we have performed fits based on three different ansatze, which led to results:

	L1	L2	L3
$\bar{m}_l^{\overline{\text{MS}},\,2\,\text{GeV}}$ [MeV]	3.55(14)	3.75(7)	3.78(17)

where:

L1 is our best fit is based on NLO ChPT with the inclusion of $\mathcal{O}(a^2)$ discretization effects. This fit corresponds to Eq. (4.17) with all parameters different from zero.

L2 same as L1 but without discretization terms, i.e. $P_2 = P_3 = P_5 = P_6 = 0$.

L3 same as L1 with the inclusion of a NNLO correction proportional to $\overline{m}_l^2$.

Adding all the systematic errors discussed in previous section in quadrature we obtain $\overline{m}_l = 3.55\,(14)\,\left(^{+28}_{-16}\right)$ MeV in the $\overline{\text{MS}}$ scheme at the renormalization scale of 2 GeV, where the two errors are statistical and systematic, respectively. We symmetrize the error and obtain:

$$\overline{m}_l^{\overline{\text{MS}},\,2\,\text{GeV}} = 3.6\,(1)\,(2)\,\text{MeV} = 3.6\,(2)\,\text{MeV}\,. \tag{4.24}$$

Note that, in the symmetrized result, the uncertainties due to discretization effects, chiral extrapolation and perturbative conversion give similar contributions to the final systematic error, at the level of 4%, 3% and 2% respectively.

4.2.5 Determination of r_0 and lattice spacings

Actually equation 4.23 provides us with the value of m_l still in units of r_0, that is: $r_0 m_l$. We can determine r_0 by taking the ratio:

$$r_0 = \frac{r_0 f_\pi \left(r_0 \bar{m}_l^{phys} \right)}{f_\pi^{phys}} , \tag{4.25}$$

(or the equivalent for M_π), where the numerator of the fraction is equation (4.18) computed at the value $r_0 \bar{m}_l^{phys}$ previously determined. The so obtained value of $r_0 = 0.440(12)\, fm$ can then be used to determine m_l from $r_0 \bar{m}_l$ [1].

The lattice spacings for each simulated β by taking the ratio:

$$a = \frac{r_0}{r_0/a} , \tag{4.26}$$

They read, at $\beta = \{3.80,\, 3.90,\, 4.05,\, 4.20\}$ respectively:

$$a = \{0.098(3)(2),\ 0.085(2)(1),\ 0.067(2)(1),\ 0.054(1)(1)\}\ \text{fm} , \tag{4.27}$$

where again the two quoted errors are statistical and systematic.

We observe that, in principle, the ratio of lattice spacings at two different values of β could be determined from the fit of the pion meson mass and decay constant, without using the information coming from r_0/a of Eq. (4.12). With our data, however, the uncertainties on the values of the quark mass renormalization constant, as well as the a priori unknown size of discretization errors affecting the pion masses and decay constants, do not allow to achieve a reliable determination of these ratios.

Other interesting low energy constant obtained from the analysis are: $2B_0^{\overline{\rm MS}\,,2\,\rm GeV} = 5.42(23)\,\text{GeV}$, and $f_0 = 121.88(18)\,\text{MeV}$.

4.2.6 Alternative way of setting the scale

The lattice spacing computed in previous section are affected by a 2-3% error. This error enters directly in the conversion to physical units of any quantity, and it is likely to dominate any other error. It would therefore be interesting to provide a more precise way to fix the scale.

Analyzing the functions 4.17 and 4.3 we noted that the product $M_\pi^2 \sqrt{f_\pi}$ is not affected by chiral logs. In fig. 4.5 this quantity is plotted as function of the renormalized quark mass. This quantity is subject to a very smooth chiral extrapolation, and at the chiral point $m = 0$ is affected by very tiny ($\leq$3%) cut-off effects.

Disposing of 3-4 sea quark mass combinations per β, one could therefore perform a simple linear chiral extrapolation of this quantity at each separate lattice spacing, without the need of any renormalization constant. Given the easiness of the extrapolation and the fact that this quantity is related to simple correlators, we propose to use it as an alternative or complementary quantity in addiction to r_0/a to set the scale and compare quantities at different lattice spacings.

[1] This value is quite different from that obtained from analysis of baryon masses by various collaboration, including ETMC. This discrepancy might be explained as an effect of chiral extrapolation, which is much more under control in the mesonic sector.

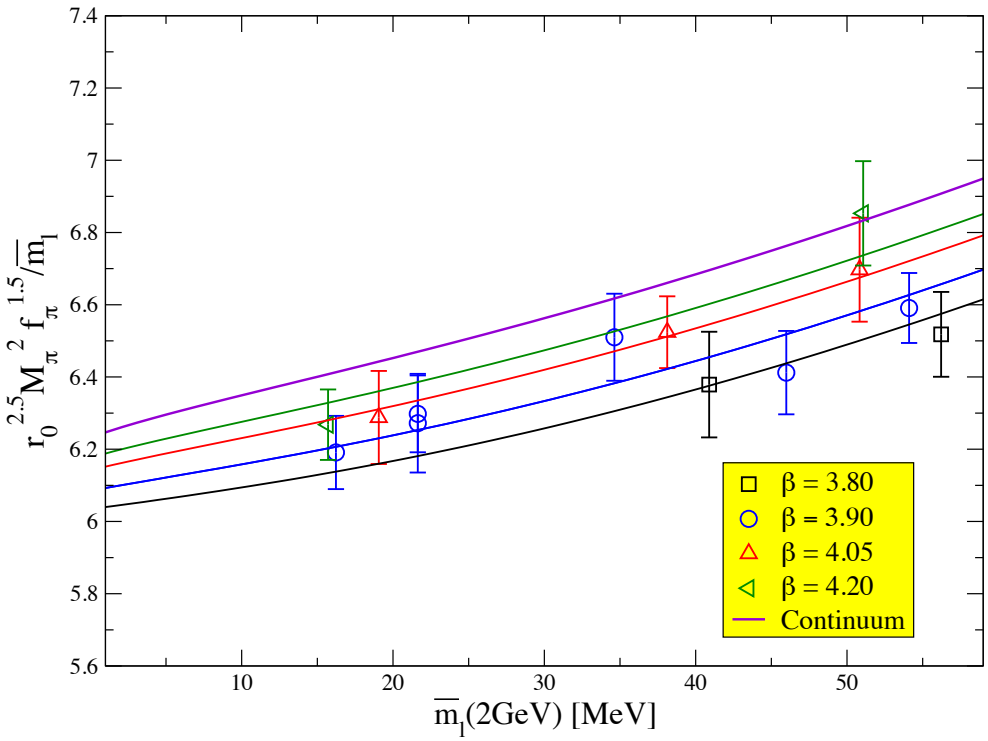

Figure 4.5: Dependence of the quantity $(M_\pi)^2 \sqrt{f_\pi}$ on the renormalized quark mass. . Lines are just the fitting functions (with chiral logs) plotted over data.

4.3 Strange quark mass

In this section we will discuss the determination of the strange quark mass inferred from the study of two different strange mesons: the Kaon and the η_s meson.

4.3.1 Determination from the Kaon mass

4.3.1.1 General strategy

Since the valence strange quark mass has not been previously tuned in our simulations, the determination of the physical strange quark mass requires an interpolation of the lattice data. In order to better discriminate the strange quark mass dependence of the kaon masses from other dependencies, we first interpolate the lattice data with quadratic spline to three reference values of the strange quark mass, which are chosen to be equal at the four lattice spacings: $\bar{m}_s^{ref} = \{80,\ 95,\ 110\}$ MeV in $\overline{\rm MS}$ at 2 GeV In figure 4.6 we show for example the interpolation of M_K^2 lattice data to the reference mass for the three sea quark masses of $\beta = 4.05$.

Then, at fixed reference strange mass, we simultaneously study the kaon mass dependence on the up/down quark mass and on discretization effects, thus performing the chiral extrapolation and taking the continuum limit. In this step we have considered chiral fits based either on $SU(2)-$ChPT [29, 30], where the chiral symmetry is assumed for the up/down quark only, or partially quenched $SU(3)-$ChPT [31], where the valence strange quark is treated as a small perturbation. In order to extrapolate the kaon mass values to the continuum and to the physical

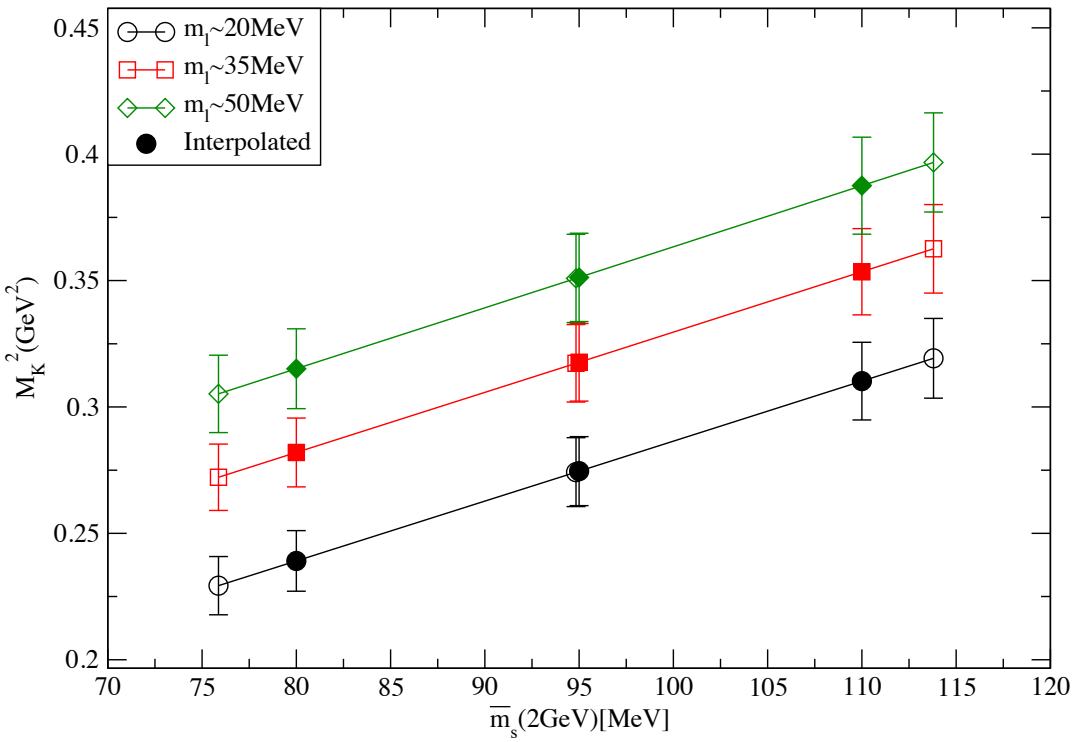

Figure 4.6: Interpolation of lattice data for M_K^2 (empty points) to reference mass for the three sea quark mass of $\beta = 4.05$.

m_l limit, we use the results for the average up/down quark mass and for the lattice spacings obtained in Eqs. (4.23) and (4.27), at each reference value of the strange quark mass. Finally, we study the kaon mass dependence on the strange quark mass, and determine the value of the physical strange quark mass using the experimental value of M_K. In order to account for the electromagnetic isospin breaking effects which are not introduced in the lattice simulation, we have used in the present analysis as "experimental" value of kaon mass the combination [32]:

$$\left(M_K^2\right)_{QCD} = \frac{1}{2}\left[M_{K^0}^2 + M_{K^+}^2 - (1+\Delta_E)\left(M_{\pi^+}^2 - M_{\pi^0}^2\right)\right] = 494.4\,\mathrm{MeV}\,, \tag{4.28}$$

where ΔE parameterize the violation of the Dashen theorem (which states that the K and π masses takes equal EM corrections at first order in e^2), and has been taken equal to 1 as suggested in [33].

4.3.1.2 Chiral and continuum extrapolation

In the first step the strange quark mass is fixed to the reference values and only the m_l and a^2 dependence of the kaon mass is studied

We have considered for the kaon meson mass functional forms based on the predictions of either NLO $SU(2)-$ChPT, which predicts the absence at this order of chiral logs:

$$M_K^2\left(m_s, m_l, a\right) = Q_1\left(m_s\right) + Q_2\left(m_s\right)\, m_l + Q_3\left(m_s\right)\, a^2\,, \quad \forall\, m_s \tag{4.29}$$

for the two steps, or $SU(3)-$ChPT:

$$M_K^2\left(m_s, m_l, a\right) = B_0\left(m_s + m_l\right)\left(1 + Q_6\left(m_s\right) + Q_7\left(m_s\right) m_l + Q_8\left(m_s\right) a^2\right), \forall\, m_s \tag{4.30}$$

where B_0 and f_0 are determined from the pion fit described in the previous section.

For illustration we show in fig. 4.6 the combined chiral/continuum fit based on $SU(2)-$ChPT, Eq. (4.29), for a fixed reference value of the strange quark mass, as a function of the light quark mass.

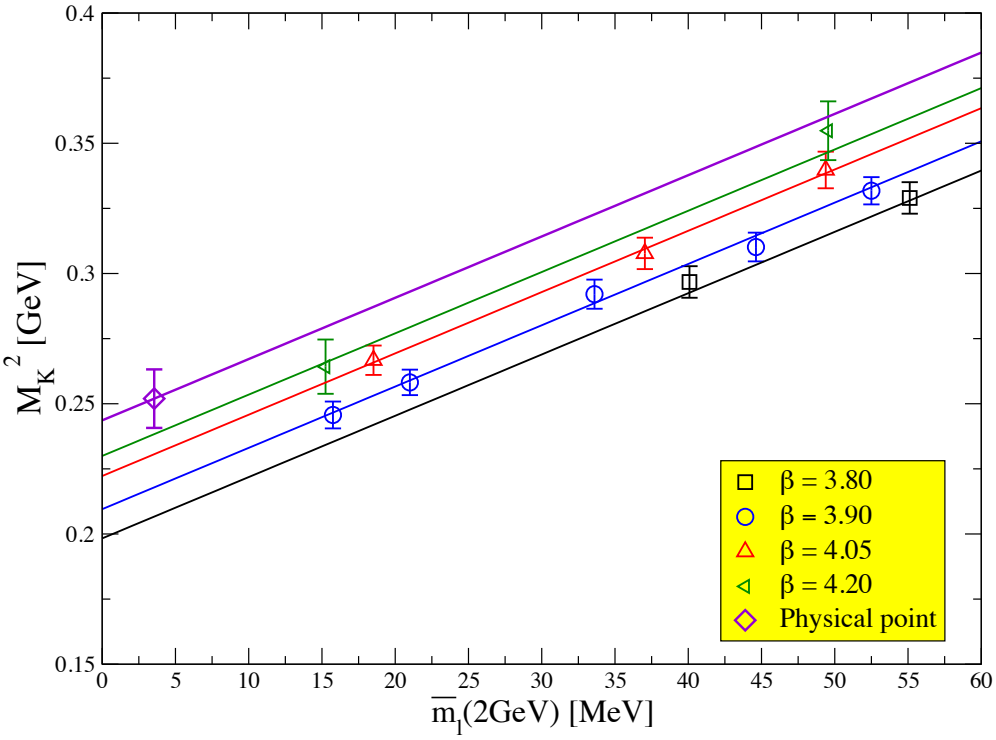

Figure 4.7: Dependence of M_K^2 on the renormalized light quark mass, for a physical strange quark mass and at the four lattice spacings.

4.3.1.3 Study in terms of m_s

The data in the continuum limit and at the physical m_l value are studied as a function of the strange quark mass. The dependence of the kaon mass on the strange quark mass is not determined by the chiral symmetry in the $SU(2)$ theory and we find that, with our choice of three reference strange masses around the physical value, a linear fit as given in Eq. (4.29) is perfectly adequate to describe the data:

$$M_K^2\left(m_s, m_l^{phys}, a = 0\right) = Q_1(m_s) + Q_2(m_s)\, m_l^{phys} = Q_4 + Q_5\, m_s\,, \tag{4.31}$$

with a value of $Q_5 = 2.5(3)\,\mathrm{GeV}$while the $SU(3)-$ChPT prediction read:

$$M_K^2\left(m_s, m_l^{phys}, a=0\right) = B_0 \cdot \left(m_s + m_l^{phys}\right)\left(1 + \frac{2\,B_0\,m_s}{(4\pi f_0)^2}\,\log\frac{2\,B_0\,m_s}{(4\pi f_0)^2} + Q_9\,m_s\right), \qquad (4.32)$$

with a value of $Q_9 = 1.2(2)\,\mathrm{MeV}$ if one takes for B_0 and f_0 the values compute in sec 4.2.5.

In fig. 4.8 the dependence on the strange quark mass is shown, in the case of the $SU(2)$ analysis (Eq. 4.31).

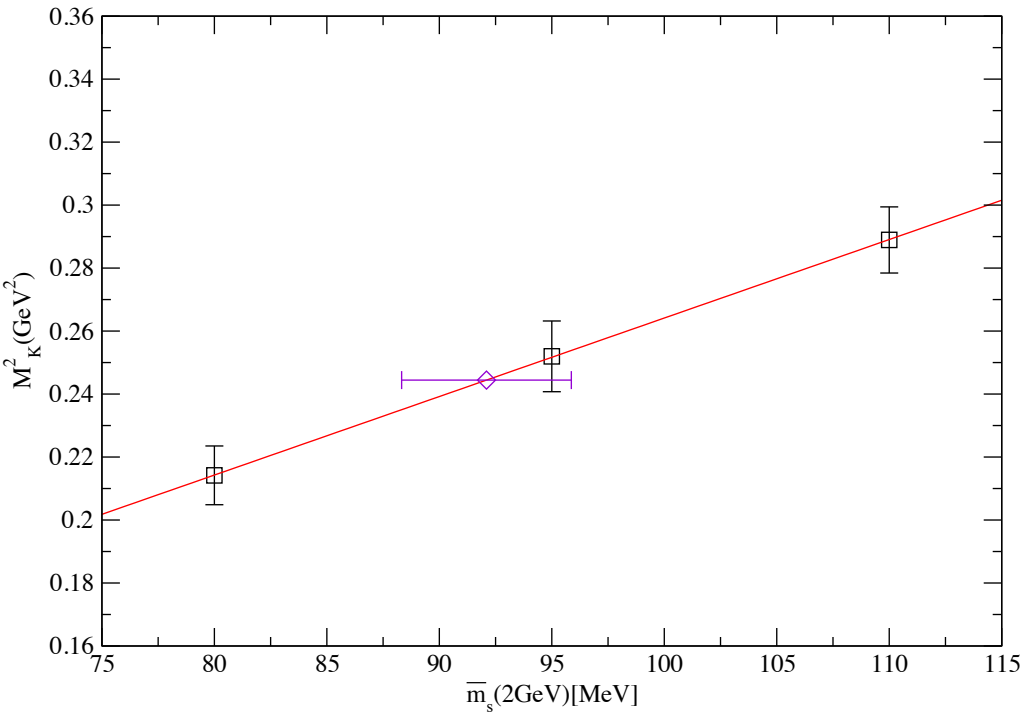

Figure 4.8: Dependence of M_K^2 in the continuum limit and at the physical up/down mass, on the strange quark mass in the $SU(2)-$ChPT analyses. Physical result is shown with empty diamond.

4.3.2 Determination from η_s mass

As an alternative way to determine the strange quark mass we have studied the dependence on m_s of a meson made up of two strange valence quarks [34]. The advantage of this approach is that the mass of this unphysical meson, denoted as η_s, is sensitive to the up/down quark mass only through sea quark effects, and it is thus expected to require only a very smooth chiral extrapolation. This expectation will be confirmed by our analysis. The price to pay is the need for an additional chiral fit required to determine the η_s mass at the physical point.

4.3.2.1 The η_s meson

In the real world, the η_s meson is known to mix with the $\left(\bar{u}u + \bar{d}d\right)$ component to produce the physical η and η' mesons. This mixing proceeds through the contribution of disconnected diagrams, which are known to be rather noisy on the lattice and therefore computationally expensive. In order to avoid this computation we consider here the two strange quarks composing the meson as degenerate in mass but distinct in flavor. Though this η_s meson does not exist in nature, its mass can be determined on the lattice [34], as we will show in the following section.

4.3.2.2 Determination of the physical η_s mass

In order to relate the mass of the η_s meson to the physically observable M_π and M_K, we have studied its dependence on the kaon and pion masses for different values of the simulated light and strange quark masses. This dependence turns out to be well described by both the functional form based on either NLO $SU(2)-$ChPT:

$$M_{\eta_s}^2 = R_1 + R_2\,\left(2\,M_K^2 - M_\pi^2\right) + R_3\,m_\pi^2 + R_4\,a^2\,, \tag{4.33}$$

or $SU(3)-$ChPT:

$$\begin{aligned} M_{\eta_s}^2 &= \left(2\,M_K^2 - M_\pi^2\right)\cdot\left[1 + (\xi_s - \xi_l)\,\log\left(2\,\xi_s\right) + (R_7+1)\,(\xi_s - \xi_l) + R_8\,a^2\right] - \\ &- M_\pi^2\,\left[-\xi_l\,\log\left(2\,\xi_l\right) + \xi_s\,\log\left(2\,\xi_s\right) + R_7\,(\xi_s - \xi_l)\right]\,, \end{aligned} \tag{4.34}$$

with $\xi_l = M_\pi^2/\left(4\,\pi\,f_0\right)^2$ and $\xi_s = \left(2\,M_K^2 - M_\pi^2\right)/\left(4\,\pi\,f_0\right)^2$, obtained from the ChPT formulae given in Eqs. (4.36 - 4.39) by replacing quark masses in terms of meson masses, and keeping terms up to NLO. We observe that, within the accuracy of our lattice data, the $\mathcal{O}(a^2)$ term in the η_s mass is found to be independent of the strange quark mass.

In fig. 4.9 we show the $SU(2)$ determination of the mass of the η_s meson. Only data near the physical point have been considered. The quantities $M_{\eta_s}^2$ and $(2M_K^2 - M_\pi^2)$ are highly correlated, and correlation has been taken into account when building the χ^2 as explained in section 3.4.4.2. In the figure we show also the prediction of the Gell-Mann-Okubo law ($M_{\eta_s}^2 = (2M_K^2 - M_\pi^2)$) for comparison.

Once the physical values of the kaon and pion mass are inserted in eqs. (4.33) and (4.34),we find that the two fits yield very close results for the η_s meson mass, namely:

$$M_{\eta_s} = 692(1)\text{MeV} \quad \text{from SU(2)}\,, \qquad M_{\eta_s} = 689(2)\text{MeV} \quad \text{from SU(3)} \tag{4.35}$$

to be compared with the leading order $SU(3)$ prediction (Gell-Man-Okubo law): $(M_{\eta_s})_{LO} = \sqrt{2\,M_K^2 - M_\pi^2} = 686\,\text{MeV}$ and with the lattice determination of [34] $M_{\eta_s} = 686(4)\,\text{MeV}$.

4.3.2.3 Chiral and continuum extrapolation

Once the mass of the η_s meson has been determined, the strange quark mass can be extracted by following the very same procedure described for the case of the kaon mass. At first, at fixed reference strange mass lattice data are extrapolated to the continuum and to the physical up/down mass.

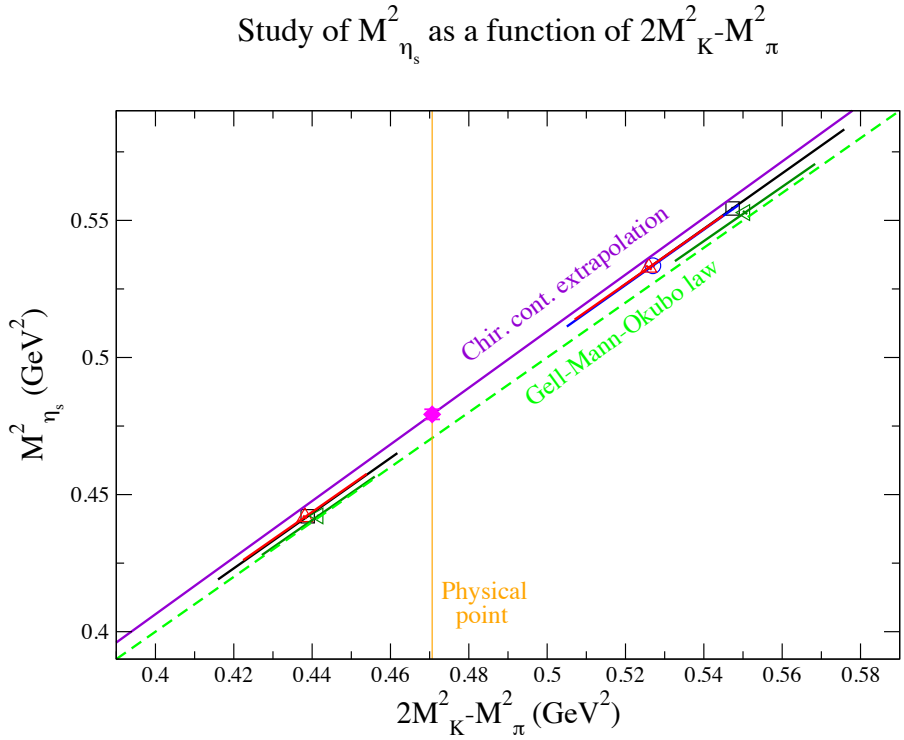

Figure 4.9: Dependence of $M^2_{\eta_s}$ from $2M^2_K - M^2_\pi$ in SU(2)-ChPT analyses. Segments show correlated errors (errors along the direction perpendicular to the diagonal are very small).

We have considered the following fitting functions based on NLO-ChPT for the dependence of the η_s meson on the (sea) up/down quark mass and on the leading discretization effects:

$$M^2_{\eta_s}(m_s, m_l, a) = T_1(m_s) + T_2(m_s)\, m_l + T_3(m_s)\, a^2\,, \quad \forall\, m_s\,, \tag{4.36}$$

in SU(2), and:

$$M^2_{\eta_s}(m_s, m_l, a) = 2\, B_0\, m_s \cdot (1 + T_6\,(m_s) + T_7(m_s)\, m_l + T_8(m_s)\, a^2)\,, \quad \forall\, m_s\,, \tag{4.37}$$

in SU(3).

In fig. (4.10) we show as example the chiral and continuum extrapolation of $M^2_{\eta_s}$ in SU(2) chiral perturbation theory. The scale on y axis has been chosen the same of fig. (4.7) to show the smallness of the chiral extrapolation compared to that of M^2_K.

4.3.2.4 Study in terms of m_s

After this extrapolation, the value of the physical strange quark mass is extracted studying the dependence on the strange mass. We have considered the following fitting functions based on NLO-ChPT for the dependence of the η_s meson on the strange quark mass:

$$M^2_{\eta_s}(m_s, m_l^{phys}, a = 0) \equiv T_1(m_s) + T_2(m_s)\, m_l^{phys} = T_4 + T_5\, m_s\,, \tag{4.38}$$

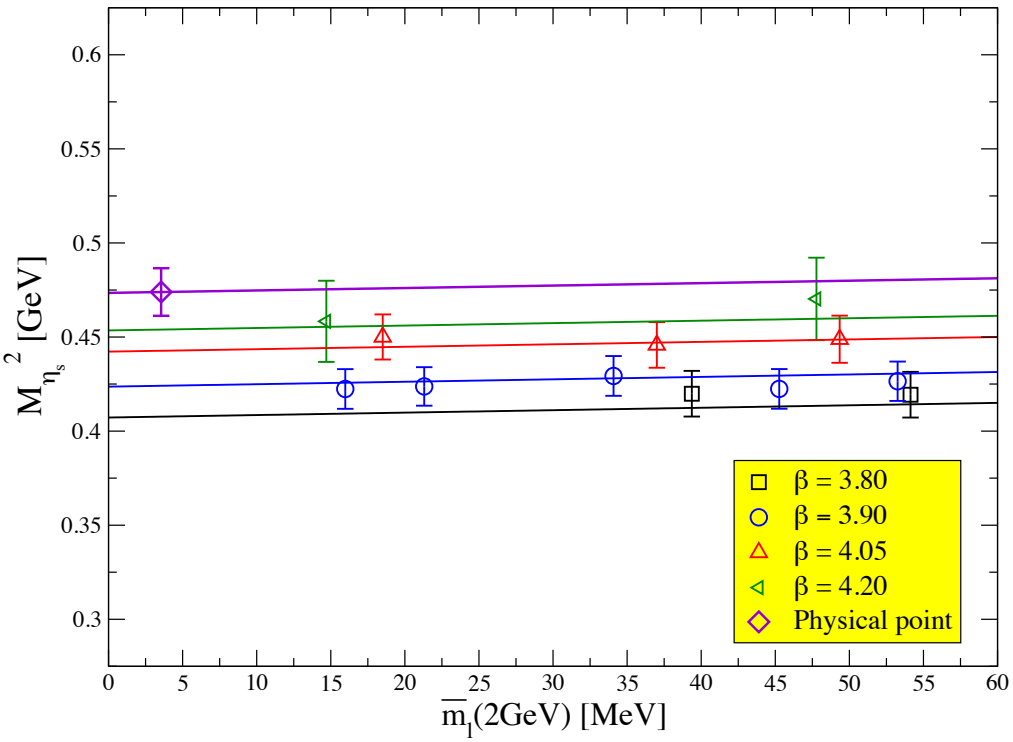

Figure 4.10: Dependence of $M^2_{\eta_s}$ on the renormalized light quark mass, for a fixed reference strange quark mass ($\overline{m}_s^{ref} = 95\,\mathrm{MeV}$) and at the four lattice spacings.

in SU(2), with a value of $T_5 = 5.10(14)$ GeV and:

$$M^2_{\eta_s}(m_s, m_l^{phys}, a=0) \equiv 2\,B_0\,m_s \cdot (1 + T_6\,(m_s) + T_7(m_s)\,m_l^{phys}) = \\ = 2\,B_0\,m_s \cdot \left(2\,\frac{2\,B_0\,m_s}{(4\pi f_0)^2}\,\log\left(2\,\frac{2\,B_0\,m_s}{(4\pi f_0)^2}\right) + T_9 + T_{10}\,m_s\right)\,, \tag{4.39}$$

in SU(3). The LECs T_2 and T_7, describing the dependence on the light quark mass, are found to be independent of the strange mass, within the accuracy of our lattice data. They are then fitted with a single parameter for all reference strange quark masses.

4.3.3 Determination of $\bar{m}_s$

In order to quote a final estimate for the strange quark mass we choose as a central value the weighted average of the results from the four determinations discussed above, namely from K and η_s and based on SU(2)- and SU(3)-ChPT. In the $\overline{\mathrm{MS}}$ scheme at 2 GeV this average reads $\overline{m}_s^{\overline{\mathrm{MS}},\,2\,\mathrm{GeV}} = 95(2)\,\mathrm{MeV}$, with the 2 MeV error representing the typical statistical and fitting uncertainty. Let us discuss the systematics uncertainty common to the two determinations of $\overline{m}_s$.

Chiral extrapolation The difference between the determinations based on the K and η_s mesons is about 3%. The results obtained from either the SU(2) or the SU(3) fits are practically the same in the analysis based on the η_s and differ by approximately 3% in the kaon case. In table (4.2) we collect the result of all these determinations of $\bar{m}_s$.

$\overline{m}_s$ [MeV]	$K-$SU(2)	$K-$SU(3)	η_s-SU(2)	η_s-SU(3)
L1	92.1(3.8)	94.7(2.2)	96.0(2.6)	95.5(2.1)
L2	91.6(3.9)	94.6(2.3)	95.4(2.6)	95.3(1.9)
L3	95.4(3.8)	94.7(2.1)	99.4(2.9)	97.7(2.2)

Table 4.2: Results for the strange quark mass in the $\overline{\rm MS}$ scheme at 2 GeV, as obtained from the different fits within the light and strange quark sectors.

Continuum extrapolation In order to evaluate the uncertainty of the continuum extrapolation we have proceeded in two ways. We have added an $\mathcal{O}(a^4)$ mass independent term in Eqs. (4.36-4.39), and we have (alternatively) excluded from these fits the data from the coarser lattice ($\beta = 3.80$). We find that the $\mathcal{O}(a^4)$ term turns out to be hardly determined in the fit, leading to three times larger uncertainties. The exclusion of $\beta = 3.80$ data, instead, yields a variation of the results of approximately 2% leaving the fitting error approximately unchanged. We then assume $\pm 2\%$ as uncertainty related to the continuum extrapolation.

Renormalization We include also in this case an uncertainty of 2% related to the truncation of the perturbative expansion in the conversion from the RI-MOM to the $\overline{\rm MS}$ scheme. The results for the strange quark mass obtained from both the kaon and the η_s meson masses turn out to be well consistent.

Final result Combining all these uncertainties in quadrature, we quote as our final estimate of the strange quark mass in the $\overline{\rm MS}$ scheme:

$$\overline{m}_s^{\overline{\rm MS},\,2\,\rm GeV} = 95(2)(6)\,\rm MeV = 95(6)\,\rm MeV\,. \tag{4.40}$$

We observe that our result for the strange mass in Eq. (4.40) is, though compatible, smaller than the value obtained by ETM collaboration in ([35]) at a fixed value of the lattice spacing ($a \simeq 0.085$fm). This is a consequence of discretization effects, which are at the level of 15% in M_K^2 on the $a \simeq 0.085$fm lattice, as shown in fig. (4.7). A further comparison can be done with the ETMC estimate of the strange quark mass that appeared in the recent work on the bag parameter B_K ([22]). Within that analysis, based on data at three β values (3.80, 3.90 and 4.05), the strange quark mass is determined from the same lattice setup by performing an $SU(2)$ chiral fit of the kaon meson mass, whose result (obtained using preliminary values for the lattice spacings and renormalization constants) reads: $\overline{m}_s^{\overline{\rm MS},\,2\,\rm GeV} = 92(5)\,\rm MeV$.

4.3.4 The m_s/m_l ratio

Using our determinations of both the strange and light quark masses, we can obtain a prediction for the ratio m_s/m_l, which is both a scheme and scale independent quantity. The several m_s/m_l values obtained from different fits are collected in Table (4.3). The result that we quote as our final estimate is

$$m_s/m_l = 27.3(5)(7) = 27.3(9)\,. \tag{4.41}$$

The results for the ratio m_s/m_l collected in Table (4.3) are slightly different from the ratios of the $\bar{m}_s$ and $\bar{m}_l$ results. This difference originates from the fact that in the ratio m_s/m_l the quark

m_s/m_l	K-SU(2)	K-SU(3)	η_s-SU(2)	η_s-SU(3)
L1	26.9(5)	27.2(5)	27.6(4)	27.3(7)
L2	27.1(5)	26.9(3)	27.5(3)	26.8(3)
L3	25.7(5)	26.0(6)	26.5(6)	26.0(7)

Table 4.3: Results for the ratio m_s/m_l, as obtained from the different fits within the light and strange quark sectors.

mass renormalization constant Z_P^{-1} exactly cancels out, whereas in the determinations of $\bar{m}_s$ and $\bar{m}_l$ the central values of Z_P are slightly modified by the fitting procedure.

4.4 Charm quark mass

The determination of the charm quark mass follows, quite closely, the strategy adopted in the determination of the strange quark mass discussed in the previous section. In this case, we use as experimental input the masses of the D, D_s and η_c mesons.

4.4.1 Preliminary interpolation

As for the strange quark case, the analysis requires an interpolation of the lattice data, being the simulated charm masses roughly in the range $0.9\, m_c^{phys} \lesssim \mu_c \lesssim 2.0\, m_c^{phys}$. In order to better study the a^2 and m_l dependence of charmed meson masses, we first use a quadratic spline fit to interpolate the data at three reference values of the charm mass which are equal at the four β values: $\bar{m}_c^{ref,\overline{\rm MS},\,2{\rm GeV}} = \{1.08\,,\ 1.16\,,\ 1.24\}\,{\rm GeV}$. We have verified that different choices of the set of reference masses leaves the charm quark results unchanged.

4.4.2 Chiral and continuum extrapolation

At fixed reference charm mass, we then study the dependence of the D, D_s and η_c meson on the up/down mass (and on the strange mass in the case of the D_s meson) and on discretization terms, thus getting the results for the meson masses in the continuum limit, at the physical values of the light (and strange) quark masses, and at the reference charm mass.

In order to fit the meson masses we have considered the following (phenomenological) polynomial fits, which turn out to describe well the dependence on the light and strange quark masses and on the lattice cutoff of the D, D_s and η_c meson masses, at fixed reference charm mass m_c,

$$m_H(m_c, m_s, m_l, a) = C_1^H(m_c) + C_2^H(m_c)\, m_l + C_3^H(m_c)\, m_s + C_4^H(m_c)\, a^2\,, \quad \forall m_c\,, \tag{4.42}$$

with $H = D, D_s, \eta_c$. From the fits, we find that the coefficients C_2^H and C_3^H turn out to be independent of the charm mass within the statistical errors. The latter coefficient C_3^H, of course, enters the fit only in the D_s case.

In fig. (4.11) we show the dependence of the D, D_s and η_c masses on the light quark mass at a fixed reference charm mass, for the four β. For the D_s and η_c mesons, which contain the light quark in the sea only, this dependence turns out to be practically invisible.

In Fig. (4.12) the meson masses at physical light and strange quark masses are shown as a function of a^2, for a reference value of the charm quark mass. As can be seen from this plot,

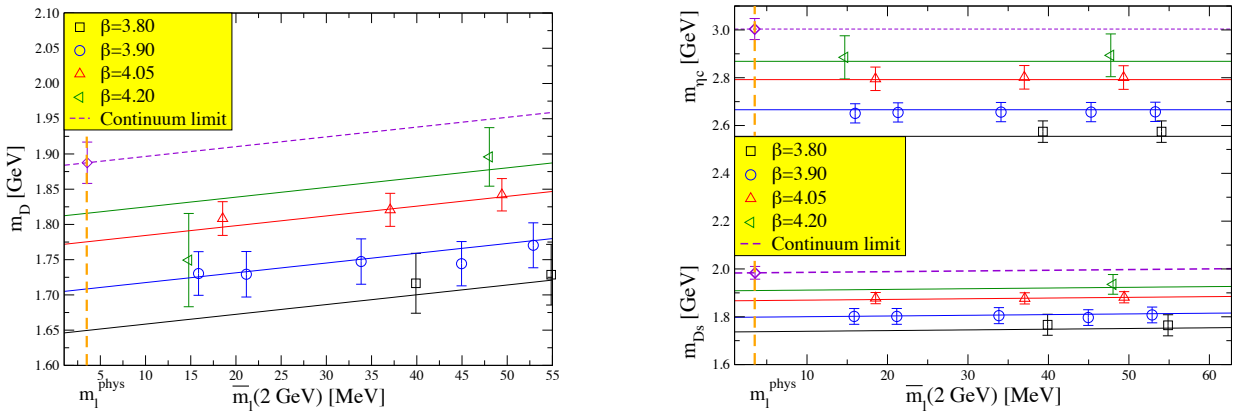

Figure 4.11: Left: Dependence of M_D (left) and M_{D_s} and M_{η_c} (right) on the light quark mass, at fixed reference charm quark mass ($\bar{m}_c^{ref} = 1.16\,\mathrm{GeV}$) and for the four simulated lattice spacings. For the D_s meson the strange quark mass is fixed to its physical value.

discretization effects on the η_c meson mass vary from approximately 4% on the finest lattice up to 14% on the coarsest one. These effects are larger than those affecting the D and D_s meson masses by approximately 30%. Fig. (4.12) also shows that the dependence of the three charmed meson masses on a^2 is very well described by a linear behavior. Attempting to vary the continuum extrapolation from the simple linear fit produces only small effects: in order to estimate the uncertainty due to the continuum extrapolation we have proceeded in two ways. We have either added in the fitting form of Eq. (4.42) an $\mathcal{O}(a^4)$ dependence, which turns out to be hardly determined thus leading to uncertainties larger by a factor three, or we have excluded the data from the coarser lattice (with $a \simeq 0.098\,\mathrm{fm}$). This latter analysis yields a variation of the results of approximately 1.5%.

4.4.3 Determination of $\bar{m}_c$

Finally, the value of the physical charm quark mass is extracted by fitting these data as a function of the charm quark mass and using as an input the experimental value of the corresponding charmed meson $M_D^{exp} = 1.870\,\mathrm{GeV}$, $M_{D_s}^{exp} = 1.969\,\mathrm{GeV}$, $M_{\eta_c}^{exp} = 2.981\,\mathrm{GeV}$[2]. In fig. 4.13 we show the dependence of the D, D_s and η_c masses on the charm mass (in the continuum limit and at physical light and strange mass).

A constant plus either a linear or a $1/m_c$ term have been considered for describing data of the D, D_s and η_c mesons, namely:

$$m_H(m_c, m_s^{phys}, m_l^{phys}, a = 0) \quad = \quad C_5^H + \frac{C_6^H}{m_c} + C_7^H\, m_c\,. \tag{4.43}$$

Since we have data at three reference charm masses (close to the physical charm), we can keep only one of the coefficients C_6^H, C_7^H different from zero. We find that both choices describe very

[2]The experimental value of the meson masses should be corrected to take into account the absence of electromagnetic effects and, in the case of the η_c, of disconnected diagrams in the lattice calculation. For the η_c meson, these corrections are estimated to be of the order of 5 MeV [34], thus affecting the extracted charm quark mass to approximately 0.2%. Similar corrections are expected for the D and D_s mesons. Given our uncertainties, we can safely neglect these corrections in the analysis.

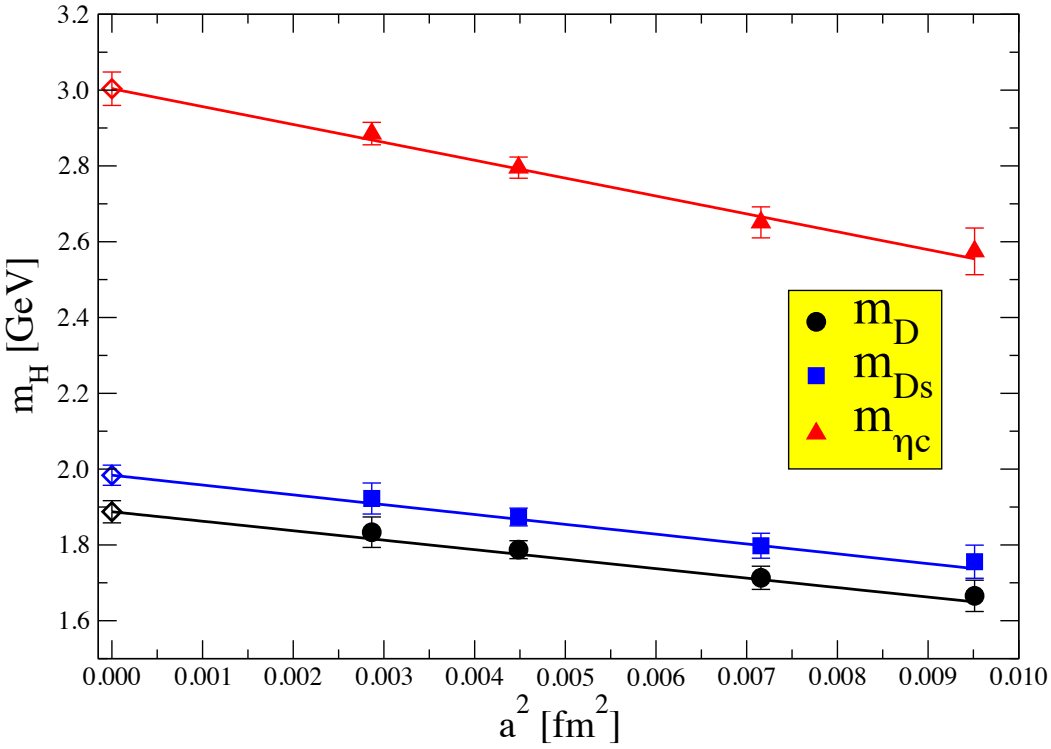

Figure 4.12: Dependence of m_D, m_{D_s} and m_{η_c}, at fixed reference charm quark mass ($\bar{m}_c^{ref,\overline{\rm MS},\,2{\rm GeV}} = 1.16\,{\rm GeV}$) and at physical up/down and strange quark mass, on the squared lattice spacing. Empty diamonds represent continuum limit results.

well the lattice data and affect only in a marginal way the interpolation to the physical charm mass. The two dependencies of the meson masses on the charm quark mass, considered in Eq. (4.43), yield results that differ by only few MeV. The systematic uncertainty then comes from the sum in quadrature of the approximately 1% spread among the three determinations from the D, D_s and η_c mesons, the 1.5% uncertainty due to discretization effects and the 2% uncertainty coming from the perturbative conversion of the renormalization constants from the RI-MOM to the $\overline{\rm MS}$ scheme.

We quote as our final result for the charm quark mass in the $\overline{\rm MS}$ scheme

$$\begin{aligned} \bar{m}_c(2{\rm GeV}) &= 1.14(3)(3)\,{\rm GeV} = 1.14(4)\,{\rm GeV} \\ \rightarrow \quad \bar{m}_c(\bar{m}_c) &= 1.28(4)\,{\rm GeV}\,, \end{aligned} \tag{4.44}$$

where the evolution to the more conventional scale given by $\bar{m}_c$ itself has been performed at N^{3}LO [29] with $N_f = 2$, consistently with our non-perturbative evaluation of the renormalization constant. Had we evolved with $N_f = 4$, which is the number of active flavors above $\mu = m_c$, the result for $\bar{m}_c(\bar{m}_c)$ would have increased by less than one standard deviation.

Our result is compatible with the preliminary estimate of the charm quark mass, $\bar{m}_c(2{\rm GeV}) = 1.23(6)$, obtained by ETMC [36] using data at three lattice spacings and preliminary values for the renormalization constants. It is also in good agreement with the HPQCD result $\bar{m}_c(\bar{m}_c) = 1.268(9)\,{\rm GeV}$ [37], with a larger uncertainty in our determination. Finally, our result is in good agreement with the recent sum rules determination $\bar{m}_c(\bar{m}_c) = 1.279(13)\,{\rm GeV}$ of [38].

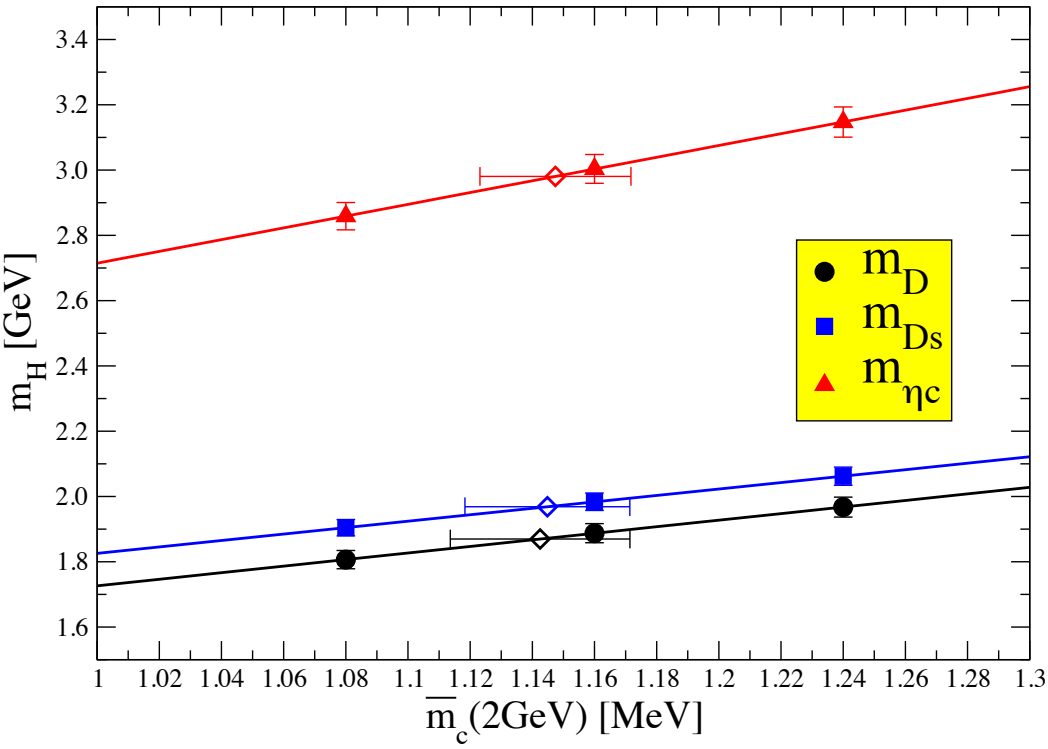

Figure 4.13: Dependence of m_D, m_{D_s} and m_{η_c}, in the continuum limit and at physical up/down and strange quarks, on the charm quark mass. The charm mass results from the three determinations are also shown, with empty diamonds.

4.4.4 The m_c/m_s ratio

We also provide a prediction for the scheme and scale independent ratio m_c/m_s. The several m_c/m_s values obtained from different fits are collected in Table (4.4).

	K-SU(2)	K-SU(3)	η_s-SU(2)	η_s-SU(3)
m_c/m_s	12.4(4)	12.1(2)	11.9(2)	12.0(3)

Table 4.4: Results for the ratio m_c/m_s, as obtained from the different fits within the strange quark sector, and from the analysis of the D meson mass in the charm sector. Determination from D_s and η are almost identical.

The result that we quote as our final estimate is

$$m_c/m_s = 12.0(3)\,, \tag{4.45}$$

in good agreement with the other recent lattice determination $m_c/m_s = 11.85(16)$ [34].

Chapter 5

B-physics

As discussed in chapter 2 the study of process involving the b quark offer important windows to indirect effects of new physics. The value of the B and B_s meson leptonic decay constant f_B and f_{B_s}, the form factors parameterizing semi-leptonic decays of $B \to D\,(D^*)\,l\nu$ and $B \to \pi\,(\rho)\,l\nu$, and the bag parameters B_B which parametrize the oscillation of neutral B meson system are decisive ingredients in extracting elements of the CKM matrix. Lattice QCD is the only method which allow one to compute these quantities non-perturbatively in a model independent manner.

Unfortunately with the available computer power it is not possible to simulate quark masses in the range of the physical b mass and at the same time keep the finite volume and discretization effects under control. In order to circumvent these problems, many different methods have been proposed so far (for a recent review see [39]).

In this work we used the $N_f = 2$ gauge ensemble already discussed in the previous chapters to determine the b quark mass and f_B, f_{B_s} decay constants. In none of these ensembles the lattice spacing is smaller than inverse b quark mass, which can be estimated to be of the order of $\sim 4\,\mathrm{GeV}$. The physical b quark mass expressed in lattice units, am_b is larger than 1 for all ensembles, and one expect large discretization effects (in principle of order 100%) when computing directly quantities at the physical b quark mass. In our work we have avoided to compute the quantities of our interest directly at the physical b quark, and have instead performed an interpolation of data computed from the c quark region together with information coming from the static limit $m_q \to \infty$.

We have used two different methods to tackle this interpolation, which differs in the way in which the static limit information is used.

In section 5.2 we will show how it is possible to introduce suitable ratio for the quantities of interest with its exactly known limit for $m_b \to \infty$ [36], and so thereby avoid to perform computation in the static limit. Using this approach (which will be referred as "ratio method" in the following) it has been possible to perform a calculation of the b quark mass and the decay constants f_B and f_{B_s} without performing any static calculation.

In section 5.3 a more standard method [40] was applied, in which the extrapolation is done using explicitly information calculated in the static limit point. This which will be called "interpolation method" in the following do not allow to determine the b quark mass. Preliminary results for f_B and f_{B_S} studied in terms of the meson mass M_B, M_{B_s} were presented in [41].

The two methods have been discussed together in the paper [**?**] where results obtained with the two approach have been found to be compatible, and their errors similar in size.

As a byproduct of this analysis we also obtain the results for f_D and f_{D_s} decay constants, which will shortly discussed in section 5.3.5. This updates and improves a previous result by the ETM collaboration [42].

Our analysis indicates that the discretization effects are not as large as one would expect them to be. In other words the discretization errors are not the main source of error in our computation: instead, the limitations to use directly the data at the physical b quark mass comes from the fact that as the quark mass increases the gap between lower lying and excited states decreases, so that the ground state is isolated at times that gets larger and larger, where the correlation functions are typically noisier. Moreover the correlation functions becomes noisier and noisier as the heavy quark mass increases. In order to make a step in the direction of using heavier masses, in section 5.4 we present preliminary results obtained with the aid of smearing techniques discussed in section 5.4, which revealed to be extremely efficient in both reducing the excited state contamination and in improving the signal to noise ratio. In the near future these techniques might be the key factors to perform calculation closer to the b quark mass.

5.1 Simulation details

At variance with the analysis of chapters 4 and 6, where only the light, strange and charm quark masses were studied, a wider range of values for the valence quark masses is considered here, in order to get closer to the physical b quark mass. The values of the simulated valence quark masses are collected in Table 5.1. The valence light quark mass, μ_ℓ, is always taken to be identical with those of the sea quarks. The heavy quark mass μ_h ranges from approximately m_c up to $(2.3 - 2.4)\, m_c$, with m_c the physical charm quark mass. Correlators at higher μ_h have been computed and were included in [41]. They are characterized by large fluctuations in the effective mass plateaux, and thus by large statistical uncertainties. As a consequence, data extracted from these correlators turns out to be irrelevant in the fits, and we have excluded them from the present analysis.

β	$a\mu_\ell$	$a\mu_s$	$a\mu_h$	t_{min}/a
3.80	0.0080, 0.0110	0.0165, 0.0200 0.0250	0.2143, 0.2406, 0.2701, 0.3032 0.3403, 0.3819, 0.4287, 0.4812	14
3.90	0.0030, 0.0040, 0.0064, 0.0085, 0.0100	0.0150, 0.0180 0.0220	0.2049, 0.2300, 0.2582, 0.2898 0.3253, 0.3651, 0.4098, 0.4600	16
4.05	0.0030, 0.0060, 0.0080	0.0135, 0.0150, 0.0180	0.1663, 0.1867, 0.2096, 0.2352 0.2640, 0.2963, 0.3326, 0.3733	21
4.20	0.0020, 0.0065	0.0130, 0.0148 0.0180	0.1477, 0.1699, 0.1954, 0.2247 0.2584, 0.2971, 0.3417	25

Table 5.1: Values of simulated bare quark masses in lattice units, for the four β values, in the light ($a\mu_\ell$), strange ($a\mu_s$) and heavy ($a\mu_h$) sectors. In the last column the minimum values of time t_{min} chosen for the 2-point function fits are collected.

In figure 5.1 we show for each β the effective mass of B mesons composed of a light quark of about 50MeV (in $\overline{\text{MS}}$ at 2 GeV) and the heaviest considered quark, together with the larger one computed in [41] but neglected in the present work. For comparison we also show the B_s meson. The horizontal lines are values of the meson masses obtained by the fits of the correlators.

The minimal time considered in the fit is the same for all the four β when expressed in physical units. This has been obtained by scaling appropriately the t_{min} of $\beta = 3.90$, in such a way that possible contaminations with scalar mesons due to the parity breaking at finite lattice spacing will be removed when taking the continuum limit.

For all values of β the ground state is clearly identified and the signal is clean within the lower plotted combinations, but the same is not true for the higher ones, and as already stated their inclusion would practically have no impact on the analysis.

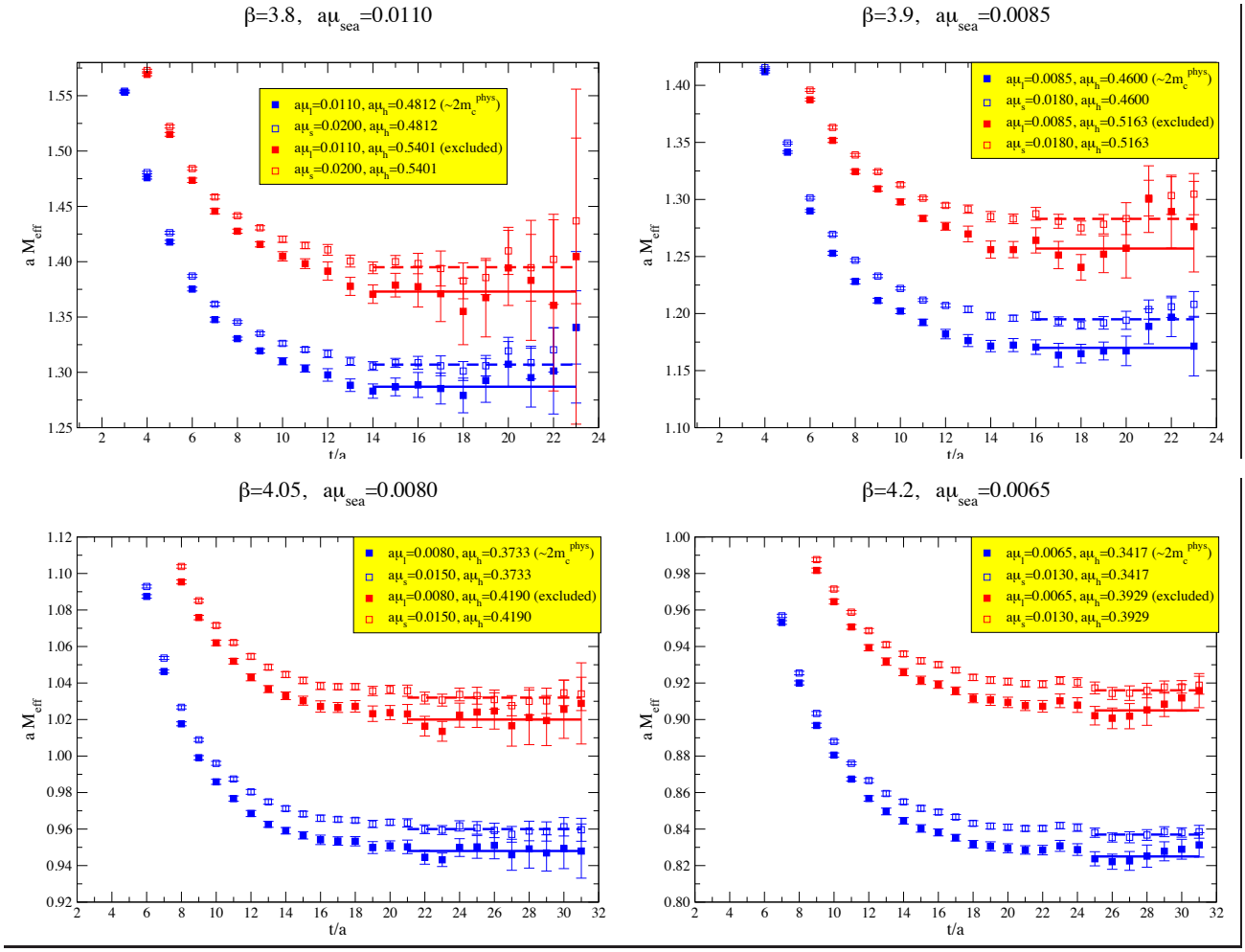

Figure 5.1: Effective masses of heaviest B (filled squares) and B_s (empty squares) mesons considered in the analysis (in blue) together with an heavier combination not considered in the present work (in red). For all mesons the light quark (valence and sea) is about 50 MeV.

5.2 Determination of $\bar{m}_b$

The method that we have used to determine the quark mass is suggested by the Heavy Quark Effective Theory (HQET) asymptotic behavior of the heavy-light meson mass $M_{h\ell}$:

$$\lim_{\mu_h^{\rm pole}\to\infty}\left(\frac{M_{h\ell}}{\mu_h^{\rm pole}}\right) = \text{constant}\ , \tag{5.1}$$

where $\mu_h^{\rm pole}$ is the pole quark mass and the limit (5.1) is approached without corrections of $\mathcal{O}(1/\log(\mu_h^{\rm pole}/\Lambda_{\rm QCD}))$. Let us describe the method in details.

5.2.1 Ratio method

As a first step we consider an appropriate sequence of heavy quark masses, $\bar{\mu}_h^{(1)}$, $\bar{\mu}_h^{(2)}$, ... , $\bar{\mu}_h^{(N)}$, with fixed ratio:

$$\frac{\bar{\mu}_h^{(n)}}{\bar{\mu}_h^{(n-1)}} = \lambda\ , \tag{5.2}$$

and ranging from the charm mass to values somewhat below the bottom mass.

Then one computes the following ratios that have an exactly known static limit:

$$\begin{aligned} y(\bar{\mu}_h^{(n)},\lambda;\bar{\mu}_\ell,a) &\equiv \frac{M_{h\ell}(\bar{\mu}_h^{(n)};\bar{\mu}_\ell,a)}{M_{h\ell}(\bar{\mu}_h^{(n-1)};\bar{\mu}_\ell,a)}\cdot\frac{\bar{\mu}_h^{(n-1)}}{\bar{\mu}_h^{(n)}}\cdot\frac{\rho(\bar{\mu}_h^{(n-1)},\mu^*)}{\rho(\bar{\mu}_h^{(n)},\mu^*)} = \\ &= \lambda^{-1}\frac{M_{h\ell}(\bar{\mu}_h^{(n)};\bar{\mu}_\ell,a)}{M_{h\ell}(\bar{\mu}_h^{(n)}/\lambda;\bar{\mu}_\ell,a)}\cdot\frac{\rho(\bar{\mu}_h^{(n)}/\lambda,\mu^*)}{\rho(\bar{\mu}_h^{(n)},\mu^*)}\,, \qquad n=2,\cdots,N\,. \end{aligned} \tag{5.3}$$

The function $\rho(\bar{\mu}_h,\mu^*)$ converts the renormalized $\overline{\rm MS}$ quark mass (at the scale μ^*) into the pole mass:

$$\mu_h^{\rm pole} = \rho\left(\bar{\mu}_h,\mu^*\right)\ \bar{\mu}_h\left(\mu^*\right)\ , \tag{5.4}$$

known up to N^{3}LO in perturbation theory [29, 43–48]. The NLO expression reads:

$$\begin{aligned} \rho(\bar{\mu}_h,\mu^*) = &\left[1+\frac{16}{3}\cdot\frac{\alpha^{\overline{\rm MS}}(\bar{\mu}_h)}{4\pi}\right]\cdot\left(\frac{\alpha^{\overline{\rm MS}}(\bar{\mu}_h)}{\alpha^{\overline{\rm MS}}(\mu^*)}\right)^{12/(33-2\,N_f)}\ \cdot \\ &\left[1+\left(\frac{2(4491-252\,N_f+20\,N_f^2)}{3(33-2\,N_f)^2}\right)\frac{\alpha^{\overline{\rm MS}}(\bar{\mu}_h)-\alpha^{\overline{\rm MS}}(\mu^*)}{4\pi}\right], \end{aligned} \tag{5.5}$$

used for $N_f=2$ in the present analysis. We notice that the dependence on the scale μ^* cancels in the ratios of ρ factors evaluated at different heavy quark masses and thus in the y ratio defined in Eq. (5.3).

From Eq. (5.1) and QCD asymptotic freedom it follows that the ratios (5.3) have the following static limit:

$$\lim_{\bar{\mu}_h\to\infty} y(\bar{\mu}_h,\lambda;\bar{\mu}_\ell,a=0) = 1\,. \tag{5.6}$$

The value of the ratio λ of Eq. (5.2), between two subsequent values of the heavy quark mass, is chosen in such a way that after a finite number of steps the heavy-light meson mass assumes the

experimental value $M_B = 5.279$ GeV (we find $\lambda = 1.1762$). In order to implement this condition, the lattice data at the four lattice spacings are interpolated at the following values of the heavy quark mass,

$$\bar{\mu}_h^{(1)} = 1.140 \text{ GeV} \ , \ \bar{\mu}_h^{(2)} = \lambda\, \bar{\mu}_h^{(1)} = 1.341 \text{ GeV} \ , \ \bar{\mu}_h^{(3)} = \lambda^2 \bar{\mu}_h^{(1)} = 1.577 \text{ GeV} \, , \tag{5.7}$$
$$\bar{\mu}_h^{(4)} = \lambda^3 \bar{\mu}_h^{(1)} = 1.855 \text{ GeV} \ , \ \bar{\mu}_h^{(5)} = \lambda^4 \bar{\mu}_h^{(1)} = 2.182 \text{ GeV} \ , \ \bar{\mu}_h^{(6)} = \lambda^5 \bar{\mu}_h^{(1)} = 2.566 \text{ GeV} \, .$$

5.2.2 Chiral and continuum extrapolation

Ratios of the kind defined in Eq. (5.3) are introduced because, besides having an exactly known static limit, they are also expected [36] to have a smooth chiral and continuum limit, as shown in the right plot of fig. 5.2. For this reason we perform a simple linear extrapolation of $M_{h\ell}$ and of y.

In fig. 5.2 (left) we show the (linear) chiral and $a^2 \to 0$ extrapolation of the heavy-light meson mass at the first heavy quark mass $\bar{\mu}_h^{(1)}$, namely $M_{h\ell}(\bar{\mu}_h^{(1)})$, for the four β values.

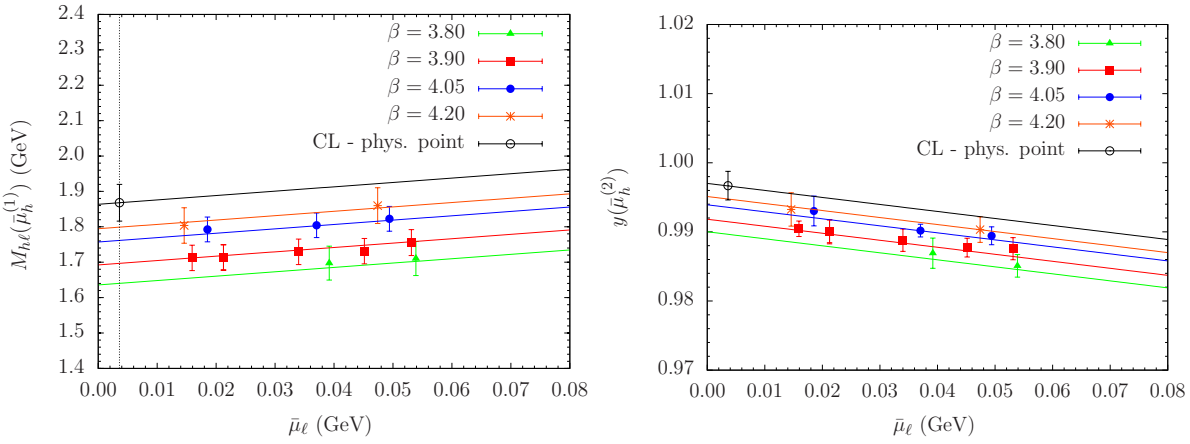

Figure 5.2: Light quark mass dependence of the meson mass $M_{h\ell}(\bar{\mu}_h^{(1)})$ (left) and of the ratio $y(\bar{\mu}_h^{(2)})$ (right) at the four values of the lattice spacing.

5.2.3 Static limit interpolation

After performing the continuum and chiral extrapolation of the ratios (5.3), we study their dependence on the inverse heavy quark mass. Inspired by HQET, we perform a polynomial fit in $1/\bar{\mu}_h$, of the form

$$y(\bar{\mu}_h) = 1 + \frac{\eta_1}{\bar{\mu}_h} + \frac{\eta_2}{\bar{\mu}_h^2} \, , \tag{5.8}$$

which imposes the constraint $y = 1$ at the static point. The fit is illustrated in fig. 5.3.

The value of the b quark mass is finally determined by considering the following equation

$$y(\bar{\mu}_h^{(2)})\, y(\bar{\mu}_h^{(3)}) \, \ldots \, y(\bar{\mu}_h^{(K+1)}) = \lambda^{-K} \, \frac{M_{hu/d}(\bar{\mu}_h^{(K+1)})}{M_{hu/d}(\bar{\mu}_h^{(1)})} \cdot \left[\frac{\rho(\bar{\mu}_h^{(1)}, \mu^*)}{\rho(\bar{\mu}_h^{(K+1)}, \mu^*)} \right] \, , \tag{5.9}$$

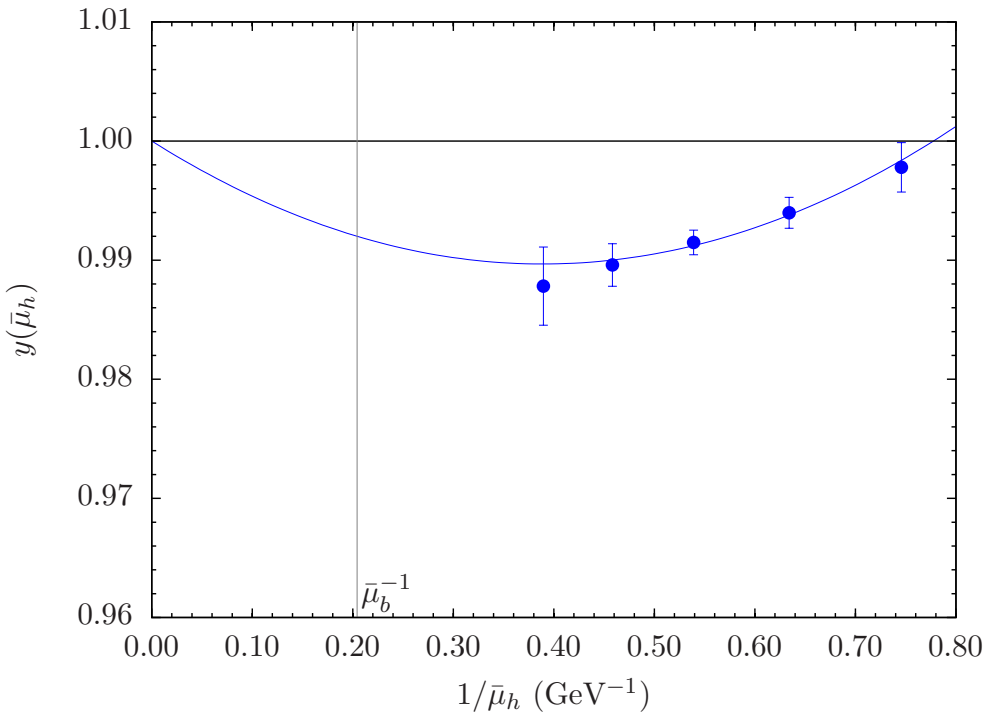

Figure 5.3: Heavy quark mass dependence of the ratio $y(\bar{\mu}_h)$ extrapolated to the physical value of the light quark mass and to the continuum limit. The vertical line represents the value of the physical b quark mass.

which should be looked at as a relation between the mass of the heavy-light meson, $M_{hu/d}(\bar{\mu}_h^{(K+1)})$, and the corresponding heavy quark mass $\bar{\mu}_h^{(K+1)}$, being $M_{hu/d}(\bar{\mu}_h^{(1)})$ the initial triggering value. The b quark mass is then determined by finding the value of K at which $M_{hu/d}(\bar{\mu}_h^{(K+1)})$ takes the experimental value of the B-meson mass, $M_B = 5.279\,\text{GeV}$. Calling K_b the solution of the resulting Eq. (5.9) (we find $K_b = 9$), one gets for $\bar{\mu}_b = \bar{m}_b^{\overline{\text{MS}},\,2\,\text{GeV}}$ the simple relation

$$\bar{\mu}_b = \lambda^{K_b}\bar{\mu}_h^{(1)} = 4.91(15)\ \ \text{GeV}\,. \tag{5.10}$$

We observe that it is always possible to guarantee that the solution K_b is an integer number through a slight variation of the parameter λ and/or of the triggering mass $\bar{\mu}_h^{(1)}$.

5.2.4 Determination from B_s meson

An equivalent method consists in determining the b quark mass by studying M_{hs} instead of $M_{hu/d}$ and using in input the experimental B_s-meson mass value, $M_{Bs} = 5.366$ GeV. A very similar result is obtained from this analysis: $\bar{\mu}_b^{\overline{\text{MS}},\,2\,\text{GeV}} = 4.92(13)$ GeV. The small difference (0.01 GeV) with respect to Eq. (5.10) indicates a good control of the chiral extrapolation which, in particular, in the heavy-strange meson case involves only the sea quark mass.

The main effect of the uncertainty due the chiral extrapolation is accounted for by the error quoted in eq. (5.10), which comes from the chiral, continuum and $1/\mu_h$ fits.

5.2.5 Systematic effects

5.2.5.1 Discretization effects

In order to estimate the residual uncertainty due to discretization effects, we have tried to include in the continuum extrapolation, besides the leading $\mathcal{O}(a^2)$ correction, an additional a^4 term. We find, however, that this sub-leading contribution cannot be fitted with our data. Therefore, we have repeated the analysis by excluding the data at the coarsest lattice spacing ($\beta = 3.80$). The difference in the determination of the b quark mass turns out to be of 0.05 GeV.

5.2.5.2 Interpolation

In order to estimate the systematic error associated to the interpolation of $y(\bar{\mu}_h)$ as a function of $1/\bar{\mu}_h$, we have repeated the whole analysis by choosing a third order polynomial in $1/\bar{\mu}_h$ (rather than a second order one, as in the ansatz (5.8)). This change resulted in an increase of the b quark mass of about 0.5%, corresponding to a shift of $\simeq 0.02$ GeV of the central value result of Eq. (5.10).

5.2.5.3 Pole mass definition

An additional uncertainty is introduced by the truncation of the perturbative series in the determination of the pole mass in Eq. (5.4), which is defined only perturbatively, and affected by renormalon ambiguities. When comparing the results obtained with the NLO definition of the pole mass to the results found with the LO one, the difference in the b quark mass is found to be small, of about 0.01 GeV. The sensitivity to the pole mass definition, which appears in the intermediate steps, thus largely cancels out in the final determination.

5.2.5.4 Global error budget

We finally quote the b quark mass at the conventional renormalization scale of m_b itself:

$$\bar{m}_b(m_b) = 4.29(13)(4) \ \text{GeV} = 4.29(14) \ \text{GeV}\,, \tag{5.11}$$

where the first error is of statistical and fitting origin and the second one is the sum in quadrature of the residual systematic uncertainties discussed above. The present result for the b quark mass has a central value which is smaller by approximately one standard deviation than the value found in [36], and an uncertainty which is reduced by almost a factor two, reflecting the various improvements implemented in the present analysis.

5.3 Determination of B and B_s meson decay constant

In this section we will determine the B and B_s mesons decay constants. In order to have better control on the chiral extrapolation, we consider as primary quantities in the present analysis the decay constant f_{B_s}, whose dependence on the light quark mass only occurs through sea effects, and the ratio f_{B_s}/f_B which provides a direct determination of the SU(3) breaking effect in the decay constant.

5.3.1 Ratio method for the decay constant

A strategy similar to that employed to determine $\bar{m}_b$ is applied to determine the B and B_s meson decay constants.

Ratio construction The HQET asymptotic prediction for the decay constant is

$$\lim_{\mu_h^{\rm pole}\to\infty} f_{h\ell}\sqrt{\mu_h^{\rm pole}} = \text{constant}\,. \tag{5.12}$$

Therefore, in this case the ratios with static limit equal to one of interest are, for f_B and f_{Bs} [36]:

$$\begin{aligned} z(\bar{\mu}_h,\lambda;\bar{\mu}_\ell,a) &\equiv \lambda^{1/2}\frac{f_{h\ell}(\bar{\mu}_h,\bar{\mu}_\ell,a)}{f_{h\ell}(\bar{\mu}_h/\lambda,\bar{\mu}_\ell,a)}\cdot\frac{C_A^{stat}(\mu_b^*,\bar{\mu}_h/\lambda)}{C_A^{stat}(\mu_b^*,\bar{\mu}_h)}\frac{[\rho(\bar{\mu}_h,\mu^*)]^{1/2}}{[\rho(\bar{\mu}_h/\lambda,\mu^*)]^{1/2}} \\ z_s(\bar{\mu}_h,\lambda;\bar{\mu}_\ell,\bar{\mu}_s,a) &\equiv \lambda^{1/2}\frac{f_{hs}(\bar{\mu}_h,\bar{\mu}_\ell,\bar{\mu}_s,a)}{f_{hs}(\bar{\mu}_h/\lambda,\bar{\mu}_\ell,\bar{\mu}_s,a)}\cdot\frac{C_A^{stat}(\mu_b^*,\bar{\mu}_h/\lambda)}{C_A^{stat}(\mu_b^*,\bar{\mu}_h)}\frac{[\rho(\bar{\mu}_h,\mu^*)]^{1/2}}{[\rho(\bar{\mu}_h/\lambda,\mu^*)]^{1/2}}\,. \end{aligned} \tag{5.13}$$

The ratio of ρ factors (raised to the appropriate power) is present to convert $\overline{\rm MS}$ heavy quark masses to pole masses as in Eq. (5.3). The factor $C_A^{stat}(\mu_b^*,\bar{\mu}_h)$, defined as

$$\Phi_{hs}(\mu_b^*) = \left[C_A^{stat}(\mu_b^*,\bar{\mu}_h)\right]^{-1}\cdot\Phi_{hs}^{\rm QCD}(\bar{\mu}_h)\,, \tag{5.14}$$

provides the matching between the decay constant in QCD for a heavy quark mass $\bar{\mu}_h$ and in HQET, and the running of the static axial current to the renormalization scale μ_b^*, and it is known up to N^{2}LO in PT [49]. The NLO expression used in the present analysis reads:

$$\begin{aligned} C_A^{stat}(\mu_b^*,\bar{\mu}_h) &= \left(\frac{\alpha^{\overline{\rm MS}}(\bar{\mu}_h)}{\alpha^{\overline{\rm MS}}(\mu_b^*)}\right)^{-\frac{6}{33-2\,N_f}}\cdot\left[1-\left(\frac{-3951+300\,N_f+60\,N_f^2+(924-56\,N_f)\pi^2}{9(33-2\,N_f)^2}\right)\right. \\ &\left.\cdot\frac{\alpha^{\overline{\rm MS}}(\bar{\mu}_h)-\alpha^{\overline{\rm MS}}(\mu_b^*)}{4\pi}\right]\cdot\left[1-\frac{8}{3}\frac{\alpha^{\overline{\rm MS}}(\bar{\mu}_h)}{4\pi}\right], \end{aligned} \tag{5.15}$$

with $N_f = 2$.

The value of f_{B_s} is obtained from the ratio z_s, while f_{B_s}/f_B from the double ratio z_s/z.

Chiral and continuum extrapolation at triggering mass For $f_{hs}/f_{h\ell}$, heavy meson chiral perturbation theory (HMChPT) predicts at the NLO a linear+logarithmic dependence on the light quark mass, since a chiral log controls the chiral behavior of f_B (see Eq. (5.17) below). In figs. 5.4 we show the chiral and continuum extrapolation of f_{hs} and $f_{hs}/f_{h\ell}$ at the initial (triggering) mass $\bar{\mu}_h^{(1)}$.

With our results, the logarithmic dependence cannot be appreciated, and we thus perform also a simpler linear fit in the light quark mass which turns out to describe well the lattice data. As discussed in section 5.3.3, we eventually average the results obtained from the HMChPT and the linear fits and include the difference in the systematic uncertainty. For f_{hs}, which depends on the light quark mass for sea effects only, we have implemented both a linear and a quadratic fit, which turn out to provide essentially identical results.

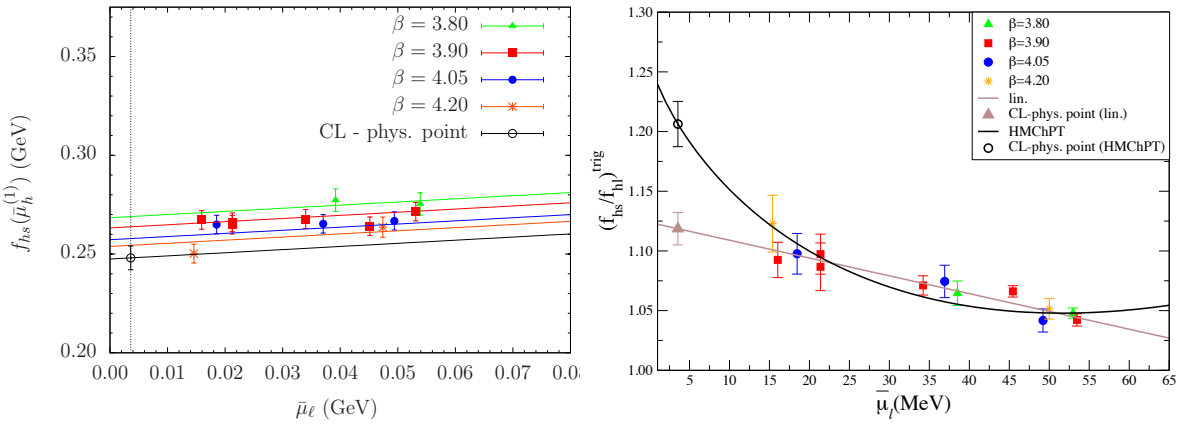

Figure 5.4: Light quark mass dependence of the decay constant $f_{hs}\left(\bar{\mu}_h^{(1)}\right)$ (left) and of the ratio of decay constants $f_{hs}\left(\bar{\mu}_h^{(1)}\right)/f_{hl}\left(\bar{\mu}_h^{(1)}\right)$ (right) at the four values of the lattice spacing.

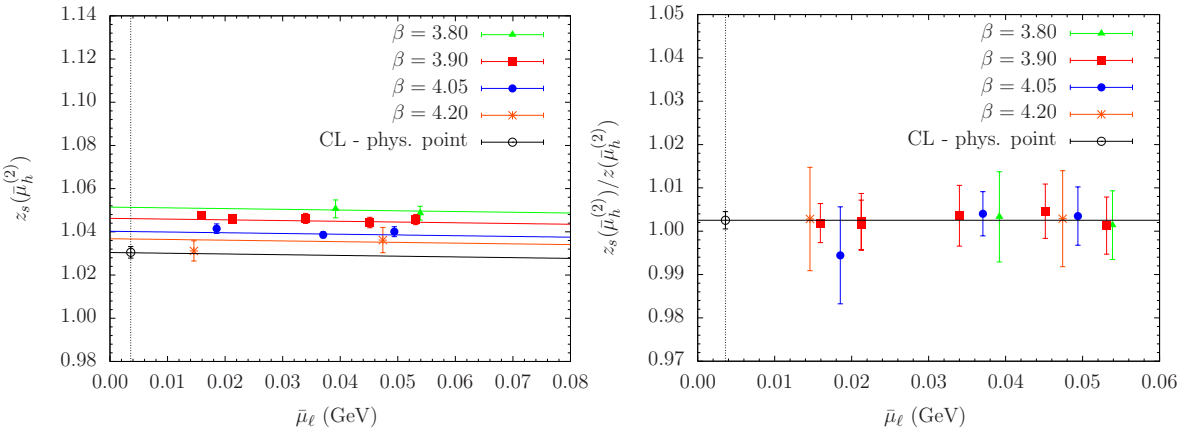

Figure 5.5: Light quark mass dependence of the ratio $z_s\left(\bar{\mu}_h^{(2)}\right)$(left) and of the double ratio $z_s\left(\bar{\mu}_h^{(2)}\right)/z\left(\bar{\mu}_h^{(2)}\right)$ (right) at the four values of the lattice spacing.

Chiral and continuum extrapolation of z Both z_s and z_s/z have a smooth chiral and continuum limit, as illustrated in fig. 5.5.

The ratio z_s has been fitted with a simple linear function of $\bar{\mu}_\ell$ and a^2 (see fig. 5.5 left).

The double ratio z_s/z is well described by both a linear and a constant behavior in both $\bar{\mu}_\ell$ and a^2 (see fig. 5.5 right). For simplicity reasons the constant fit ansatz was chosen.

Interpolation to $\bar{m}_b$ Finally, we study the dependence of the ratio z_s and the double ratio z_s/z on the heavy quark mass, which are shown in fig. 5.6.

For z_s we perform a quadratic interpolation to the b quark mass as for the ratio $y(\bar{\mu}_h)$ in Eq. (5.8). For z_s/z, the dependence on the heavy quark mass is barely visible, so that in this case we perform either a linear interpolation in $1/\bar{\mu}_h$ or we fix this ratio equal to its asymptotic heavy-quark mass limit, $z_s/z = 1$.

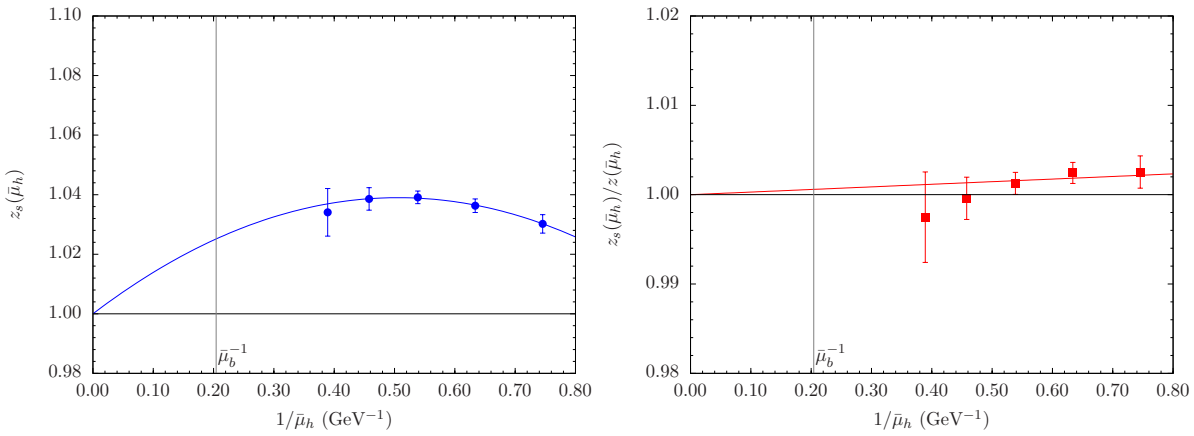

Figure 5.6: Heavy quark mass dependence of the ratio $z_s(\bar{\mu}_h)$ (left) and of the double ratio $z_s(\bar{\mu}_h)/z(\bar{\mu}_h)$ (right) extrapolated to the physical value of the light and strange quark masses and to the continuum limit. The vertical line represents the value of the physical b quark mass.

5.3.2 Interpolation method

As already mentioned, the interpolation method consists in interpolating to the b quark mass the results in the theory with the propagating heavy quark obtained for values of the heavy quark masses in the range around and above the physical charm (up to twice to three times its value) and the result evaluated in the static limit by simulating the HQET on the lattice. In the following we will address the calculation with lattice QCD in the charm mass region (section 5.3.2.1) and the interpolation among the two sets of results (section 5.3.2.2).

The calculation within the HQET on the lattice has been carried on by Andrea Shindler, Chris Michael and Marc Wagner and details on the calculations can be found in [?].

5.3.2.1 Decay constants in QCD

The lattice data with the propagating heavy quark for the meson masses and decay constants are the same used for the ratio method. We considered in the analysis four values of the lattice spacing and the values of valence quark masses collected in Table 5.1.

First, we slightly interpolate the lattice data to reach a set of reference heavy quark masses equal at the four β values, namely $\bar{\mu}_h = \{1.25,\ 1.50,\ 1.75,\ 2.00,\ 2.25\}$ GeV in the $\overline{\rm MS}$ scheme, at $\mu = 2\,\text{GeV}$.

This allows us to perform chiral extrapolation and to study discretization effects at fixed heavy quark mass. As for the ratio method, we consider as primary quantities f_{hs} and the ratio $f_{hs}/f_{h\ell}$ obtained in the present analysis from Φ_{hs} and $\Phi_{hs}/\Phi_{h\ell}$, where:

$$\Phi_{hs} = f_{hs}\sqrt{M_{hs}} \qquad \text{and} \qquad \frac{\Phi_{hs}}{\Phi_{h\ell}} = \frac{f_{hs}}{f_{h\ell}}\sqrt{\frac{M_{hs}}{M_{h\ell}}}\,. \tag{5.16}$$

An alternative analysis based on the definition of $\Phi_{h\ell(s)}$ in terms of the pole mass, rather than the meson mass, i.e. $\Phi_{h\ell(s)} = f_{h\ell(s)}\sqrt{\mu_b^{\rm pole}}$, has been also performed, leading to fully equivalent results.

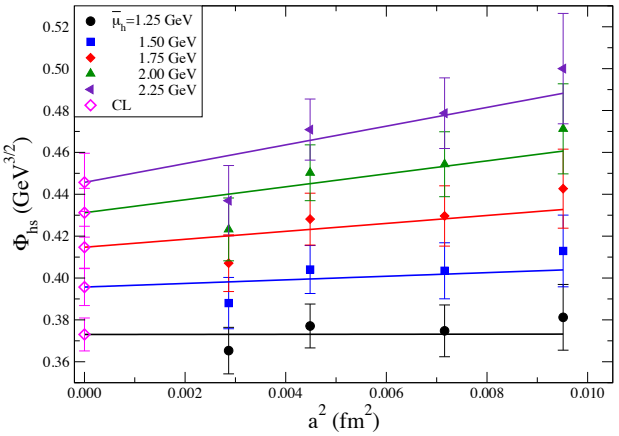

Figure 5.7: Dependence of Φ_{hs} on the squared lattice spacing, at the five reference values of the heavy quark mass (for a fixed value of the up/down and strange quark masses).

The light quark mass dependence predicted for $\Phi_{h\ell}$ and Φ_{hs} by HMChPT [50–52] at the NLO reads:

$$\Phi_{h\ell}\,(a,\bar{\mu}_\ell,\bar{\mu}_h) = A_h\,\left[1 - \frac{3\,(1+3\hat{g}^2)}{4}\,\frac{2\,B_0\,\bar{\mu}_\ell}{(4\,\pi\,f_0)^2}\,\log\left(\frac{2\,B_0\,\bar{\mu}_\ell}{(4\,\pi\,f_0)^2}\right) + B_h\,\bar{\mu}_\ell + C_h\,a^2\right]\,,$$

$$\Phi_{hs}\,(a,\bar{\mu}_\ell,\bar{\mu}_s,\bar{\mu}_h) = D_h\,\left(1 + E_h\,\bar{\mu}_\ell + F_h\,\bar{\mu}_s + G_h\,a^2\right)\,, \qquad (5.17)$$

where we have also included in the above expressions a linear dependence on a^2 to account for leading discretization effects. The subscript h in the fit parameters of Eq. (5.17) denotes the dependence on the heavy quark mass.

Details on chiral extrapolation As previously discussed for the ratio method, the contribution of chiral logs in the ratio $\Phi_{hs}/\Phi_{h\ell}$, predicted by HMChPT, cannot be appreciated with our data (see fig. 5.4 right). Thus, in order to perform the chiral extrapolation to the physical light quark mass, we also perform a simple linear fit in $\bar{\mu}_\ell$ and eventually take the average of the two results. In the fit based on HMChPT we take for the parameter $\hat{g}$ the value $\hat{g} = 0.61(7)$ obtained from the experimental measurement of the $g_{D^*D\pi}$ coupling [53]. We choose this value, instead of the HQET prediction $\hat{g} = 0.44(8)$ [54, 55], as we fit data that are close to the charm mass region and in order to conservatively include in the average the maximum spread resulting from the different ways of performing the chiral extrapolation of our data (larger value of $\hat{g}$ increase the effects of chiral logs). For Φ_{hs}, as for f_{hs} within the ratio method (see fig. 5.4 left), we have tried both a linear and a quadratic fit in $\bar{\mu}_\ell$, obtaining very similar results.

Details on discretization effects The size of discretization effects in the calculation of Φ_{hs} is shown in fig. 5.7, for a simulated value of the light quark mass of about 50 MeV (in $\overline{\rm MS}$ at 2 GeV) and with $\bar{\mu}_s \approx \bar{\mu}_s^{phys}$.

It is interesting to note that lattice artifacts turn out to be small. We find that this is a consequence of a partial cancellation between discretization terms in the decay constant and in the rooted meson mass, which are of similar size and opposite sign. For the same reason, the ratio $\Phi_{hs}/\Phi_{h\ell}$ (not shown) turns out to be practically independent of the lattice spacing.

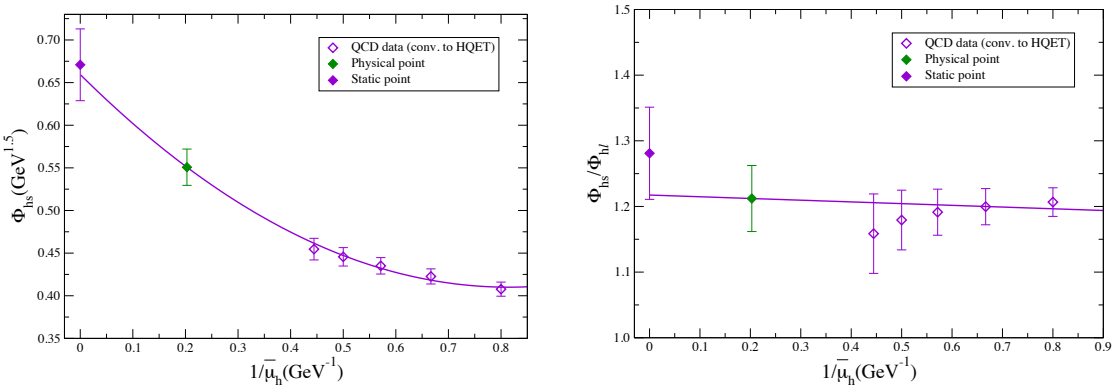

Figure 5.8: Dependence of Φ_{hs} (left) and $\Phi_{hs}/\Phi_{h\ell}$ (right), in the chiral and continuum limit, on the inverse of the heavy quark mass.

5.3.2.2 Interpolation to physical b

In order to perform a combined fit static and $b-$propagating data, we convert the values of Φ_{hs} from QCD to HQET, by using the NLO matching and evolution factor C_A^{stat} (see Eqs.(5.14) and (5.15)). The renormalization scale is chosen to be $\mu_b^* = 4.5$ GeV as for the static data. Note that in the ratio $\Phi_{hs}/\Phi_{h\ell}$ the C_A^{stat} factor cancels out.

The interpolation is then performed, as shown in fig. 5.8, through a fit in $1/\bar{\mu}_h$, which is quadratic for Φ_{hs} (similarly to Eq. (5.8)) and only linear for $\Phi_{hs}/\Phi_{h\ell}$, where a much smoother dependence on the heavy quark mass is found, as expected. It is clear from the plots that the static point data has a quite significant influence on the shape of the fitting curve.

Finally, the physical results for the decay constants are obtained by inserting the "physical" value of the b quark mass determined from the ratio method, given in Eqs. (5.10)-(5.11). The uncertainty on the b quark mass has been propagated by assuming a Gaussian distribution of the errors.

5.3.3 Results for the decay constants

In this section we present and discuss the final results obtained for the decay constants f_{Bs}, f_{Bs}/f_B and f_B from the ratio and the interpolation methods.

As discussed in the previous sections, in order to estimate the uncertainty due to the chiral extrapolation we compare the results of two different chiral fits. This comparison is relevant in particular for the ratio $\Phi_{hs}/\Phi_{h\ell}$, from which Φ_{Bs}/Φ_B is extracted. In this case, the two fits are based either on the linear + logarithmic dependence on the light quark mass predicted by HMChPT (Eq. (5.17)) or on a polynomial (quadratic) behavior. For Φ_{hs} we have tried both the linear fit of Eq. (5.17) and a quadratic fit. The analogous chiral fit ansatz employed in the analysis of $f_{hs}(\bar{\mu}_h^{(1)})/f_{h\ell}(\bar{\mu}_h^{(1)})$ within the ratio method framework have been discussed in sect. 5.3.1. The results are collected in Table 5.2 for both the ratio and the interpolation method. The first error quoted in the table is the one coming from the fit, and includes both the statistical error and the systematic uncertainty due to the chiral and continuum extrapolation and to the interpolation to the b quark mass.

The second error accounts for the additional systematic uncertainties and it has been evaluated

f_{Bs}[MeV]				f_{Bs}/f_B			
Ratio Method		Interpol. Method		Ratio Method		Interpol. Method	
Lin.	Quad.	Lin.	Quad.	HMChPT	Polyn.	HMChPT	Polyn.
225(7)(4)	225(7)(4)	237(9)(4)	238(9)(4)	1.22(2)(0)	1.14(2)(0)	1.22(5)(2)	1.16(6)(2)
225(7)(4)		238(9)(4)		1.18(2)(4)		1.19(5)(3)	
232(10)				1.19(5)			

Table 5.2: Collection of the results obtained for f_{Bs} and f_{Bs}/f_B from the ratio and interpolation methods. The statistical and systematic uncertainties are summed in quadrature. The third and fourth lines provide info on the results obtained by extrapolating to the physical pion mass point by using different chiral fit ansatz (see text). The final values, given in the last row, are an average of the results of the two methods.

as discussed in the following.

Continuum limit When performing the continuum limit, both in the ratio and the interpolation method, we consider a linear fit in a^2. Since an additional a^4 term cannot be fitted with our data, we estimate the uncertainty due to discretization effects by excluding data at the coarsest lattice ($\beta = 3.80$). The central values for f_{Bs} change by 2 and 1 MeV for the ratio and the interpolation method respectively. The corresponding changes in the values of the ratio f_{Bs}/f_B are instead negligible.

Heavy mass dependence Within the interpolation method we estimate the uncertainty in reaching the physical bottom mass by including, for each β, data at two larger values of μ_h, and by choosing slightly different values for the reference masses. We find that with these variations the central values obtained for f_{Bs} change by approximately 3 MeV, while the results for the ratio f_{Bs}/f_B are practically unaffected. In the context of the ratio method analysis in order to estimate the systematic error associated to the determination of $z_s(\bar{\mu}_b)$ we have varied the fit ansatz by considering either a second order or a third order polynomial in $1/\bar{\mu}_h$. This change produces only a 1 MeV decrease in the final value of $f_{Bs} \simeq 225$ MeV (see Table 5.2). Even smaller is the relative uncertainty in the $1/\bar{\mu}_h$ interpolation of the double ratio $z_s(\bar{\mu}_h)/z(\bar{\mu}_h)$, owing to the very flat profile of data within errors, as it is seen from fig. 5.6 (right).

Pole mass As the pole mass is affected by renormalon ambiguities, in the analysis based on the ratio method we compare the results obtained by using the NLO definition of the pole mass to the results found with the LO definition. Within the interpolation method, instead, we have also considered the alternative definition of $\Phi_{h\ell(s)}$ in terms of the pole mass (rather than the meson mass), again using either the NLO or the LO definition of the pole mass. In both cases, the differences are found to be small, at the level of 1 MeV, for the decay constants, as the sensitivity to the pole mass definition, which appears in the intermediate steps of the calculation, largely cancels out in the final determinations. The results for the ratio f_{Bs}/f_B are practically unaffected.

Mismatch of the strange quark mass in the static simulation The static-strange correlators have been calculated with a value of the strange quark mass that was estimated from an analysis at fixed lattice spacing, and turned out to be larger with respect to the continuum limit

estimate by approximately 22% at $\beta = 3.90$ and 13% at $\beta = 4.05$. In order to evaluate the systematic uncertainty due to this mismatch, we have analyzed the data with propagating heavy quark for Φ_{hs} which are available at several values of the strange quark mass. By using the continuum estimate of the strange quark mass, Φ_{Bs} decreases by approximately 2%. A similar effect can be thus expected for the static data. We have thus repeated the interpolation to the b quark mass using for the static points results smaller by 2%. We find that the B_s decay constant decreases by 3 MeV and f_{Bs}/f_B by 0.015. We conservatively ignore the sign of the variation and consider these changes as a symmetric contribution to the systematic uncertainty. This uncertainty does not affect the ratio method, since in this case the static limit of z_s and z_s/z is exactly known.

Final results For both methods we add in quadrature the systematic uncertainties and, finally, as shown in the last row of Table 5.2, we average the results of the two methods obtaining

$$f_{Bs} = 232(10)\ \text{MeV}\,, \qquad \frac{f_{Bs}}{f_B} = 1.19(5)\,, \tag{5.18}$$

and for the B decay constant, which is determined for each analysis as $f_B = f_{Bs}/(f_{Bs}/f_B)$,

$$f_B = 195(12)\ \text{MeV}\,. \tag{5.19}$$

These values are in agreement and improve the results obtained in [36] and [41].

5.3.4 Comparison of the two methods

The systematic uncertainties due to the chiral and continuum extrapolation and to the interpolation to the physical b quark mass, as well as the sensitivity to the definition of the pole mass used in the ratio method, have been carefully studied. An important uncertainty affecting the determination of the ratio f_{B_s}/f_B and, in turn, of f_B, is introduced by the chiral extrapolation to the physical value of the average up/down quark mass. We note, in this respect, that given an assumption for the chiral extrapolation fitting function, i.e. either including or not the leading chiral logarithm, the results obtained for the ratio f_{B_s}/f_B by using the ratio and the interpolation method are in perfect agreement within each other (see Table 5.2). In order to reduce the uncertainty due to the chiral extrapolation, simulations at smaller values for the light quark masses, closer to their physical values, are needed.

The difference between the results obtained for f_{B_s} by using the ratio and the interpolation method (approximately 5%, see Table 5.2) provides an indication of the uncertainty due to the interpolation to the heavy b quark mass. In this respect, the main advantage of the ratio method is that the static limit of the ratios is exactly known (by definition), so that the approach does not require a dedicated lattice computation within the HQET.

5.3.5 D and D_s meson decay constants

As a byproduct of the analysis we also obtain the decay constants for the D and D_s mesons. In order to determine these quantities, we only consider three values for the heavy quark reference masses around the physical charm quark mass. By interpolating to the physical value $\overline{m}_c(\overline{m}_c) = 1.28(4)$ GeV, obtained in [41], we find

$$f_D = 212(8)\ \text{MeV}\,, \qquad f_{Ds} = 248(6)\ \text{MeV}\,, \qquad \frac{f_{Ds}}{f_D} = 1.17(5)\,, \tag{5.20}$$

to be compared with the results $f_D = 197(9)$ MeV, $f_{Ds} = 244(8)$ MeV and $f_{Ds}/f_D = 1.24(3)$ of [42]. With respect to [42], the present analysis is improved essentially for the reasons discussed for f_B and f_{Bs}, namely: the statistics is increased for some ensembles, data at the finest lattice spacing ($\beta = 4.20$) are now included, the continuum extrapolation is performed at fixed (reference) heavy quark masses. Moreover, as discussed for f_{Bs}/f_B, we perform the chiral extrapolation of $f_{hs}/f_{h\ell}$ either following HMChPT or a linear dependence on μ_ℓ. In [42] the value $f_{D_s}/f_D = 1.24(3)$ was obtained from the HMChPT fit only, while the result given in Eq. (5.20) is an average of $f_{Ds}/f_D = 1.21(2)$ from HMChPT and $f_{Ds}/f_D = 1.12(2)$ from the linear fit. By considering both results we have increased the uncertainty associated to the chiral extrapolation.

5.4 Smearing tests

Increasing the mass of the heavy quark results in a smaller gap between the lowest and excited states. One needs to go to larger time to isolate the ground state in the correlation functions. Given that in two points correlation functions the signal decrease faster than gauge sampling and stochastic noise (if random source are used), at increasing quark masses the determination of matrix elements and hadron masses becomes more and more difficult, end eventually impossible.

When computing correlation functions one create out from the vacuum the state of its interest $|s\rangle$ (which we will suppose for simplicity to be a single particle state) through an appropriate operator O carrying quantum numbers of the state s. The operator O in general will create all state with the same quantum numbers of s and not just the fundamental:

$$O|0\rangle = |s\rangle + \left|s^{(1)}\right\rangle + \left|s^{(2)}\right\rangle + \dots . \tag{5.21}$$

Nevertheless it must exist a set of operator O_s that when applied to the vacuum create only the state[1] s. The prove of this is simple: given the (non unique) operator O, an operator O_s can be defined as $O_s \equiv |s\rangle \langle s| O$.

The operator O_s will be in general a non-local combination of fields at different space points, corresponding to the wave function of the state. Knowing the distribution of such fields one could build the interpolating operator and compute correlation functions containing just the state s at all times, highly improving signals.

In order to build an operator which approximate O_s and have therefore a better overlap with state $|s\rangle$, one have to make some guess on the shape of hadron wave function. The general criteria used to build such improved creation operator is that the wave function of an hadron of mass M extend over a region of space of order $1/M$. Increasing the spatial extent of operators one can achieve better overlap with the lower lying state and thus obtain correlation functions with minor excited states contamination. One can assume the shape of the wave function to be Gaussian-like, and build a creation operator with such form.

5.4.1 Gaussian Smearing

One possibility called *Gaussian smearing* is to substitute the creation operator O with:

$$O_s = G^n(k)\, O, \qquad G(k) \equiv \frac{1 + kH}{1 + 6k}, \tag{5.22}$$

[1] The operator $\mathcal{O}_s$ is not unique: different choice of operator $\mathcal{O}$ lead to different operators $\mathcal{O}_s$, which differ for the normalization and their action on states different from the vacuum.

where H is given by:

$$H_{x,y} \equiv \sum_{\mu=1,2,3} \left(U_{x;\mu} \delta_{y,x+\hat{\mu}} + U^{\dagger}_{x-\hat{\mu};\mu} \delta_{y,x-\hat{\mu}} \right) , \tag{5.23}$$

with U being the gauge links, k a real number, and n an integer number called the *smearing level*.

Let us consider the computation of two points correlation functions between bilinear operator such as $O_i = \bar{\psi} \Gamma_i \psi$, and to be interested in the calculation of the correlation functions $C_{s_2 s_1} \left\langle O^{\dagger}_{s_2} O_{s_1} \right\rangle$ between smeared operators:

$$O_{s_i} = G^{n_i} (k_i) \, O_i, \quad i \in 1, 2 \, . \tag{5.24}$$

It can be shown that the correlation function wrote in terms of these operator is given by the contraction:

$$C_{\vec{x},t} = - \left\langle \mathrm{Tr} \left[\Gamma_2 \left(M^{SS} \right)^{-1}_{x,0} \Gamma_1 \left(M^{SS} \right)^{-1}_{0,x} \right] \right\rangle , \tag{5.25}$$

where we have defined the sink and source smeared (SS) propagator $\left(M^{SS} \right)^{-1}$, which can be expressed in terms of the usual propagator as:

$$\left(M^{SS}_{x,0} \right)^{-1} = G^{n_2} (k_2)_{x,y} \left(M_{y,z} \right)^{-1} G^{n_1} (k_1)_{z,0} \, . \tag{5.26}$$

This can be achieved first of all by defining a vector $\eta_x = \delta_{x,0}$, then applying over it the source smearing operator:

$$\phi_y = G^{n_1} (k_1)_{y,x} \, \eta_x , \tag{5.27}$$

then solving for the vector χ the linear system:

$$M_{x,y} \chi_y = \phi_y \, , \tag{5.28}$$

and lastly applying the sink smearing operator:

$$\left(M^{SS} \right)^{-1}_{x,0} \equiv G^{n_2} (k_2)_{x,y} \, \chi_y \, . \tag{5.29}$$

The effect of the source smearing operator is to build an extended source ϕ on which to invert the fermionic matrix. If the original source η is a Kronecker delta at the origin, the extended or "smeared" source η is a Gaussian-like distributed in space, mainly:

$$|\eta|^2_x \propto e^{-\left(\frac{|\vec{x}|}{2\sigma} \right)^2} \delta_{t,0} \, , \tag{5.30}$$

where the parameter σ is an increasing function of k and n, which must be tuned in order to obtain the wanted Gaussian width. Increasing the number of iteration n decreasing at the same time the smearing strength k one can achieve (approximatively) the same source width σ.

At fixed σ, larger n will correspond to a greater gaussianity of the shapes of the source. This is not a very relevant point anyway, given that the true wave-function of lowest state does not need to be gaussian.

In Fig. 5.9 we show for example the profile density as a function of the distance of a smeared source, obtained by smearing with parameters $k = 4$, $n = 50$ using a $\beta = 3.90$, $am = 0.0064$ gauge configuration. The gaussianity of the smeared source is evident.

The smearing of propagator sink act in a very similar way, enhancing the overlap of operator O_2 between vacuum and the state s.

This discussion apply also when working with stochastic sources with (or without) using one-end trick.

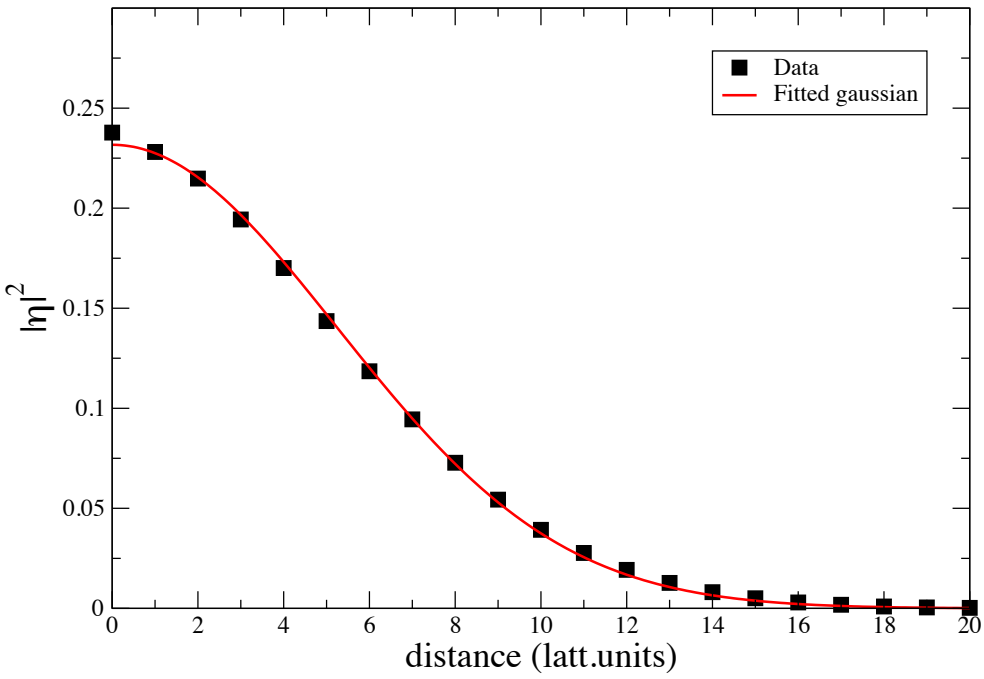

Figure 5.9: Density profile of a smeared source obtained by smearing with $k = 4$, $n = 50$ using a $\beta = 3.90$, $am = 0.0064$, $V = 24^3 \times 48$ gauge configuration. The curve is a plot of the fitting gaussian.

5.4.2 Comparison between different smearing combinations

In general one can build one can build correlation function with smearing parameters in the source and in the sink. For the sake of simplicity we have limited to analyze correlation functions with the same smearing level in the source and in the sink, or with one of the two set to zero (local). To summarize we have considered four kind of correlation functions: the simple local-local which has been used through all previous work, which we indicate in the following as LL (where L stand for Local); the source smeared correlation functions, which we call SL; the sink smeared correlation function LS; and the source and sink smeared, SS.

We made a test by computing pseudo-scalar correlation functions on the $\beta = 3.90$, $am = 0.0064$, $V = 24^3 \times 48$ gauge ensemble using 240 gauge configurations, with a large list of heavy quark masses, fixing the parameter $k = 4$ and with four different number of iterations: 0, 30, 60, 90.

In Fig. 5.10 we plot the effective mass relative to four level smearing of the meson composed by light ($am = 0.0064$) quark and an heavy quark of a mass approximately double of the physical charm.

As expected in smeared correlation functions the ground state is isolated much better and at shorter time than the simple local-local correlator. Increasing the number of smearing iterations does not improve the suppression of excited state contamination, while enhance errors.

We noted that the error on correlation function is an increasing function of the number of smearing iterations applied to the sink. In figure 5.11 we show the correlation function effective mass obtained fixing the number of iterations in the source to 30 and varying the number of iteration in the sink. It is evident that the suppression of excited states do not worsen much

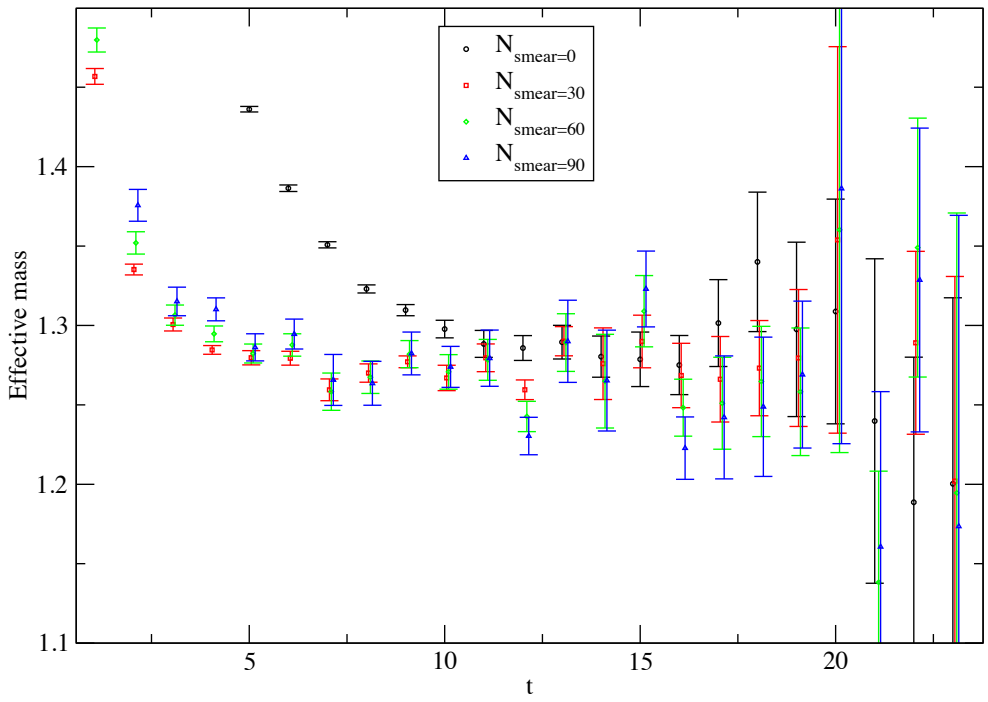

Figure 5.10: Comparison of the effective mass of the pseudo-scalar correlation function with four different numbers of iterations. The function is compute over 240 gauge configuration of $am = 0.0064$, $\beta = 3.90$, $V = 24^3 \times 48$ ensemble. Data is slightly displaced horizontally for better readability. The number of iterations in the sink is always equal to the source.

neither at $n_{sink} = 0$.

The signal behaves much better if the sink of the propagator is not smeared at all.

It turns instead out that the signal to noise ratio in the SL (source smeared, sink local) correlation function is quite largely improved with respect to the simple local-local correlation. There is indeed an apparent difference between the effects of the smearing on the source and on the sink. We suggest that this feature might be related to the usage of random wall sources: the increase of noise is known to be a general feature of usage of smearing, but when performed on a stochastic source it could help to cancel part of the stochastic noise, possibly by averaging a larger number of gauge variant terms end therefore improving the stochastic closure of the source indices. This topic could be investigated in future by comparing the effects of smearing also in presence of a simple point source.

5.4.3 Preliminary study of the B meson mass

We decided to fix the number of smearing iteration in the sink to 30 and on the sink to 0, and perform a preliminary calculation of the pseudo-scalar correlation functions. We studied a single gauge setup for each of the three $\beta \in \{3.80, 3.90, 4.05\}$, in order to check the feasibility of the determination of the b quark mass and of the decay constant f_B and f_{B_s} directly at the physical b quark mass, or by making a more limited heavy extrapolation.

The bare sea quark mass for each setup has been chosen to correspond approximately to the same renormalized light mass (in $\overline{\text{MS}}$ at 2 GeV.) of about 30 MeV. In Fig 5.12 we show the

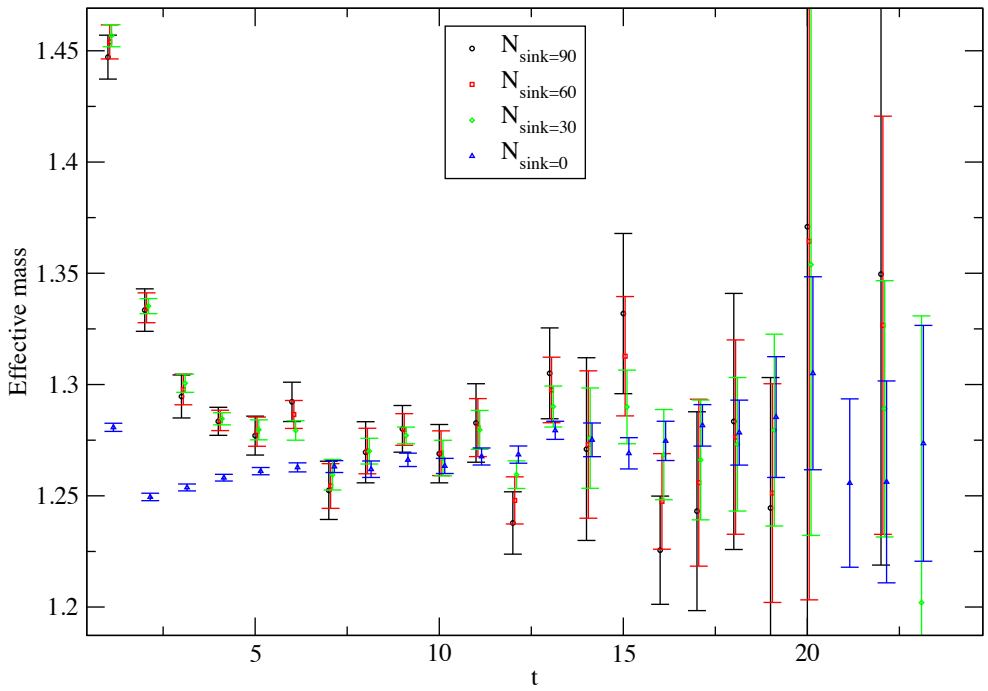

Figure 5.11: Comparison fixing the number of source iteration to 30 and changing the number of smearing iteration on the sink.

effective mass of the correlation function computed approximately at the physical b quark mass. It is evident that a clear plateaux can still be seen starting from $t \sim 12$.

In figure 5.13 we show the continuum extrapolation of the meson mass as determined at the three lattice spacing, for a set of four different b quark masses. It is remarkable that even at the physical b quark discretization effects seem to be not larger than 20%. Of course this is a preliminary result, which must be checked more carefully with a fourth lattice spacing and analyzing a larger number of sea quark masses.

As a last check we studied the decay constant f_B on the gauge ensemble $\beta = 3.90$, $am = 0.0064$ already analyzed for previous test. In order to build the meson decay constant, the local interpolating field Z_L is needed. The source smeared correlator is expected to behave as:

$$C^{SL}(t) = \frac{Z_S Z_L}{M_B} e^{-TM_B/2} \cosh\left[M_B\left(T/2 - t\right)\right] , \tag{5.31}$$

over times where only lowest state dominates, with Z_S being an unknown function of Z_L and smearing parameters. Only the combination $Z_S Z_L$ and the mass M_B can be determined through the fit of the SL correlation functions. In order to determine the simple Z_L factor one need to determine separately the factor Z_S by fitting the source and sink smeared (SS) correlation function, which is expected to behave as:

$$C^{SS}(t) = \frac{Z_S^2}{M_B} e^{-TM_B/2} \cosh\left[M_B\left(T/2 - t\right)\right] , \tag{5.32}$$

and obtain Z_L by dividing appropriately the fitted constant $Z_S Z_L$. Being the meson mass M_B contained in both 5.31 and 5.32 formulae, this can (and should) be done in a combined fit of the two correlation functions.

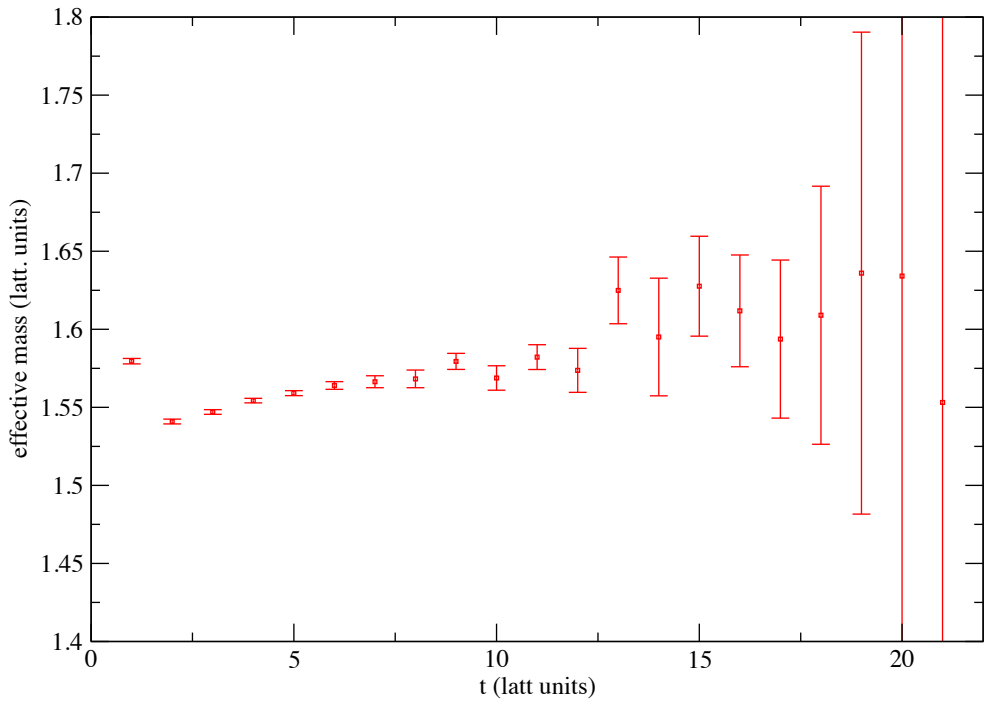

Figure 5.12: Effective mass of the correlation function at $\beta = 3.90$ for the B meson composed of a light quark of renormalized quark mass of approximately 30 MeV (in $\overline{\text{MS}}$ at 2 GeV) and the physical b quark. .

In figure 5.14 we show the result of the B meson decay constant f_B obtained at various heavy quark masses up to the physical b, using or not using smearing techniques. With smearing it is possible to determine f_B with high precision up to the physical B and thus it could be possible to determine it by making small or null extrapolation.

Having the test been done at a fixed lattice spacing and sea quark mass, the comparison with the results obtained in previous chapter does not allow to say anything definitive over them, but nonetheless is very encouraging.

To summarize, the usage of smearing techniques seem to be a very promising tool to study b physics, and we plan to start a full analysis of b quantities with these techniques in the near future.

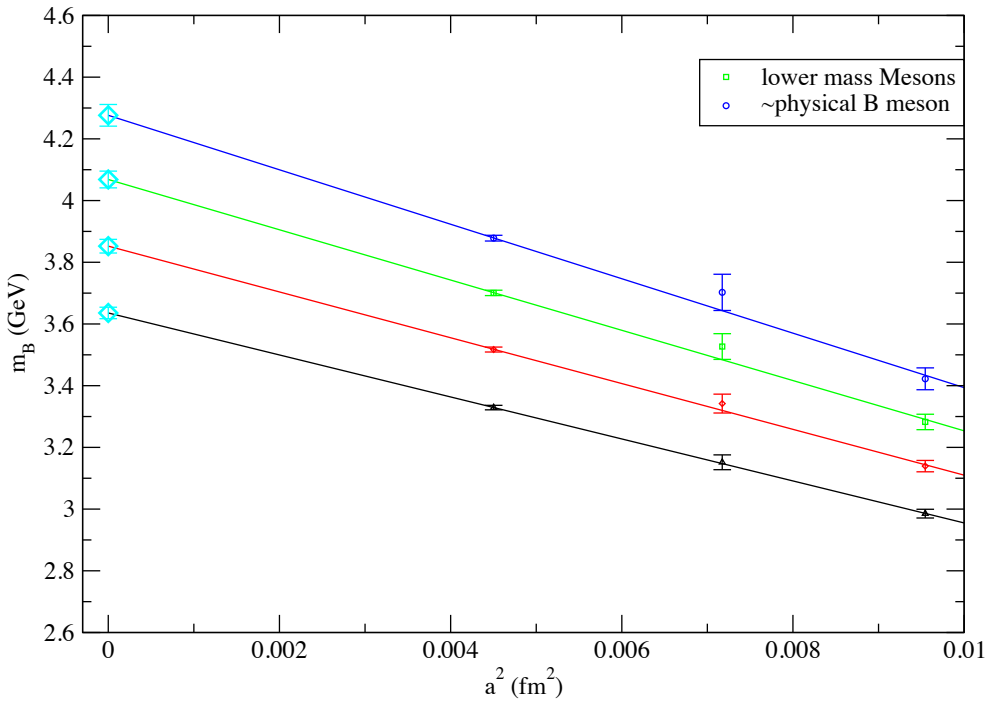

Figure 5.13: Continuum extrapolation (at approximately fixed renormalized light quark mass ~ 30MeV, in $\overline{\text{MS}}$ at 2 GeV) at three lattice spacings. The heaviest data is approximately at the physical b mass.

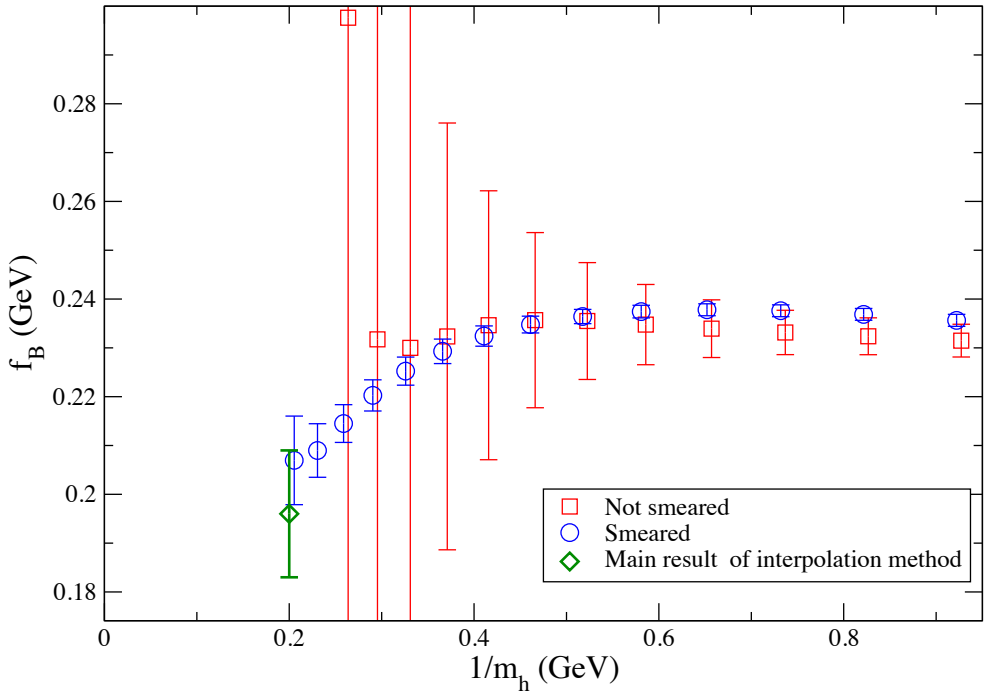

Figure 5.14: B meson decay constant f_B at a fixed lattice spacing ($\beta = 3.90$) and renormalized light quark mass (30 MeV in $\overline{\text{MS}}$ at 2 GeV) as function of reciprocal heavy quark mass. We compare results obtained using smeared and not-smeared correlation functions together with the main results of analysis of previous section 5.

Chapter 6

Isospin breaking effects

Isospin symmetry is an almost exact property of strong interactions as described by the QCD Lagrangian. As already mentioned, this symmetry hold because of the difference between the up and down quark masses is much smaller than the QCD scale, $(m_d - m_u)/\Lambda_{QCD} \ll 1$, and it remains true also when electromagnetic interactions are switched on, because isospin breaking effects due to the different quark electric charges ($q_u \neq q_d$) are suppressed by the electromagnetic coupling constant, $\alpha_{em} \sim 1/137$. For these reasons most of theoretical predictions assume isospin symmetry, i.e. the masses of the up and down quarks are taken equal and the electromagnetic effects are neglected. The calculations presented in the previous chapters are obtained in the isospin symmetric limit.

Nowadays, with the increasing precision of the experimental determinations of many physical quantities, and in some cases with the improvement of the theoretical predictions, the control over isospin breaking effects is becoming phenomenologically relevant. This is the case, for example, of the form factors parameterizing K_{ℓ_3} decays. Isospin breaking effects are important also for hadron spectroscopy, for the meson decay constants, for the $\pi - \pi$ scattering length, for the chiral condensate and for many other quantities.

In this chapter we will describe a new method to take into account the correction arising from quark mass difference, and present some example of applications. In particular we will compute the up-down quark mass difference, determine the QCD corrections to the Kaon meson decay constant f_K, the semi-leptonic $K\ell_3$ form factors and predict the proton-neutron mass difference.

6.1 Motivation and method

In the past, isospin breaking effects due to the light quarks mass difference (in the following referred to as *QCD Isospin Breaking effects* or simply QIB effects) have been accommodated within the ChPT framework, while several attempts to compute electromagnetic effects for the meson spectroscopy in lattice QCD have been presented.

It is much harder to take into account in numerical simulations QCD isospin breaking because the effect is in general rather small and comparable with the errors in the determination of, say, the meson masses or decay constants. Furthermore, in order to perform unitary dynamical simulations of two light quarks of different mass the single quark determinant must be positive and this happens only in the case of lattice discretizations of the fermion action that are very expensive from the numerical point of view.

Our method is instead based on a perturbative expansion in the up-down quark mass difference. Let us start by considering the evaluation of any generic euclidean correlation function used to extract information about physical quantities as masses, decay constants, form factors etc.

$$\langle \mathcal{O} \rangle = \frac{\int D\phi \, \mathcal{O} e^{-S}}{\int D\phi \, e^{-S}} \,, \tag{6.1}$$

where D represents generically the full functional integration measure of the theory. By neglecting for the moment electromagnetic corrections and possible isospin breaking terms that may arise because of lattice artifacts with particular choices of the lattice fermion action, we can write the Lagrangian density as a term which is $SU(2)_V$ symmetric plus the isospin breaking term:

$$\mathcal{L} = \underbrace{\mathcal{L}_{kin} + \frac{m_d + m_u}{2} \left(\bar{u} u + \bar{d} d \right)}_{\mathcal{L}_0 = \mathcal{L}_{kin} + m_{ud} \bar{q} q} - \underbrace{\frac{m_d - m_u}{2} \left(\bar{u} u - \bar{d} d \right)}_{\varepsilon_{ud} \bar{q} \tau_3 q = \varepsilon_{ud} \hat{\mathcal{L}}} \,, \tag{6.2}$$

where $q \equiv (u,\, d)$, $m_{ud} \equiv (m_d + m_u)/2$ and $\varepsilon_{ud} \equiv (m_d - m_u)/2$. By expanding at first order the exponential of the action, $S = \sum_x \mathcal{L}(x)$, with respect to ε_{ud} we obtain

$$\langle \mathcal{O} \rangle \simeq \frac{\int D\phi \mathcal{O} \left(1 + \varepsilon \hat{S} \right) e^{-S_0}}{\int D\phi \left(1 + \varepsilon \hat{S} \right) e^{-S_0}} = \frac{\langle \mathcal{O} \rangle_0 + \varepsilon_{ud} \left\langle \mathcal{O} \hat{S} \right\rangle_0}{1 + \varepsilon_{ud} \cancel{\left\langle \hat{S} \right\rangle_0}} = \langle \mathcal{O} \rangle_0 + \varepsilon_{ud} \left\langle \mathcal{O} \hat{S} \right\rangle_0 \,, \tag{6.3}$$

The correction in the denominator vanishes because of isospin symmetry. Concerning the Wick contractions of the correlation functions $\left\langle \mathcal{O} \hat{S} \right\rangle_0$, isospin symmetry makes also vanish disconnected contributions of the form:

$$\varepsilon_{ud} \left\langle [\text{Wick contractions of } \mathcal{O}] \times \text{tr} \left[\hat{\text{S}} \right] \right\rangle_0 = 0 \,, \tag{6.4}$$

since these are proportional to the trace of the flavor matrix τ_3. The previous observation is a particular case of the following general recipe to be used in order to compute leading QIB effects on the lattice:

- consider a given correlation function in the full theory with $m_u \neq m_d$, and draw all the Wick contractions
- expand the up and down quark propagators with respect to ε_{ud} according to

$$\begin{array}{rcl} S_u(x_1, x_2) & = & S_\ell(x_1, x_2) + \varepsilon_{ud} \sum_y S_\ell(x_1, y) S_\ell(y, x_2) + \dots \,, \\ S_d(x_1, x_2) & = & S_\ell(x_1, x_2) + \varepsilon_{ud} \sum_y S_\ell(x_1, y) S_\ell(y, x_2) + \dots \,, \end{array} \tag{6.5}$$

- retain the terms linear in ε_{ud} and compute the corresponding diagrams.

In the following sections we shall discuss in details how to extract physical informations from the resulting correlation functions. To this end we need to set the notation we are going to use in drawing Feynman diagrams. Eqs. 6.5 can be represented diagrammatically as in figure 6.1, where the up quark line in the full theory is drawn in light blue color while the down quark line in green.

All the black lines refer to S_ℓ, the propagator with the symmetric mass m_{ud} in the isospin symmetric theory: $y \longrightarrow x = S_\ell(x - y) = \left\langle \ell(x) \bar{\ell}(y) \right\rangle$, whereas the insertion of the scalar

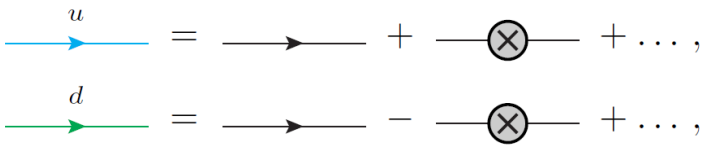

Figure 6.1: Diagrammatic expansion of up and down quark propagators

density is represented by a cross $\otimes = \varepsilon_{ud} \sum_z \bar{\ell}(z)\,\ell(z) = \varepsilon_{ud}^L \sum_z \left[\bar{\ell}(z)\,\ell(z)\right]^L$, with ℓ being either u or d. Here and in the following the superscript L stays for bare lattice quantity. In particular we have:

$$\varepsilon_{ud} = Z_{\Delta m} \varepsilon_{ud}^L \,, \tag{6.6}$$

but as already stressed previously, in tmQCD at maximal twist the non-singlet scalar density renormalizes as $Z_P = 1/Z_{\Delta m}$ so that the combination $\varepsilon_{ud} \sum_z \bar{\ell}(z)\,\ell(z)$ is renormalization group invariant.

The square of the S_ℓ propagator entering Eqs. 6.5 can be easily calculated on the lattice by using S_ℓ itself as the source vector of a new inversion.

It is useful to introduce the following operators acting as absolute variations:

$$\Delta_d \mathcal{O} = \mathcal{O}(d) - \mathcal{O}(\ell)\,, \qquad \Delta_u \mathcal{O} = \mathcal{O}(\ell) - \mathcal{O}(u)\,, \qquad \Delta\mathcal{O} = \frac{\Delta_d \mathcal{O} + \Delta_u \mathcal{O}}{2} \quad ,$$

and the relative variation operator:

$$\delta_d \mathcal{O} = \frac{\Delta_d \mathcal{O}}{\mathcal{O}(\ell)}\,, \qquad \delta_u \mathcal{O} = \frac{\Delta_u \mathcal{O}}{\mathcal{O}(\ell)}\,, \qquad \delta\mathcal{O} = \frac{\Delta\mathcal{O}}{\mathcal{O}(\ell)}\,. \tag{6.7}$$

6.2 Determination of $m_d - m_u$

In order to compute the QIB corrections to any observable, we must first of all fix the value of the quantity ε_{ud}. This is can be achieved as already done in chapter 4 to fix any other mass, by requiring a certain quantity depending (at first order) from the light quarks mass splitting ε_{ud} to reproduce its physical value.

A first trivial observation comes from Eq. (6.4) telling us that all the quantities that do not involve a light valence quark propagator do not get corrected at first order in ε_{ud}. This is the case for example of heavy-heavy and heavy-strange meson's masses and decay constants, etc.

Pions' masses and decay constants too do not get corrected at first order. This can be shown diagrammatically as follows:

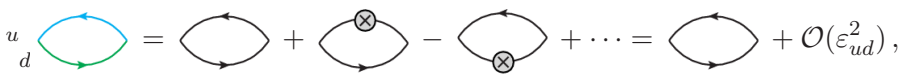

for the charged pions two point function $C_{\pi^+\pi^-}(t) = \sum_{\vec{x}} \langle\, \bar{u}\gamma_5 d(x)\ \bar{d}\gamma_5 u(0)\,\rangle$, and:

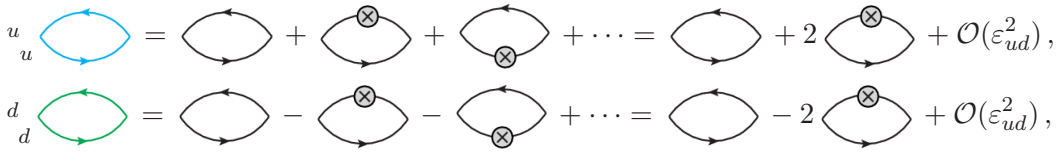

for the connected diagrams entering neutral pion two point function $C_{\pi^0\pi^0}(t) = \frac{1}{2}\sum_{\vec{x}} \langle\, (\bar{u}\gamma_5 u - \bar{d}\gamma_5 d)(x)\ (\bar{u}\gamma_5 u - \bar{d}\gamma_5 d)(0)\,\rangle$. It is easy to show that the first order corrections cancel also for the disconnected diagrams contributing to $C_{\pi^0\pi^0}(t)$ in the full theory.

First order corrections to masses and decay constants are instead different from zero for flavored mesons. Here we discuss the case of strange particles but the discussion proceeds unchanged if the strange is replaced with a charm or a bottom quark. The QIB correction to the two-point correlation functions of the strange mesons are

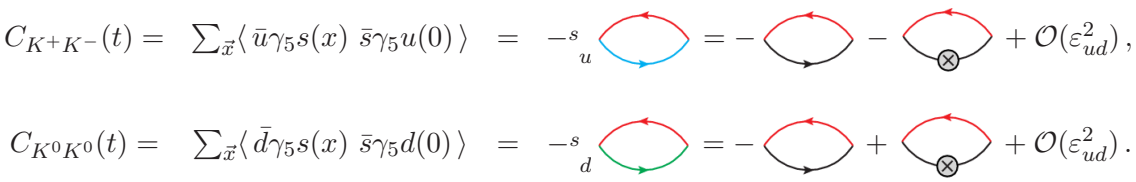

(6.8)

In the diagrams above and in the following the strange quark line is red. Note that the correction to the neutral mesons is equal in magnitude and opposite in sign with respect to that to the charged particles, i.e. $\Delta_d C_{KK}(t) = \Delta_u C_{KK}(t)$.

We can therefore use the Kaon mass splitting $M_{K^0} - M_{K^+}$ to fix the value of the parameter ε_{ud}. In the full theory the correlation functions of Eqs. 6.8 behave as:

$$\begin{aligned} C_{K^+K^-}(t) &= \frac{Z^2_{K^\pm}}{M_{K^\pm}} e^{-TM_{K^\pm}/2} \cosh\left[M_{K^\pm}\,(T/2-t)\right] \\ C_{K^0K^0}(t) &= \frac{Z^2_{K^0}}{M_{K^0}} e^{-TM_{K^0}/2} \cosh\left[M_{K^0}\,(T/2-t)\right], \end{aligned}$$

where the ground state dominates. In these formulae the mass and Z are function of the quark masses, and in particular of the parameter ε_{ud}. Expanding at first order in ε_{ud} we get:

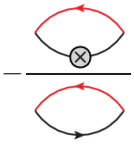

(6.9)

We can therefore use the correction to the Kaon mass to fix the value of ε_{ud}, as illustrated in the following sections.

6.2.1 Correlation function analysis

By applying the method explained in previous section, we have computed the correlation function ratio $\delta C_{K,K}(t)/\varepsilon_{ud}$ over the whole set of $N_f = 2$ gauge ensembles already used for the quark masses determination, considering about 150 configurations for each ensemble.

The data of $\delta C_{K,K}(t)/\varepsilon_{ud}$ has been fitted with Eq. 6.9, leaving Z_K, M_K, $\delta Z_K/\varepsilon_{ud}$ and $\delta M_K/\varepsilon_{ud}$ as free parameters. The parameters M_K, Z_K are constrained by fitting simultaneously the function $C_{K,K}(t)$ with the expression:

$$C_{K,K}(t) = \frac{Z_K^2}{M_K} e^{-TM_K/2} \cosh\left[M_K\left(T/2 - t\right)\right]. \tag{6.10}$$

In Fig. 6.2 we show the fit of the correlation function $C_{K,K}$ and $\delta C_{K,K}/\varepsilon_{ud}$. It is clear that the two correlation functions are well fitted by the mentioned functions.

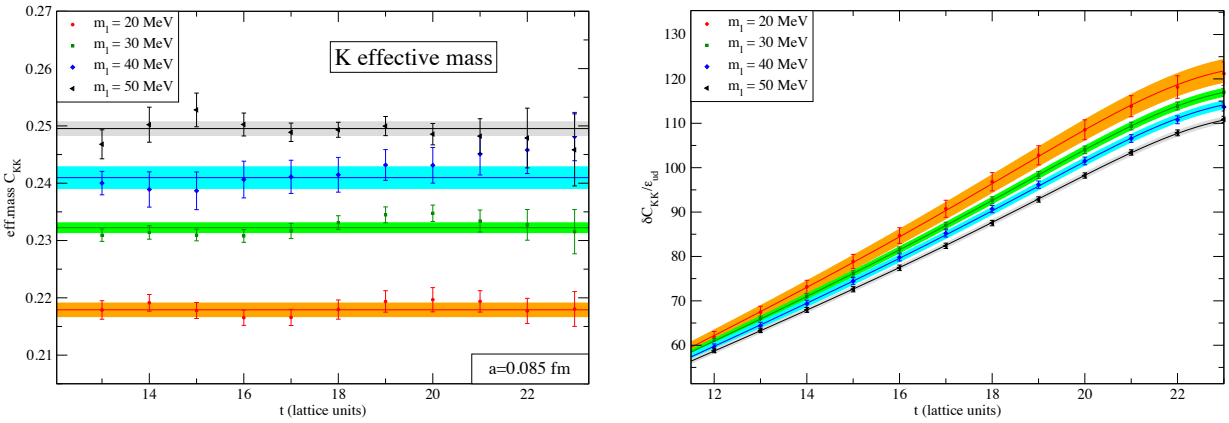

Figure 6.2: Left panel: effective mass of $C_{K,K}$ correlation function. Right panel: ratio $\delta C_{K,K}(t)/\varepsilon_{ud}$. Data is shown for a single lattice spacing ($\beta = 3.80$) at four different values of the sea quark mass. The colored band show the 68% C.L contour of the fit of Eq. 6.9 over the computed data. Light quark mass is in $\overline{\text{MS}}$ at 2 GeV.

6.2.2 Continuum and chiral extrapolation

After determining the parameter $\delta M_K/\varepsilon_{ud}$ on each gauge ensemble we have performed the continuum and chiral fit. We shall now discuss the chiral and continuum extrapolations. The chiral formulae for ΔM_K^2 and δF_K were obtained long ago within the $SU(3)_V$ effective theory in ref. [56]. It is useful to consider the correction to the meson's mass square because this is a finite quantity in the chiral limit. The relevant formulae are:

$$\begin{aligned} M_\pi^2 &= 2B_0 m_{ud}\,, \\ M_K^2 &= B_0(m_{ud} + m_s)\,, \\ M_\eta^2 &= 2B_0(m_{ud} + 2m_s)/3\,, \\ \mu_P &= \frac{M_P^2}{16\pi^2 f_0^2}\ln(M_P^2/\mu^2)\,, \end{aligned} \tag{6.11}$$

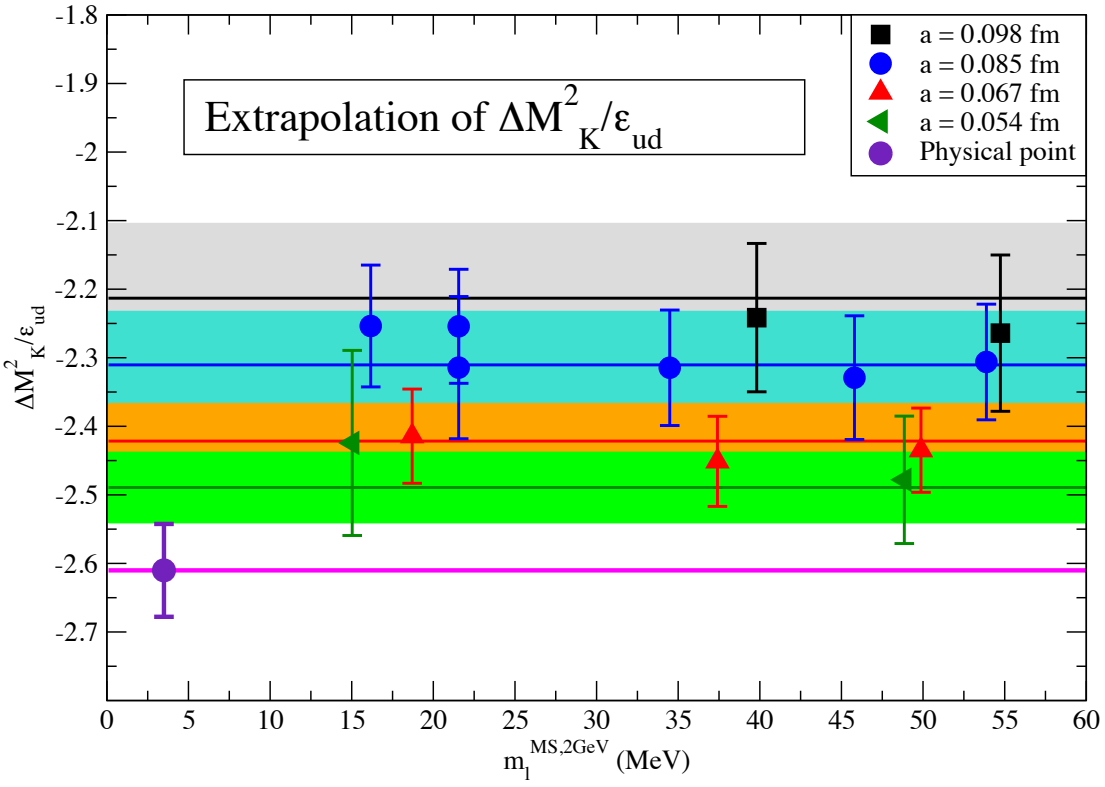

Figure 6.3: Combined chiral and continuum extrapolations of $\Delta M_K^2/\varepsilon_{ud}$.

Since our results have been obtained by quenching the strange quark ($N_f = 2$), we have chosen to fit our data with the formulae resulting by expanding the r.h.s. of Eqs. (6.11) with respect to m_{ud}/m_s. This procedure is justified when the average light quark mass is sufficiently small as appears to be the case by looking at our data shown in Figure 6.3.

Our results, obtained at four different lattice spacings for several values of the average light quark mass, do not show a visible dependence with respect to m_{ud} that can be quantified within the plotted errors. These errors combine the statistical and systematic errors coming from the uncertainties on the lattice spacing and on the renormalization constants). We have consequently fitted the numerical data with the following functional form:

$$\left[\frac{\Delta M_K^2}{\varepsilon_{ud}}\right](m_{ud}, a) = \left[\frac{\Delta M_K^2}{\varepsilon_{ud}}\right]^{QCD} + C_M a^2. \tag{6.12}$$

The results of the fit is $\Delta M_K^2/\varepsilon_{ud} = -2.61(7)\,\mathrm{MeV}$.

After having determined $\Delta M_K^2/\varepsilon_{ud}$ we can use the physical value of the $K^\pm - K^0$ mass difference as input to determine $[m_d - m_u]^{QCD}$. But before doing this, we have to understand how to deal with the isospin breaking corrections to the Kaon mass originating from electromagnetism.

6.2.3 Electromagnetic corrections

When comparing the theoretical predictions with the experimental numbers we cannot neglect the isospin breaking corrections induced by electromagnetic interactions. As an effect of ultraviolet

divergences, the separation of the electromagnetic and strong QIB effects is artificial and ambiguous [57, 58]: the amount of each of the two contributions depend on the definition by which they are separated, whereas they do not correspond to any physical observable.

In this work we only consider the QCD corrections: this is equivalent to say that we follow the common procedure of separating the two isospin breaking contributions by switching off electromagnetism. Obviously the attempt to use physical quantities to fix ε_{ud}^{QCD} fails, since there are no data with electromagnetic interactions switched off and, for this reason, we shall use the definition and determination of the electromagnetic corrections done by other groups.

According to Dashen's theorem [59], electromagnetic corrections are the same for $M^2_{K^0} - M^2_{K^+}$ and $M^2_{\pi^0} - M^2_{\pi^+}$ in the chiral limit while, as discussed in the previous sections, pions' masses are not affected by first order QCD corrections. Beyond the chiral limit it is customary [60] to parametrize violations to the Dashen's theorem in terms of small parameters and, concerning $M^2_{K^0} - M^2_{K^+}$, we have:

$$\left[M^2_{K^0} - M^2_{K^+}\right]^{QCD} = \left[M^2_{K^0} - M^2_{K^+}\right]^{exp} - (1+\varepsilon_\gamma)\left[M^2_{\pi^0} - M^2_{\pi^+}\right]^{exp}, \tag{6.13}$$

where we have neglected QCD contributions of the second order $O(\varepsilon^2_{ud})$ in the pion's mass difference. Using chiral perturbation theory and results from lattice QCD calculations of the electromagnetic corrections [60] estimates:

$$\begin{aligned} &\varepsilon_\gamma = 0.7(5)\,, \\ &\left[M^2_{K^0} - M^2_{K^+}\right]^{QCD} = 6.05(63) \times 10^3 \text{ MeV}\,. \end{aligned} \tag{6.14}$$

6.2.4 Determination of $m_d - m_u$

By using Eqs. (6.14) and the results of the fits of our data shown in Figure 6.3 to the functional forms given in Eqs. (6.12) and (6.20) we get the following results:

$$[m_d - m_u]^{QCD}\,(\overline{\text{MS}}, 2\text{GeV}) = 2\varepsilon_{ud}^{QCD} = 2.27(24) \text{ MeV}. \tag{6.15}$$

After having fixed the value of ε_{ud} we can proceed to evaluate the other observables of our interest.

6.3 Isospin breaking effects in f_K

The value of the Kaon leptonic decay constant f_K is used together with the Pion's one f_π to determine the ratio between the CKM matrix elements $\left|\frac{V_{us}}{V_{ud}}\right|$, as explained in chapter 2. The world average value for the ratio f_K/f_π computed in the isospin symmetric limit is 1.193(5). This value is corrected for IB using chiral perturbation theory. A recent calculation [61] gives:

$$\left[\frac{f_{K^+}/f_{\pi^+}}{f_K/f_\pi} - 1\right]^{QCD} = -0.22(6)\%\,. \tag{6.16}$$

This correction is quite poorly known, and its error is of the same order of magnitude of the statistical error of f_K/f_π itself. Moreover it is obtained within an effective theory, and it would

be interesting to have a first principle computation to compare. We will provide our estimate of the QIB corrections to f_K using the method exposed in sect. 6.1.

The WI formula for f_K is:

$$f_K \equiv \frac{(\mu_s + \mu_l)\, Z_K}{M^2}\,, \tag{6.17}$$

with μ_l and μ_s being respectively the light and strange bare quark masses, and Z_K the matrix element of the K local interpolating operator. It is immediate to show that:

$$\delta f_K = \frac{f_{K^+} - f_{K^-}}{2 f_K}\,, \tag{6.18}$$

is given by:

$$\delta f_K = \frac{\varepsilon_{ud}}{\mu_s + \mu_l} + \delta Z_K - 2\delta M_K. \tag{6.19}$$

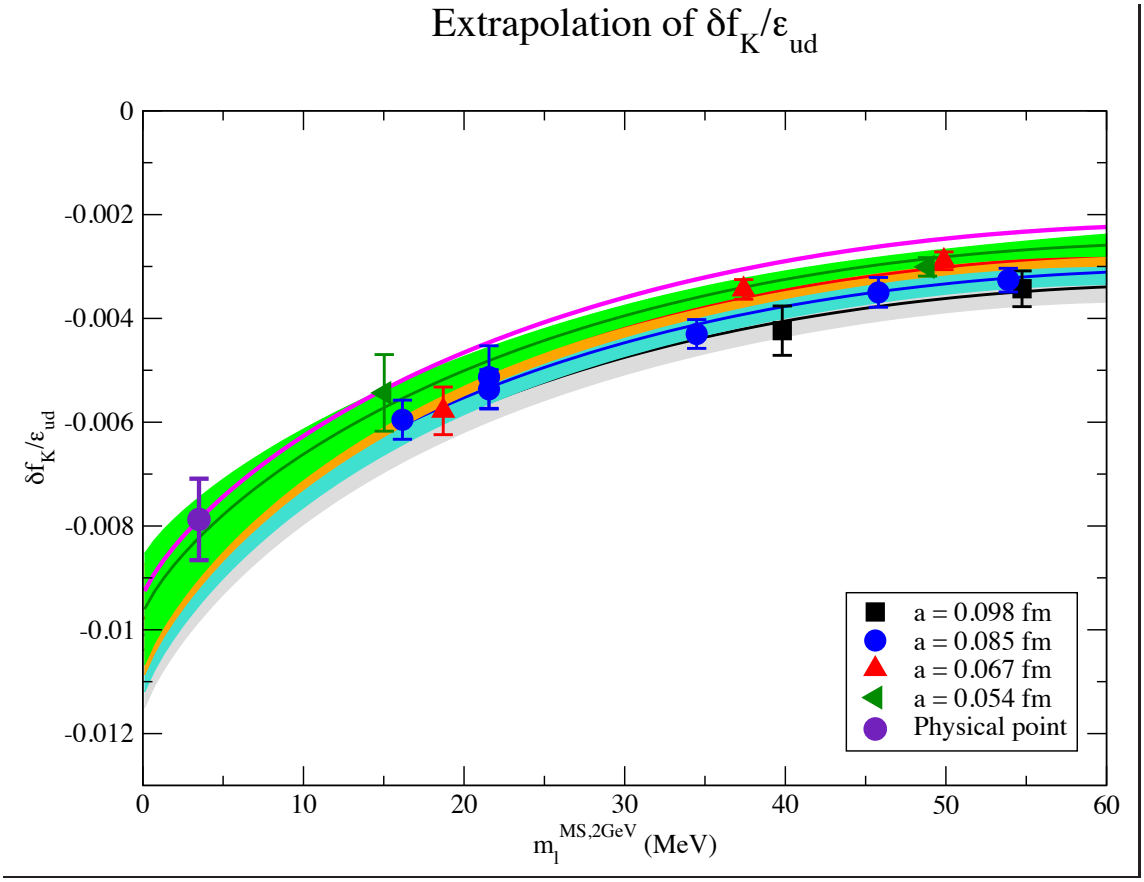

Figure 6.4: Combined chiral and continuum extrapolations of $\delta f_K/\varepsilon_{ud}$.

This can be computed directly using the parameters $\delta Z_K/\varepsilon_{ud}$ and $\delta M_K/\varepsilon_{ud}$ fitted from the time behavior of the δC_{KK} correlation function of previous section.

After having determined δf_K on each gauge ensemble we have to perform the chiral and continuum extrapolation of the data. We have performed a fit of the data with the formula:

$$\frac{\delta f_K\,(m_l, a)}{\varepsilon_{ud}} = A + B\, m_l \log m_l + C\, m_l + D\, a^2\,, \tag{6.20}$$

which is the $SU(2)$ Chiral Perturbation Theory prediction plus a quadratic dependence from the lattice spacing.

In Fig. 6.4 we show the fit of the simultaneous fit of our data. The dependence from m_l is clearly visible, although the two terms m_l and $m_l \log m_l$ are only marginally fitted simultaneously.

Using the value of ε_{ud} determined in the previous section we get:

$$\left[\frac{f_{K^+}/f_{\pi^+}}{f_K/f_\pi} - 1\right]^{QCD} = \left[\frac{f_{K^+}}{f_K} - 1\right]^{QCD} = -0.38(6)\%\,, \tag{6.21}$$

which is almost double than the straight Ch-PT perturbation theory 6.16.

6.4 Neutron - Proton mass splitting

An interesting quantity to compute is the proton-neutron mass splitting. We have performed a preliminary determination of this quantity at a fixed lattice spacing, on which we shall report in the following.

6.4.1 Relevant correlations

One of the simplest[1] color singlet operator which is possible to build from two u and one d quark fields, with definite parity and transforming as a spin $1/2$ representation is given by:

$$O_N^{\pm} = \epsilon_{abc} \frac{1 \pm \gamma^0}{2} u_c \left(u_a C\gamma_5 d_b^T\right)\,. \tag{6.22}$$

The proton mass can therefore be determined from the correlation function:

$$C_{pp}^{\pm}(t) = \sum_{\vec{x}} \langle \left[\epsilon_{abc}\left(\bar{u}_a C\gamma_5 \bar{d}_b^T\right) \bar{u}_c \frac{1 \pm \gamma^0}{2}\right](x) \left[\epsilon_{def} \frac{1 \pm \gamma^0}{2} u_d \left(u_e^T C\gamma_5 d_f\right)\right](0) \rangle\,, \tag{6.23}$$

while the neutron from the correlation:

$$C_{nn}^{\pm}(t) = \sum_{\vec{x}} \langle \left[\epsilon_{abc}\left(\bar{d}_a C\gamma_5 \bar{u}_b^T\right) \bar{d}_c \frac{1 \pm \gamma^0}{2}\right](x) \left[\epsilon_{def} \frac{1 \pm \gamma^0}{2} d_d \left(d_e^T C\gamma_5 u_f\right)\right](0) \rangle\,. \tag{6.24}$$

Each correlation function corresponds to two different contractions, diagrammatically:

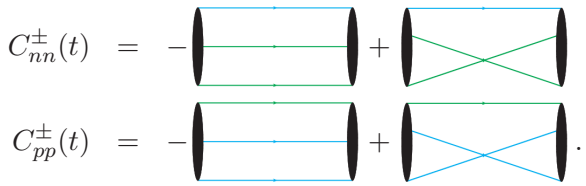

Moreover the proton propagates only in the first half of the correlation function C^+ and in the second half of C^-, while its negative parity partner propagate in the other halves, and in order

[1] there are other possible interpolators as simple as the proposed one, but this choice maximize the signal/noise ratio.

to increase statistical, we shall extract nucleon masses from the combinations:

$$\begin{aligned} C_{nn}(t) &= C^{+}_{nn}(t) - C^{-}_{nn}(T-t)\,, \\ C_{pp}(t) &= C^{+}_{pp}(t) - C^{-}_{pp}(T-t)\,. \end{aligned} \tag{6.25}$$

In the isospin symmetric limit there is no difference between the two correlation functions, which are identically equivalent. The correction to the isospin symmetric limit is given by:

$C^{\pm}_{nn}(t) = -$ 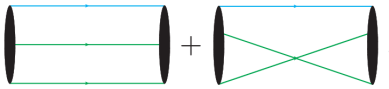 ,

$C^{\pm}_{pp}(t) = -$ 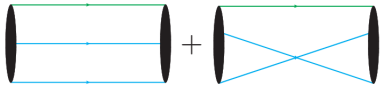 ,

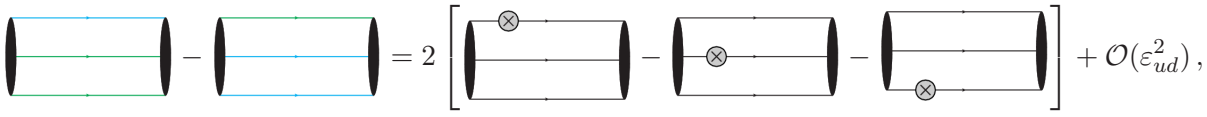

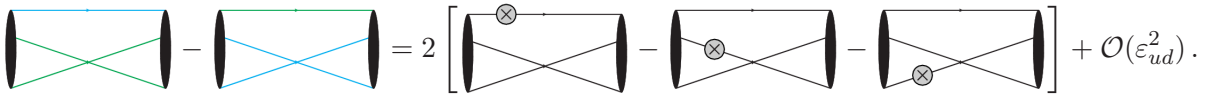

(6.26)

6.4.2 Correlation computation and analysis

The nucleon correlation functions are known to be much noisier than the mesonic ones, and the signal to noise ratio increases very fast with the increasing of the time, therefore it is important to isolate the lowest state the sooner it is possible. For this reason the quark fields entering the source interpolating operators have been "Gaussian smeared" as already explained in section (5.4.1), using for the parameters k and n values optimized in ref. [62] where the same gauge configurations of this study have been used.

The extraction of physical informations from nucleons euclidean two point functions proceeds along the same lines described in details in the case of the Kaon. By using the diagrammatic analysis of Eqs. (6.26) we have:

$$C_{NN}(t) = -$$ 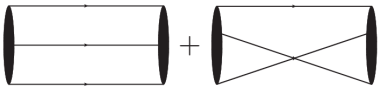 $$= W_N e^{-M_N t} + \cdots\,, \tag{6.27}$$

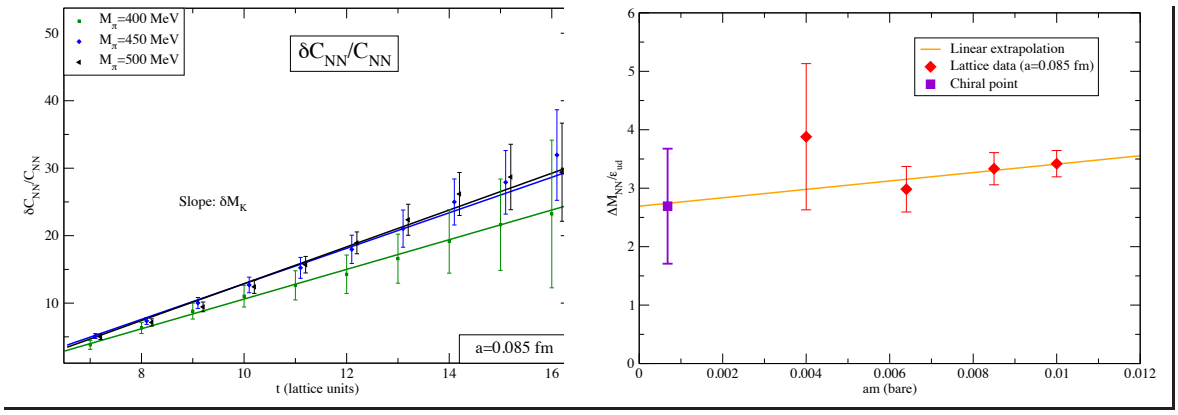

Figure 6.5: *Left panel*: correlation functions $\delta C_{NN}(t)/a\varepsilon^L_{ud}$. The data are at fixed lattice spacing $a = 0.085\,\text{fm}$ for different values of m_l. *Left panel*: linear extrapolation of the neutron-proton mass splitting.

and

$$\delta C_{NN}(t) \;=\; -$$

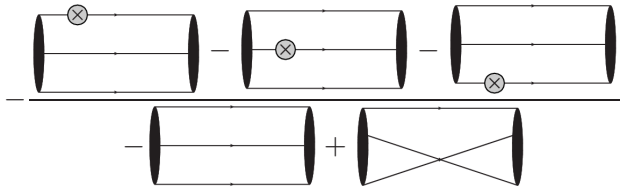

$$+$$

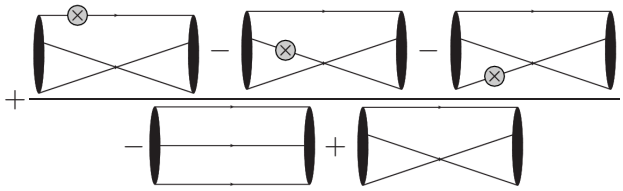

$$= \quad \delta W_N - t\Delta M_N + \cdots\,, \tag{6.28}$$

where the dots represent sub leading exponentials contributing to the correlation functions. By extracting the slope in t of $\delta C_{NN}(t)$, we can determine $\Delta M_N = (M_n - M_p)/2$. In the left panel of Figure 6.5 we show the effective masses $M_N^{eff}(t)$ as extracted from the correlation functions $\delta C_{NN}(t)/a\varepsilon^L_{ud}$ that we have fitted to straight lines, according to Eq. (6.28), i.e. without taking into account the finite time extent of the lattice because it affects the correlation functions only at large times where no signal can be extracted within our errors. In the right panel of Figure 6.5 we show the chiral extrapolation of $\Delta M_N/\varepsilon_{ud}$ performed by using a simple linear fitting function [63].

By using the results of the fit and the value of ε^{QCD}_{ud} previously found we get:

$$[M_n - M_p]^{QCD} = 2\varepsilon^{QCD}_{ud}\left[\frac{\Delta M_N}{\varepsilon_{ud}}\right]^{QCD} = 2.7(9)\ \text{MeV}\,, \tag{6.29}$$

This number is our best estimate at present but it has been obtained at fixed lattice spacing and with limited statistics. We plan to refine the calculation in future.

6.5 Isospin breaking effects in $K_{\ell 3}$

The method exposed in this chapter allow to determine QIB corrections to many other quantities, such as the semi-leptonic form factors involved in $K_{\ell 3}$ decays. The determination of the correction to such quantity is of primary importance given the strong impacts that they may have on the determination of V_{us} CKM matrix element.

6.5.1 Semi-leptonic form factors

Let us first describe how the semi-leptonic form factors are determined on lattice.

Our aim is to determine the $f_+^{K\to\pi}$ as a function of transferred momentum, with particular attention to the value assumed at 0 transferred momentum. The form factor is defined by the decomposition:

$$\langle\pi(p')|V_\mu|K(p)\rangle = \left[f_+\left(q^2\right)\left(p+p'\right)_\mu + f_-\left(q^2\right)\left(p-p'\right)_\mu\right] \ , \qquad q^2=(p-p')^2. \tag{6.30}$$

In order to determine such matrix element we start by defining the three point function:

$$C^{K\pi}_{p_K,p_\pi;\mu}(t) = \quad = \sum_{\vec{x},\vec{y}} \left\langle O^{p_\pi}_\pi\left(t_{sink},\vec{y}\right)\ \widehat{V}_\mu\left(t,\vec{x}\right)\ O^{p_K\dagger}_K\left(0\right)\right\rangle \ , \tag{6.31}$$

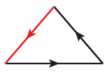

where $O^p_K(0)$ is the operator which creates a Kaon in the origin and $O^p_\pi\left(t_{sink},\vec{y}\right)$ a Pion in the point $\left(t_{sink},\vec{y}\right)$, with t_{sink} kept fixed. The p means that the two particles are created in a system in presence of twisted boundary conditions, which force particles to have at least momentum p (this allow to change continuously the values of the momentum injected in the system and study kinematics region not accessible otherwise). This correlation function can be computed by taking the contraction:

$$C^{K\pi}_{p_K,p_\pi;\mu}(t) = \mathrm{Tr}\left[S^{p_K}_s\left(0,y\right)\gamma_\mu\Sigma^{p_\pi}_{s,l}\left(y,0\right)\gamma_5\right] \ , \tag{6.32}$$

where $S^{p_K}_s$ is the propagator satisfying the Dirac equation for the strange:

$$D_s\left(x,y\right)S^{p_K}_s\left(0,y\right) = e^{-ip_Kx}\delta\left(x,0\right) \ , \tag{6.33}$$

and $\Sigma^{p_K,p_\pi}_{s,l}$ is the *sequential* propagator, satisfying the Dirac equation:

$$D_l\left(x,y\right)\Sigma^{p_\pi}_{s,l}\left(y,0\right) = e^{-ip_\pi x}\gamma_5 S^{p_K=0}_s\left(x,0\right)\delta_{x_0=t_{sink}}. \tag{6.34}$$

In these equations D_i is the fermionic matrix for the quark i. It is possible to show that the evaluation of S_s requires an inversion of the fermionic matrix for each value of p_K, and $\Sigma_{s,l}$ an additional inversion for each value of p_π.

Where ground state dominates, correlation function 6.32 behaves as:

$$C^{K,\pi}_{p_K,p_\pi;\mu}(t) = \frac{1}{\sqrt{Z^K_V Z^\pi_V}}\frac{Z_K Z_\pi}{4E^K_{p_K}E^\pi_{p_\pi}}e^{-t\left(E^K_{p_K}-E^\pi_{p_\pi}\right)}e^{-TE^\pi_{p_\pi}/2}\left\langle K_{p_K}\right|V_\mu\left|\pi_{p_\pi}\right\rangle \ , \tag{6.35}$$

with E being meson energy (equal to the mass in the case $\vec{p}=\vec{0}$).

It is possible to build smart ratio in which almost all coefficients but the matrix element of interest cancel out. In particular we define:

$$R_\mu \equiv \frac{C^{K,\pi}_{p_K,p_\pi;\mu}(t)\, C^{\pi,K}_{p_\pi,p_K;\mu}(t)}{C^{K,K}_{p_K,p_K;\mu}(t)\, C^{\pi,\pi}_{p_\pi,p_\pi;\mu}(t)} =$$

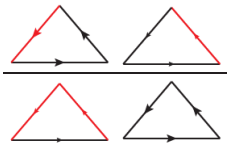

$$= \frac{1}{4E^K_{p_K} E^\pi_{p_\pi}} \left|\langle K_{p_K}| V_\mu |\pi_{p_\pi}\rangle\right|^2 , \qquad (6.36)$$

where $C^{K,K}$ and $C^{\pi,\pi}$ are degenerate case of three point correlation functions (in which case the form factor is 1 because of the conservation of vectorial current). By measuring the value of E from the simple two points function we are left with $|\langle K_{p_K}| V_\mu |\pi_{p_\pi}\rangle|$ which can be studied in terms of p_K and p_π to determine form factors.

6.5.2 QIB corrections to form factor

In the present section we will list the contractions relevant to determine the QIB corrections to the form factors. The diagrams entering the correction to the ratio 6.36 are:

$$\delta R^\mu_{K\pi}(t) =$$

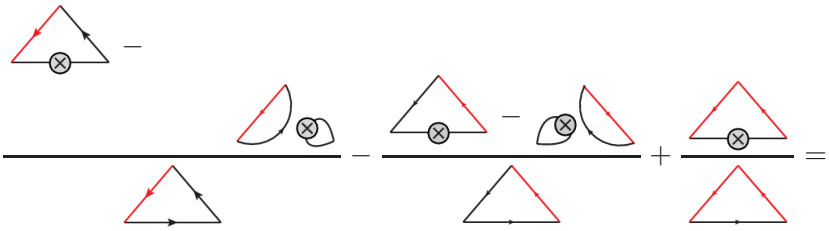

$$= 2\delta\left[\langle\pi|V^\mu_{su}|K\rangle\right] - \delta E_K + \cdots .$$

Given the strong complication involved in the precise determination of disconnected diagrams, in this work we have not calculated disconnected diagrams and we cannot show results for $\delta f^{K\pi}_\pm(q^2)$. For the time being and in order to show that our method works also in the case of three point functions and form factors, we have calculated the difference of $f^{K^0\pi^-}_+(q^2)$ with respect the isospin symmetric value $f^{K\pi}_+(q^2)$, i.e $\delta_d f^{K\pi}_+(q^2)$. This is a quantity that cannot be measured directly because the missing contribution, $\delta_u f^{K\pi}_+(q^2)$, is neither equal nor related in a simple way to $\delta_d f^{K\pi}_+(q^2)$. The two different contributions are associated to two independent isospin channels, nonetheless its computation is interesting to show the various possible applications of our method. Neglecting disconnected contribution we can compute only:

$$\delta_d R^\mu_{K\pi}(t) =$$

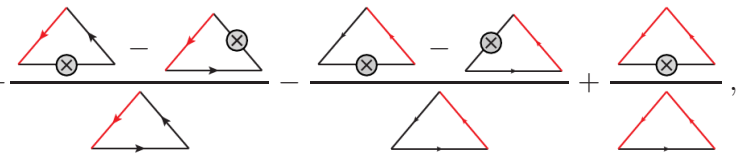

$$= 2\delta_d\left[\langle\pi|V^\mu_{su}|K\rangle\right] - \delta E_K + \cdots . \qquad (6.37)$$

In Fig. 6.6 we show the ratios $R^0_{K\pi}(t)$ and their corrections computed on a single ensemble of gauge configurations. The good precision of the correlation function means that the method will

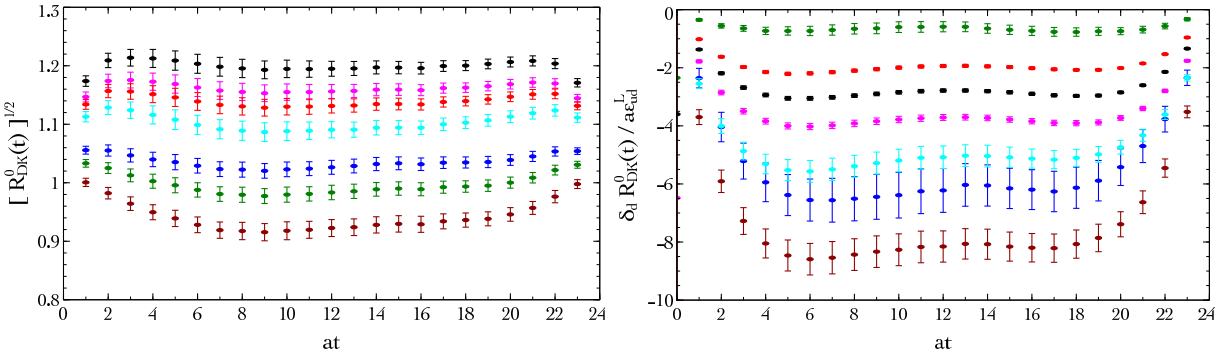

Figure 6.6: *Left panel*: we show our results for $\sqrt{R^0_{K\pi}(t)}$ for several values of the momentum transfer. *Right panel*: we show our results for $\delta_d R^0_{K\pi}(t)/a\varepsilon^L_{ud}$ for several values of the momentum transfer. The data are obtained a fixed lattice spacing $a = 0.085$ fm and at fixed $am^L_{ud} = 0.0064$.

allow - when completed with the computation of disconnected diagrams - to determine the QIB correction to the f_+ form factors and provide stronger bound on the value of V_{us} CKM matrix element.

Chapter 7

$N_f = 2 + 1 + 1$ simulations

As explained in section 3.5.2.3 the quenching of the strange and charm quark is believed to have quite small effects on physical observable (and b quark even smaller). Nonetheless a direct evaluation of the amount of the corrections induced by the unquenching of these quarks is difficult and still lacking. The partial quenching of s and c quarks induces therefore a systematic effect which is not quantifiable. The only practical way to estimate it is to perform a lattice QCD computation including these two quarks, and to compare the results obtained with partially quenched simulations.

In this chapter we will discuss briefly the preliminary results obtained from a set of $N_f = 2 + 1+1$ simulations recently carried out by ETM [64,65]. We will briefly explain how a non degenerate doublet of quark s and c can be introduced maintaining the automatic $\mathcal{O}(a)$ improvement, describe the lattice ensemble produced and list all correlation functions computed on them. On the end we will present preliminary results for selected quantities.

7.1 Twisted mass with s and c quarks

7.1.1 Un-degenerate doublet

On its simplest form twisted mass QCD describes a degenerate doublet of quarks. In order to introduce the strange and charm quarks, which have a quite different mass, we must generalize the structure of the twisted mass terms in order to accommodate for a mass splitting, by writing the mass term of the Lagrangian as:

$$S_{heavy} \equiv \bar{\chi}_h \left(m + i\mu_\sigma \gamma_5 \tau_1^{flav} + \mu_\delta \tau_3^{flav} \right) \chi_h, \qquad \chi_h = \begin{pmatrix} \chi_s \\ \chi_c \end{pmatrix}. \tag{7.1}$$

The μ_δ induces a splitting between the mass of the doublet, and comparing this expression with the one presented in section 3.3.4 we can notice that the twisting term $i\mu_\sigma\gamma_5$ is not anymore diagonal in the flavor isospin. This is needed because the direction z has been used to induce the splitting, and in order to have a real quark determinant the twist term must be taken orthogonal to it, as shown in [66].

The bare parameters μ_σ, μ_δ are related to the renormalized strange and charm mass through

the relation:

$$\begin{aligned} m_s^{ren} &= Z_P^{-1}\left(\mu_\sigma - Z_P/Z_S\mu_\delta\right) \\ m_c^{ren} &= Z_P^{-1}\left(\mu_\sigma + Z_P/Z_S\mu_\delta\right). \end{aligned}$$

The value of μ_σ and μ_δ must be tuned appropriately in order to reproduce the physical value of the s and c quarks.

The automatic order a improvement can be obtained using the same value of the critical parameter $m = 1/2\kappa - 4$ used for the light sector.

7.1.2 Gauge action and renormalization procedure

When adding a second doublet of quarks, the value of the light quark mass for which exceptional configurations shows up increases significantly at fixed physical situation [67]. For this reason being interested in considering quark mass as near the chiral point as done in the $N_f = 2$ simulations, a different gauge action was chosen for $N_f = 2 + 1 + 1$ computations. Iwasaki gauge action has proved to be more efficient in suppressing exceptional configuration with respect to the tree-level-Symanzik improved action [68], and therefore has been used through all the simulations here considered.

When calculating renormalization constants in the RI/MOM scheme, one has to perform a chiral extrapolation of the constants. This must be done in unitary setup in which both sea and valence quark masses are send to zero, and therefore means that one needs to produce dedicated gauge ensembles with four degenerate quarks in order to compute renormalization constants. An additional problem comes again from exceptional configuration, which in presence of a second *light* doublet are present at much higher quark mass than when in presence of an *heavy* doublet, even using Iwasaki gauge action. The solution in this case is to work off maximal twist: in this situation, lower quark masses can be reached without incur in exceptional configuration. In order to achieve $\mathcal{O}(a)$ improvement, average between quantities computed at opposite twist angle must be performed. This strategy has been pursued by ETM collaboration. All these technical problems render the computation of the renormalization constants much more difficult than in the $N_f = 2$ case, indeed the computation is still going one well after the production of the gauge configurations. This is the main reason for which all the results presented in this chapter are still preliminary.

7.1.3 Setup used for the correlation function measurement

The structure of the heavy twisted mass Lagrangian term 7.1 is non-diagonal in the twist isospin space. This means that at finite lattice spacing s and c quarks can mix among themselves. This imply that interpolating operator containing the c quark will produce correlation functions whose large time behavior will be dominated by stranged hadron in place of the expected charmed ones. This effect goes away when taking the continuum limit, but makes very hard to extract the true values of mass and matrix elements of hadrons containing s or c quarks.

For this reason we have preferred to work in a non-unitary setup in which the s and c mesons are separate part of a light-type doublet of the kind presented in Eq. 3.52. In the computation of correlation functions we have used alternatively only one of the two strange or charm quark present in each doublet, as already done in all previous $N_f = 2$ work. The effects of non-unitarity

are expected to be quite mild, as the difference between sea and valence quark in this case are only discretization effects and therefore are expected to go away in the continuum limit.

7.1.4 Simulation details

These are the parameters of our analysis:

- three different lattice spacings, $\beta = 1.90,\ 1.95,\ 2.10 \rightarrow a \sim 0.06 - 0.09\,\mathrm{fm}$
- several sea masses corresponding to $M_\pi = 230 - 500\,\mathrm{MeV}$
- 3 heavy valence quark masses around the physical strange mass $M_K = 450 - 700\,\mathrm{MeV}$
- three volumes: $24^3 \times 48,\ 32^3 \times 64,\ 48^3 \times 96$.

7.2 B_K parameter

In this section we will briefly report about the computation of the B_K parameter. As the renormalization constant of the operator has been computed only on one of the three lattice spacings, it is not possible to perform the continuum limit and therefore the analysis is presented at the fixed lattice spacing $\beta = 1.95$ although the bare values of B_K are available for all the lattice spacing reported in section 7.1.4.

In order to compute the value of B_K according to what shown in chapter 2, it is necessary to take the ratio between the matrix element of operator:

$$Q_1 = \frac{1}{4}\left[\bar{s}\gamma_\mu\left(1-\gamma_5\right)d\right]\left[\bar{s}\gamma_\mu\left(1-\gamma_5\right)d\right]\,, \tag{7.2}$$

between Kaon and anti-Kaon states and the square of the matrix element of the axial current:

$$A_0 = \left[\bar{s}\gamma_0\gamma_5 d\right]\,, \tag{7.3}$$

between Kaon (or anti-Kaon) and the vacuum.

This means that we should determine these matrix elements from the long time behavior of appropriate correlators, but actually we can take advantage of the definition of B_K as a ratio and work directly with the correlation function itself. Putting an operator interpolating for the Kaon at time t_{source} and another at time t_{sink} we can compute the ratio between the correlation functions:

$$B\left(t\right) = \frac{\sum_{\vec{x}}\left\langle \bar{K}^0\left(\vec{x}, t_{sink}\right)\middle| Q_1\left(t\right)\middle| K^0\left(\vec{0}, t_{source}\right)\right\rangle}{\frac{8}{3}\left(\sum_{\vec{y}}\left\langle \bar{K}^0\left(\vec{y}, t_{sink}\right)\middle| A_0\left(t\right)\middle|0\right\rangle\right)\left(\sum_{\vec{z}}\left\langle 0\middle| A_0\left(t\right)\middle| K^0\left(\vec{z}, t_{source}\right)\right\rangle\right)}\,. \tag{7.4}$$

This ratio behaves as:

$$B\left(t\right) = \frac{B_1 f_B^2 M_K^2 e^{-(t_{sink}-t)M_K-(t-t_{source})M_K}+\dots}{\frac{8}{3}f_B^2 M_K^2 e^{-(t_{sink}-t)M_K-(t-t_{source})M_K}+\dots} = B_K^{bare} + E\left(t\right)\,, \tag{7.5}$$

where the dots and $E\left(t\right)$ contain all the contributions coming from excited states. Therefore B_K is simply given by the ratio between correlation functions taken only where lower lying state

dominates. It is important to choose $t_{sep} \equiv t_{sink} - t_{source}$ large enough in order to allow some point t to be in the range where ground state dominates, but not too large, otherwise the signal will be destroyed by noise. A common choice is to take $t_{sep} = T/2$, which allows to improve statistics averaging between the two halves of the time lattice extension.

Stochastic sources can be used to improve the signal, but as we have to ensure the stochastic closure of the sources, careful attention must be placed in taking two different stochastic walls at source and sink (otherwise, non-local closure of the sink can take place).

The correlation at the numerator of 7.4 is given by two different Wick contractions:

$$C_3(t) \equiv \sum_{\vec{x}} \left\langle \bar{K}^0(\vec{x}, t_{sink}) \middle| Q_1(t) \middle| K^0\left(\vec{0}, t_{source}\right) \right\rangle = \tag{7.6}$$

$$= 2 \sum_{\vec{x},\vec{y}} \mathrm{Tr}\left[S_d(\vec{x}, t_{sink}; \vec{y}, t) \Gamma S_s\left(\vec{y}, t; \vec{0}, t_{source}\right) \gamma_5 S_d\left(\vec{y}, t; \vec{0}, t_{source}\right) \Gamma S_s(\vec{x}, t_{sink}; \vec{y}, t) \right] -$$

$$- \mathrm{Tr}\left[S_d(\vec{x}, t_{sink}; \vec{y}, t) \Gamma S_s(\vec{x}, t_{sink}; \vec{y}, t) \gamma_5 \right] \cdot \left[S_d\left(\vec{y}, t; \vec{0}, t_{source}\right) \gamma_5 S_s\left(\vec{y}, t; \vec{0}, t_{source}\right) \Gamma \right] .$$

In Fig. 7.1 we show the ratio of Eq. 7.4 compute on two different gauge ensembles, on which we fitted the data with a constant over the indicated interval.

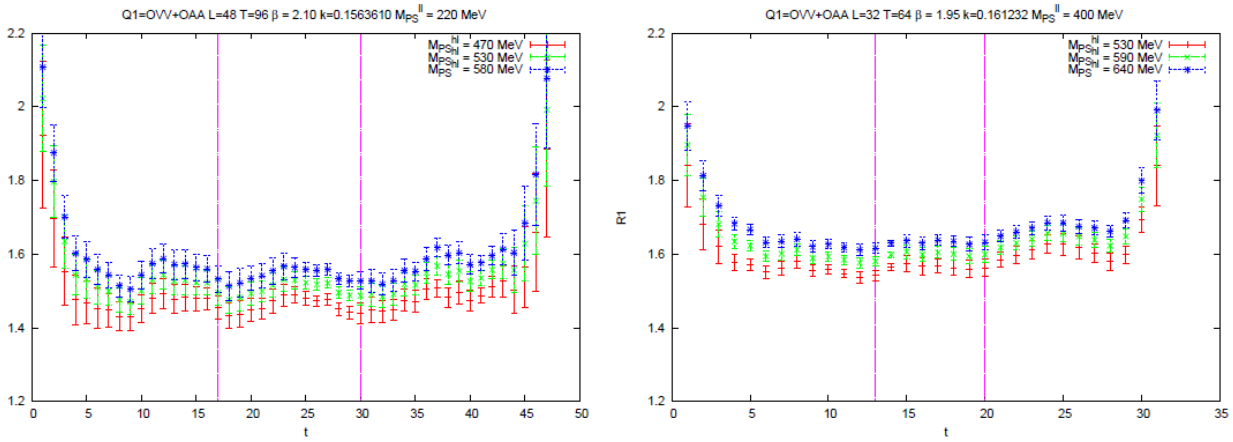

Figure 7.1: Ratio defined Eq. 7.4 (still missing the 3/8) factor) measured on two fixed gauge ensembles (*left panel:* $\beta = 2.10$, $V = 48^3 \times 96$, $am = 0.0015$; *right panel*: $\beta = 1.95$, $V = 32^3 \times 64$, $am = 0.0055$) considering 3 different strange masses. The vertical purple lines define the fit interval of the correlation functions ratio (images courtesy of Nuria Carrasco).

After determining the ratios, the data at $\beta = 1.95$ has been extrapolated to the physical point by fitting separately at each strange mass the five available light quark masses with the $SU(2)$ – ChPT prediction at next leading order:

$$B_K^{bare}(M_{ll}) = B_{K,hh}^{chir} \left[1 + A_{hh} M_{ll} - \left(\frac{M}{4\pi f} \right)^2 \log \frac{M_{ll}}{4\pi f_0} \right] \forall M_{hh} , \tag{7.7}$$

where the constant A_{hh} and $B_{K,hh}^{chir}$ are different for each value of the strange quark. In the left panel of plot Fig. 7.2 we show the data at the and fit function simultaneously.

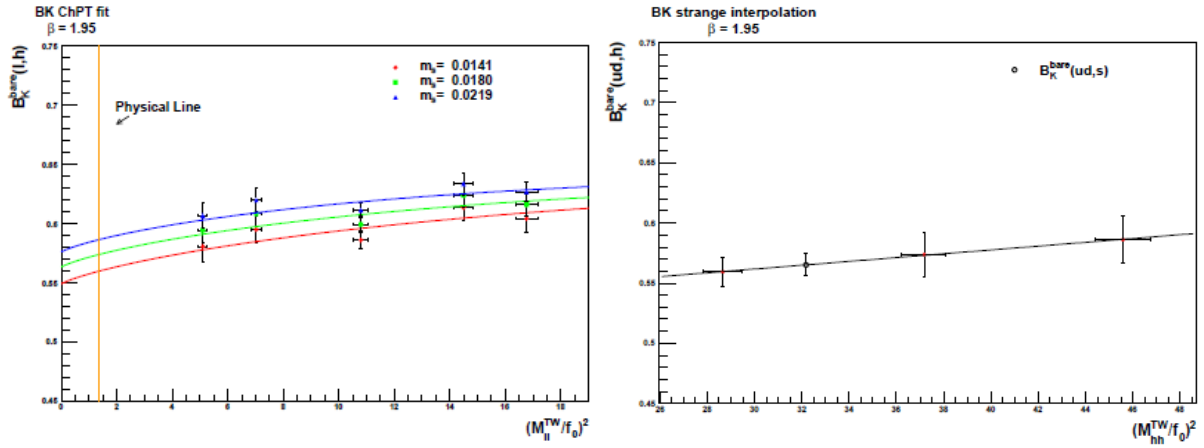

Figure 7.2: *Left panel:* chiral extrapolation at $\beta = 1.95$ for the three considered strange mass. *Right panel:* interpolation of chiral data (red points) to the physical strange (empty point).

After performing the chiral extrapolation, we interpolated the result at the physical strange by studying the value of B_K^{bare} in terms of the strange meson mass, interpolating linearly to the physical point, as shown in the right panel of Fig. 7.2.

The final result on the $\beta = 1.95$ lattice is $B_K^{bare} = 0.565(9)$.

The renormalization constant of the B_K parameter has been computed in RI/MOM scheme and evolved in the RGI scheme by N.Carrasco and reads:

$$Z_{B_K} = 1.334(18)\,. \tag{7.8}$$

In the present work this constant will be taken only as external input: the details on its calculation are quite involved and, not having been part of the present thesis, will not be presented in this work. We remind to the published literature [11] for details on the calculation. Putting the value of such renormalization constant together with B_K^{bare} we get:

$$B_K^{\rm RGI}\,(N_f = 2+1+1,\ \beta = 1.95) = Z_{B_K} B_K^{bare} = 0.754(16)\,. \tag{7.9}$$

The lack of knowledge of the renormalization constant for other two lattice spacings ($\beta = 1.95$, $\beta = 2.10$) do not allow to take continuum limit, so present result is still preliminary.

Nonetheless this value compares very well with the results obtained in previous $N_f = 2$ computation carried on by ETM collaboration obtained performing a full continuum limit analysis:

$$B_K^{\rm RGI}\,(N_f = 2, \text{cont}) = 0.729(30)\,. \tag{7.10}$$

This seem to suggest that the quenching effects on the calculation of the B_K parameter is quite small compared to the statistical error.

In the near future the availability of the missing renormalization constants will allow to present also for $N_f = 2+1+1$ a continuum extrapolated result.

7.2.1 $K_{\ell 3}$ form factors

As a last topic we present a preliminary determination of the $K_{\ell 3}$ form factor applying the method has been described in Sec. 6.5.1.

We have measured the three point correlation functions 6.32 on all $N_f = 2+1+1$ gauge ensembles previously considered. In Fig. 7.3 we show an example of such measure performed on a single gauge ensemble $\left(\beta = 1.90,\ V = 24^3 \times 48,\ M_\pi \sim 440\,\text{Mev}\right)$ at a particular value of q^2, corresponding to the maximum possible transfer momentum $q^2_{MAX} = M_K^2 - M_\pi^2$.

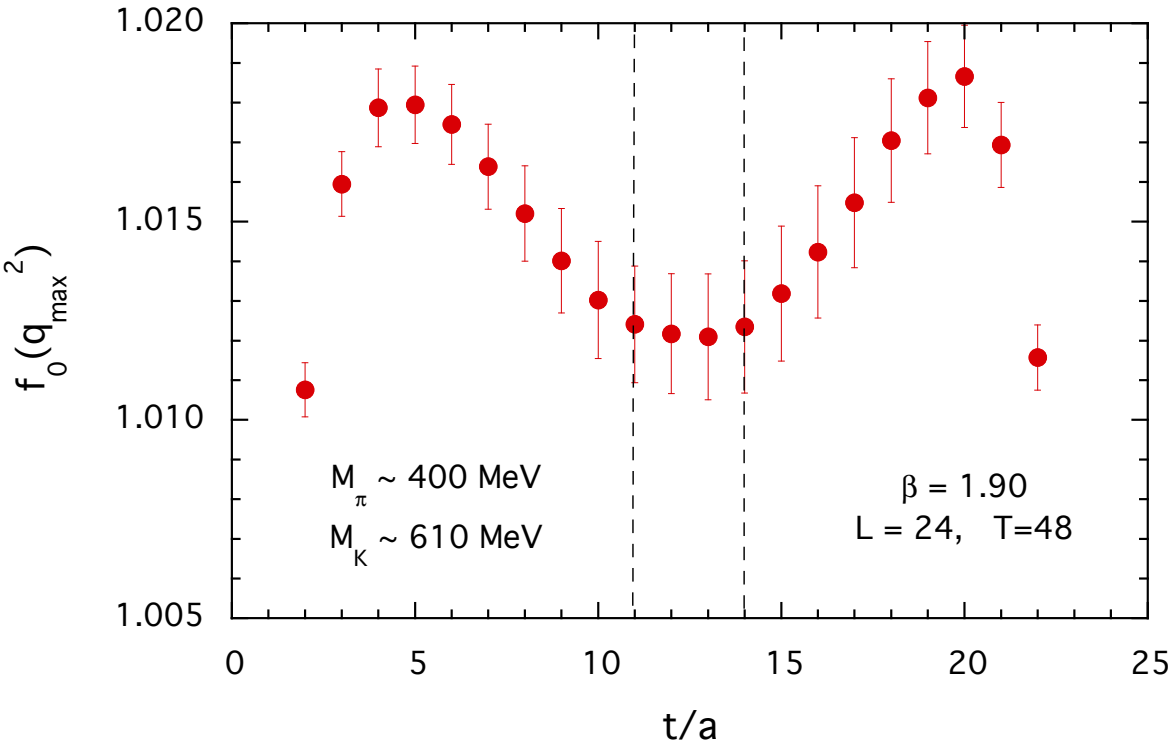

Figure 7.3: Ratio 6.36 measured at maximal value of q^2, where it equals f_0. Vertical lines bounds fit interval.

Fitting to constant such ratios over appropriate interval gives us the value of the matrix element.

Measuring such ratio for various combination of values of p_K and p_π we have been able to cover a large kinematic range. In Fig. 7.4 we show the f_+ and f_0 form factors in terms of q^2.

In future, the full analysis of the value of $f_+\left(q^2\right)$ will take into account the chiral extrapolation and interpolation of strange to its physical value.

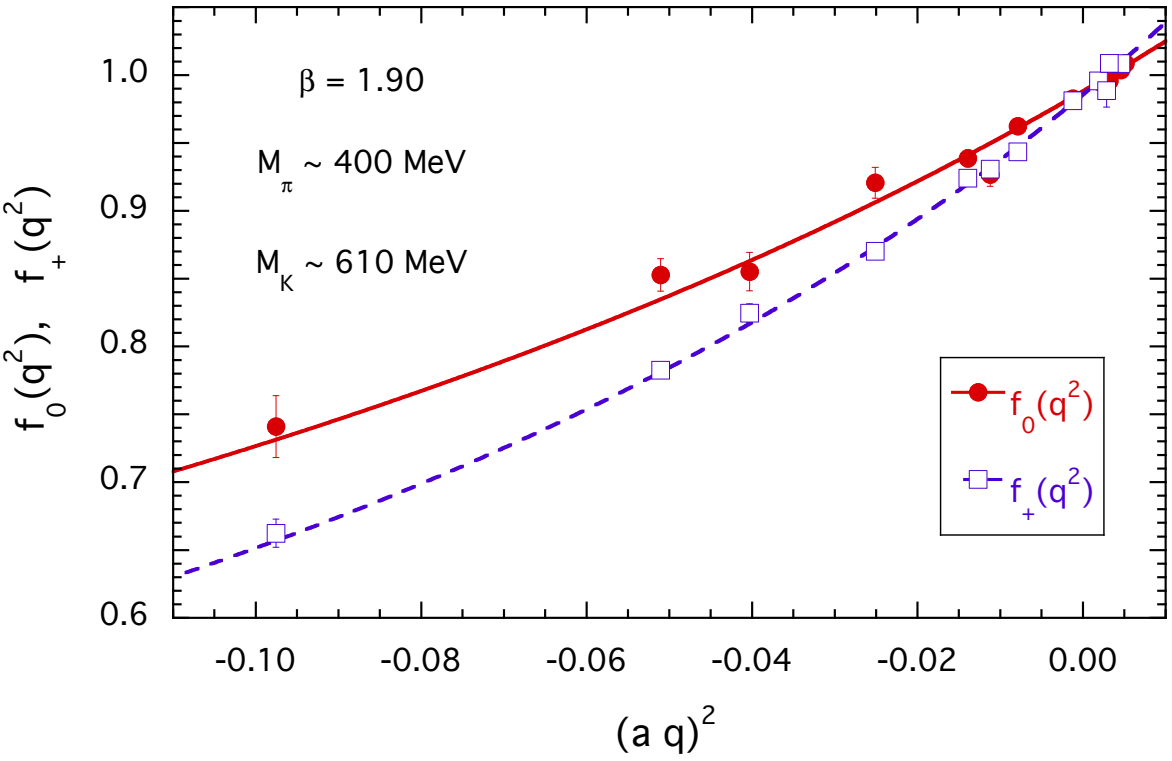

Figure 7.4: Form factors f_+ and f_0 determined on a single gauge ensemble shown in terms of q^2.

Chapter 8

Conclusions

In the present Ph.D work we have carried out the determination of various parameters of the Standard Model. This allow to test the model predictions against physical measurement and to enlighten the possible presence of new physics. Here we will summarize the main achievements of this work.

Quark masses

In chapter 4 we performed a non-perturbative determination of the u/d, s, c quark masses. The value of quark masses have been determined by tuning them in such a way to reproduce the observed spectrum of pseudo-scalar mesons. For the average up-down quark mass we have considered pion, for strange quark we have considered Kaon and the $\eta^{'}$, and for charm we chose D D_s and η_c mesons. Quark masses has been renormalized within the RI-MOM scheme, and converted to physical units considering lattice spacings values fixed from f_π. By taking into account carefully the continuum limit and chiral extrapolation we have been able to present results where the two main sources of systematic errors are properly taken into account and removed from the analysis.

The final values of the quark mass in $\overline{\rm MS}$ scheme at 2 GeV are:

$$\begin{aligned} \overline{m}_l^{\overline{\rm MS},\,2\,\rm GeV} &= 3.6\,(1)\,(2)\ \text{MeV} &&= 3.6\,(2)\ \text{MeV}\,, \\ \overline{m}_s^{\overline{\rm MS},\,2\,\rm GeV} &= 95\,(2)\,(6)\ \text{MeV} &&= 95\,(6)\ \text{MeV}\,, \\ \overline{m}_c^{\overline{\rm MS},\,2\rm GeV} &= 1.14\,(3)\,(3)\ \text{GeV} &&= 1.14\,(4)\ \text{GeV}\,. \end{aligned} \tag{8.1}$$

Where the first error is statistic and the second systematic, and the two have been summed in quadrature.

For the charm we also report the running mass:

$$\overline{m}_c\,(\overline{m}_c) = 1.28\,(4)\ \text{GeV}\,. \tag{8.2}$$

b-physics

In chapter 5 we presented a specific approach to deal with b quark extrapolation, and we have applied it to b quark mass and f_B and f_{B_s} leptonic decay constants determination. By building suitable ratios of appropriate quantities having exactly known static limit it has been possible to determine the b quark mass:

$$\overline{m}_b(\overline{m}_b) = 4.29(13)(4)\,\text{GeV} \ = 4.29\,(14)\ \text{GeV}\,, \tag{8.3}$$

for which we also report the value in $\overline{\rm MS}$ at 2 GeV:

$$\overline{m}_b^{\overline{\rm MS},\,2\,\rm GeV} = 4.92\,(13)\ \rm GeV\,. \tag{8.4}$$

By interpolating between the charm quark masses and the static limit computed in HQET it has been possible to compute f_B and f_{B_s}, which have been compared also with the results obtained with the ratio methods:

$$f_{Bs} = 232(10)\ \ \rm MeV\,, \qquad f_B = 195(12)\ \ \rm MeV\,, \qquad \frac{f_{Bs}}{f_B} = 1.19(5)\,. \tag{8.5}$$

We explored also the impact of usage of smearing techniques, finding them very effective in improving the appearance of ground state. In future this techniques will allow for the determination of these quantities to reach the level of accuracy required by future experiments.

Isospin breaking

In chapter 6 we present a new fully non-perturbative method to to take into account the isospin breaking effects related to this difference. In particular by expanding the full QCD lagrangian at first order in the $u-d$ quark mass difference and treating the isospin breaking therms as a perturbation, we have computed the $u-d$ quark mass difference from first principles which results in $\overline{\rm MS}$ at 2 GeV:

$$[m_d - m_u]^{\overline{\rm MS},\,2\rm GeV} = 2.27(24)\ \rm MeV\,. \tag{8.6}$$

We also computed the isospin breaking corrections on the K leptonic decay constant with unprecedented accuracy:

$$\left[\frac{f_{K^+}}{f_K} - 1\right] = -0.38(6)\%\,. \tag{8.7}$$

We also provide a preliminary determination of the proton-neutron mass splitting at fixed lattice spacing:

$$[M_n - M_p]^{QCD} = 2.7(9)\ \rm MeV\,, \tag{8.8}$$

Moreover we studied the feasibility of the calculation of the isospin breaking correction to the K semi-leptonic form factors.

Simulations with $n_f = 2+1+1$

In chapter 7 we present preliminary results obtained in new computations which take into accounts two heavier flavors of quarks (strange and charm) with respect to previous computations. We showed in particular a preliminary computation of the B_K parameter involved in neutral K mixing, and a preliminary computation of the pion electromagnetic form factor. When terminated, these results will be the first to take into account both strange and charm dynamical quarks.

Future perspective

The most relevant systematics effects still affecting flavor lattice computations are the chiral extrapolation and the neglecting of electromagnetism.

In future with the increasing of availability of computational power it will be possible to reach lower and lower light quark mass, and so eventually reach the physical point. This will allow to avoid to perform the chiral extrapolation and to provide more reliable lattice computed quantities.

Regarding the electromagnetism, various lattice collaborations are already producing gauge ensemble with actions which includes the QED. These QCD+QED dynamical simulations are quite more difficult than the simple QCD ones. We suggest that an extension of the δm_{ud} expansion method present in chapter 6 to the expansion in powers of e^2 (electric charge) will provide alternative and possibly simpler way to compute QED corrections to computed quantities. We already started working on this promising simulation program and we hope to provide feasibility studies in future publications.

A large source of uncertainty comes from the quite poor knowledge of lattice spacings. In future in order to reach a precision lower than 2% on dimensional quantities, a more precise determination of lattice spacings will be needed. In section 4.2.6 we provided a possible alternative way to fix the scale, which we promise to investigate in the near future.

Bibliography

[1] M. Ciuchini et al. 2003, hep-ph/0307195.

[2] M. Bona et al. 2007, 0709.0451.

[3] Mario Antonelli et al. 2009, 0907.5386.

[4] William J. Marciano. *Phys.Rev.Lett.*, 93:231803, 2004, hep-ph/0402299.

[5] M. Bona et al. *Phys.Lett.*, B687:61–69, 2010, 0908.3470.

[6] Kenneth G. Wilson. *Phys. Rev.*, D10:2445–2459, 1974.

[7] K. Symanzik. *Nucl.Phys.*, B226:187, 1983.

[8] B. Sheikholeslami and R. Wohlert. *Nucl.Phys.*, B259:572, 1985.

[9] Roberto Frezzotti, Pietro Antonio Grassi, Stefan Sint, and Peter Weisz. *JHEP*, 08:058, 2001, hep-lat/0101001.

[10] R. Frezzotti and G.C. Rossi. *JHEP*, 0408:007, 2004, hep-lat/0306014.

[11] M. Constantinou et al. *Phys. Rev.*, D83:014505, 2011, 1009.5606.

[12] J. Gasser and H. Leutwyler. *Annals Phys.*, 158:142, 1984.

[13] P. Hasenfratz and H. Leutwyler. *Nucl.Phys.*, B343:241–284, 1990.

[14] Elvira Gamiz, Christine T.H. Davies, G.Peter Lepage, Junko Shigemitsu, and Matthew Wingate. *Phys.Rev.*, D80:014503, 2009, 0902.1815.

[15] C. Albertus, Y. Aoki, P.A. Boyle, N.H. Christ, T.T. Dumitrescu, et al. *Phys.Rev.*, D82:014505, 2010, 1001.2023.

[16] G. Martinelli, C. Pittori, Christopher T. Sachrajda, M. Testa, and A. Vladikas. *Nucl. Phys.*, B445:81–108, 1995, hep-lat/9411010.

[17] Stefano Capitani. *Phys.Rept.*, 382:113–302, 2003, hep-lat/0211036.

[18] B. Blossier et al. *Phys. Rev.*, D82:114513, 2010, 1010.3659.

[19] Ph. Boucaud et al. *Phys. Lett.*, B650:304–311, 2007, hep-lat/0701012.

[20] Petros Dimopoulos et al. *PoS*, LATTICE2008:103, 2008, 0810.2873.

[21] M. Foster and Christopher Michael. *Phys.Rev.*, D59:074503, 1999, hep-lat/9810021.

[22] M. Constantinou et al. *JHEP*, 08:068, 2010, 1004.1115.

[23] Remi Baron et al. *JHEP*, 08:097, 2010, 0911.5061.

[24] R. Sommer. *Nucl. Phys.*, B411:839–854, 1994, hep-lat/9310022.

[25] Philippe Boucaud et al. *Comput.Phys.Commun.*, 179:695–715, 2008, 0803.0224.

[26] Oliver Bar. *Phys. Rev.*, D82:094505, 2010, 1008.0784.

[27] P. Dimopoulos, R. Frezzotti, C. Michael, G. C. Rossi, and C. Urbach. *Phys. Rev.*, D81:034509, 2010, 0908.0451.

[28] Gilberto Colangelo, Urs Wenger, and Jackson M. S. Wu. *Phys. Rev.*, D82:034502, 2010, 1003.0847.

[29] K.G. Chetyrkin and A. Retey. *Nucl.Phys.*, B583:3–34, 2000, hep-ph/9910332.

[30] C. Allton et al. *Phys. Rev.*, D78:114509, 2008, 0804.0473.

[31] Stephen R. Sharpe. *Phys. Rev.*, D56:7052–7058, 1997, hep-lat/9707018.

[32] C. Aubin et al. *Phys. Rev.*, D70:031504, 2004, hep-lat/0405022.

[33] Johan Bijnens and Joaquim Prades. *Mod.Phys.Lett.*, A22:767–782, 2007, hep-ph/0702170.

[34] C. T. H. Davies et al. *Phys. Rev. Lett.*, 104:132003, 2010, 0910.3102.

[35] B. Blossier et al. *JHEP*, 0804:020, 2008, 0709.4574.

[36] B. Blossier et al. *JHEP*, 1004:049, 2010, 0909.3187.

[37] I. Allison et al. *Phys.Rev.*, D78:054513, 2008, 0805.2999.

[38] K.G. Chetyrkin, J.H. Kuhn, A. Maier, P. Maierhofer, P. Marquard, et al. *Phys.Rev.*, D80:074010, 2009, 0907.2110.

[39] C. Aubin. *PoS*, LAT2009:007, 2009, 0909.2686.

[40] C.R. Allton, Christopher T. Sachrajda, V. Lubicz, L. Maiani, and G. Martinelli. *Nucl.Phys.*, B349:598–616, 1991.

[41] B. Blossier et al. *PoS*, LATTICE2009:151, 2009, 0911.3757.

[42] B. Blossier et al. *JHEP*, 0907:043, 2009, 0904.0954.

[43] Kirill Melnikov and Timo van Ritbergen. *Phys.Lett.*, B482:99–108, 2000, hep-ph/9912391.

[44] K. G. Chetyrkin and M. Steinhauser. *Phys. Rev. Lett.*, 83:4001–4004, 1999, hep-ph/9907509.

[45] K. G. Chetyrkin. *Phys. Lett.*, B404:161–165, 1997, hep-ph/9703278.

[46] J.A.M. Vermaseren, S.A. Larin, and T. van Ritbergen. *Phys.Lett.*, B405:327–333, 1997, hep-ph/9703284.

[47] N. Gray, David J. Broadhurst, W. Grafe, and K. Schilcher. *Z.Phys.*, C48:673–680, 1990.

[48] David J. Broadhurst, N. Gray, and K. Schilcher. *Z.Phys.*, C52:111–122, 1991.

[49] K.G. Chetyrkin and A.G. Grozin. *Nucl.Phys.*, B666:289–302, 2003, hep-ph/0303113.

[50] Stephen R. Sharpe and Yan Zhang. *Phys.Rev.*, D53:5125–5135, 1996, hep-lat/9510037.

[51] J.L. Goity. *Phys.Rev.*, D46:3929–3936, 1992, hep-ph/9206230.

[52] Benjamin Grinstein, Elizabeth Ellen Jenkins, Aneesh V. Manohar, Martin J. Savage, and Mark B. Wise. *Nucl.Phys.*, B380:369–376, 1992, hep-ph/9204207.

[53] K. Nakamura et al. *J.Phys.G*, G37:075021, 2010.

[54] Damir Becirevic, Benoit Blossier, Emmanuel Chang, and Benjamin Haas. *Phys.Lett.*, B679:231–236, 2009, 0905.3355.

[55] Hiroshi Ohki, Hideo Matsufuru, and Tetsuya Onogi. *Phys.Rev.*, D77:094509, 2008, 0802.1563.

[56] J. Gasser and H. Leutwyler. *Nucl.Phys.*, B250:465, 1985.

[57] J. Gasser, A. Rusetsky, and I. Scimemi. *Eur.Phys.J.*, C32:97–114, 2003, hep-ph/0305260.

[58] Johan Bijnens. *Phys.Lett.*, B306:343–349, 1993, hep-ph/9302217.

[59] Roger F. Dashen. *Phys.Rev.*, 183:1245–1260, 1969.

[60] Gilberto Colangelo, Stephan Durr, Andreas Juttner, Laurent Lellouch, Heinrich Leutwyler, et al. *Eur.Phys.J.*, C71:1695, 2011, 1011.4408.

[61] Vincenzo Cirigliano and Helmut Neufeld. *Phys.Lett.*, B700:7–10, 2011, 1102.0563.

[62] C. Alexandrou et al. *Phys.Rev.*, D78:014509, 2008, 0803.3190.

[63] J. Gasser and H. Leutwyler. *Phys.Rept.*, 87:77–169, 1982.

[64] R. Baron, Ph. Boucaud, J. Carbonell, A. Deuzeman, V. Drach, et al. *JHEP*, 1006:111, 2010, 1004.5284.

[65] Remi Baron et al. *Comput.Phys.Commun.*, 182:299–316, 2011, 1005.2042.

[66] R. Frezzotti and G. C. Rossi. *Nucl. Phys. Proc. Suppl.*, 128:193–202, 2004, hep-lat/0311008.

[67] T. Chiarappa et al. *Eur. Phys. J.*, C50:373–383, 2007, hep-lat/0606011.

[68] F. Farchioni, K. Jansen, I. Montvay, E.E. Scholz, L. Scorzato, et al. *Phys.Lett.*, B624:324–333, 2005, hep-lat/0506025.